NATIONAL CENTER FOR EARTHQUAKE ENGINEERING RESEARCH

State University of New York at Buffalo

SEISMIC FRAGILITY ANALYSIS OF PLANE FRAME STRUCTURES

by

Howard H.M. Hwang and Yeng Keong Low

Center for Earthquake Research and Information
Memphis State University
Memphis, Tennessee 38152

Technical Report NCEER-88-0028

July 31, 1988

This research was conducted at Memphis State University and was partially supported by the National Science Foundation under Grant No. ECE 86-07591.

NOTICE

This report was prepared by Memphis State University as a result of research sponsored by the National Center for Earthquake Engineering Research (NCEER). Neither NCEER, associates of NCEER, its sponsors, Memphis State University, or any person acting on their behalf:

a. makes any warranty, express or implied, with respect to the use of any information, apparatus, method, or process disclosed in this report or that such use may not infringe upon privately owned rights; or

b. assumes any liabilities of whatsoever kind with respect to the use of, or for damages resulting from the use of, any information, apparatus, method or process disclosed in this report.

SEISMIC FRAGILITY ANALYSIS OF PLANE FRAME STRUCTURES

by

Howard H.M. Hwang[1] and Yeng Keong Low[2]

July 31, 1988

Technical Report NCEER-88-0028

NCEER Contract Number 87-1004

NSF Master Contact Number ECE 86-07591

1 Associate Research Professor, Center for Earthquake Research and Information, Memphis State University

2 Graduate Research Assistant, Center for Earthquake Research and Information, Memphis State University

NATIONAL CENTER FOR EARTHQUAKE ENGINEERING RESEARCH
State University of New York at Buffalo
Red Jacket Quadrangle, Buffalo, NY 14261

50272-101

REPORT DOCUMENTATION PAGE	1. REPORT NO. NCEER 88-0028	2.	3. Recipient's Accession No. PB89-131445/AS

4. Title and Subtitle
Seismic fragility analysis of plane frame structures

5. Report Date
July 31, 1988

6.

7. Author(s)
Howard H.M. Hwang and Yeng Keong Low

8. Performing Organization Rept. No.

9. Performing Organization Name and Address
National Center for Earthquake Engineering Research
State University of New York at Buffalo
Red Jacket Quadrangle
Buffalo, NY 14261

10. Project/Task/Work Unit No.

11. Contract(C) or Grant(G) No.
(C) 87-1004 & ECE 86-07591
(G)

12. Sponsoring Organization Name and Address

13. Type of Report & Period Covered
Technical Report

14.

15. Supplementary Notes
This research was conducted at Memphis State University and was partially supported by the National Science Foundation under Grant No. ECE 86-07591.

16. Abstract (Limit: 200 words)
~~This~~ THIS report presents a practical and simplified fragility analysis method for plane reinforced concrete frame structures subject to in-plane earthquake ground accelerations. The frame modeling is based on the approach used in the computer program TABS77. A condensation technique is used in TABS77 to transform the frame structure into a stick model with lumped mass at each floor level. Dynamic characteristics of the structure such as natural frequencies and mode shapes are also obtained using TABS77. The earthquake ground acceleration is represented by a segment of stationary Gaussian random process with mean zero and a Kanai-Tajimi power spectrum. The power spectrum together with the dynamic characteristics of the structure are utilized in the random vibration analysis to derive the covariance matrices of the structural response. A simplified limit analysis procedure is utilized to determine the failure mechanism and the corresponding story shear capacity of the frame structure. Thus, the limit state used in this study is the failure mechanism established by the simplified limit analysis. For this failure mechanism, the limit state probability of each story, i.e. the story limit state probability, can be evaluated. Then, the limit state probability of the structure is measured in terms of the largest story limit state probability. The fragility curve for the frame structure is generated by evaluating the limit state probability at different levels of peak ground acceleration. A four-story test structure is used for numerical illustration. A five-story building assumed to be located in New York City is also evaluated.

17. Document Analysis a. Descriptors

b. Identifiers/Open-Ended Terms

EARTHQUAKE ENGINEERING
STRUCTURAL RESPONSE ANALYSIS
FRAGILITY ANALYSIS
REINFORCED CONCRETE STRUCTURES
DYNAMIC STRUCTURAL ANALYSIS
PLANE FRAME STRUCTURES

c. COSATI Field/Group

18. Availability Statement	19. Security Class (This Report)	21. No. of Pages
Release unlimited	Unclassified	119
	20. Security Class (This Page) Unclassified	22. Price A06

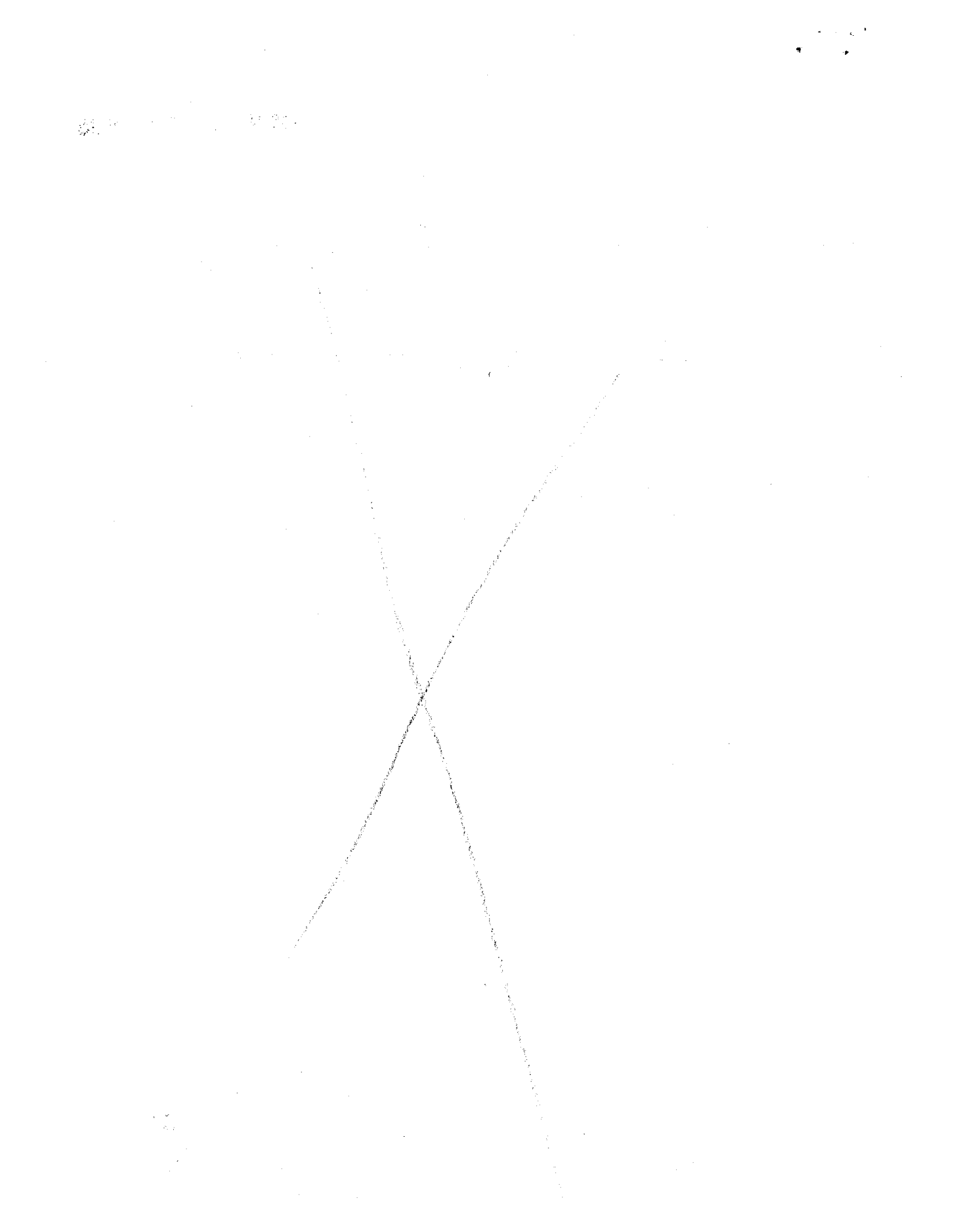

PREFACE

The National Center for Earthquake Engineering Research (NCEER) is devoted to the expansion of knowledge about earthquakes, the improvement of earthquake-resistant design, and the implementation of seismic hazard mitigation procedures to minimize loss of lives and property. The emphasis is on structures and lifelines that are found in zones of moderate to high seismicity throughout the United States.

NCEER's research is being carried out in an integrated and coordinated manner following a structured program. The current research program comprises four main areas:

- Existing and New Structures
- Secondary and Protective Systems
- Lifeline Systems
- Disaster Research and Planning

This technical report pertains to Program 1, Existing and New Structures, and more specifically to Reliability Analysis and Risk Assessment.

The long term goal of research in Existing and New Structures is to develop seismic hazard mitigation procedures through rational probabilistic risk assessment for damage or collapse of structures, mainly existing buildings, in regions of moderate to high seismicity. This work relies on improved definitions of seismicity and site response, experimental and analytical evaluations of systems response, and more accurate assessment of risk factors. This technology will be incorporated in expert systems tools and improved code formats for existing and new structures. Methods of retrofit will also be developed. When this work is completed, it should be possible to characterize and quantify societal impact of seismic risk in various geographical regions and large municipalities. Toward this goal, the program has been divided into five components, as shown in the figure below:

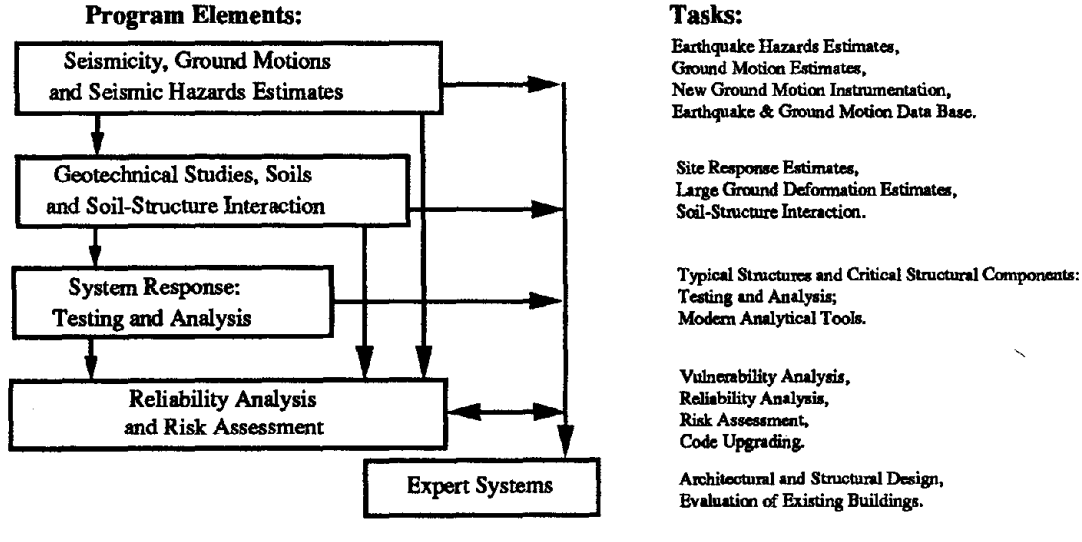

Reliability Analysis and Risk Assessment research constitutes one of the important areas of Existing and New Structures. Current research addresses, among others, the following issues:

1. Code issues - Development of a probabilistic procedure to determine load and resistance factors. Load Resistance Factor Design (LRFD) includes the investigation of wind vs. seismic issues, and of estimating design seismic loads for areas of moderate to high seismicity.
2. Response modification factors - Evaluation of RMFs for buildings and bridges which combine the effect of shear and bending.
3. Seismic damage - Development of damage estimation procedures which include a global and local damage index, and damage control by design; and development of computer codes for identification of the degree of building damage and automated damage-based design procedures.
4. Seismic reliability analysis of building structures - Development of procedures to evaluate the seismic safety of buildings which includes limit states corresponding to serviceability and collapse.
5. Retrofit procedures and restoration strategies.
6. Risk assessment and societal impact.

Research projects concerned with Reliability Analysis and Risk Assessment are carried out to provide practical tools for engineers to assess seismic risk to structures for the ultimate purpose of mitigating societal impact.

Seismic probabilistic risk assessment procedures can be used in estimating the seismic risk of urban centers and other important man-made facilities consisting of a large number of structural systems, the majority of which are building structures. This report presents the result of a fragility analysis performed for plane frame structures subjected to inplane ground accelerations. For this purpose, random vibration theory is used under the limit state condition corresponding to structural collapse described in approximation with the aid of linear analysis by utilizing experience-based response modification factors. Best-estimate fragility curves are obtained that can be used for the seismic risk assessment of individual buildings and eventually of urban centers.

ABSTRACT

This report presents a practical and simplified fragility analysis method for plane reinforced concrete frame structures subject to in-plane earthquake ground accelerations. The frame modeling is based on the approach used in the computer program TABS77. A condensation technique is used in TABS77 to transform the frame structure into a stick model with lumped mass at each floor level. Dynamic characteristics of the structure such as natural frequencies and mode shapes are also obtained using TABS77. The earthquake ground acceleration is represented by a segment of stationary Gaussian random process with mean zero and a Kanai-Tajimi power spectrum. The power spectrum together with the dynamic characteristics of the structure are utilized in the random vibration analysis to derive the covariance matrices of the structural response. A simplified limit analysis procedure is utilized to determine the failure mechanism and the corresponding story shear capacity of the frame structure. Thus, the limit state used in this study is the failure mechanism established by the simplified limit analysis. For this failure mechanism, the limit state probability of each story, i.e. the story limit state probability, can be evaluated. Then, the limit state probability of the structure is measured in terms of the largest story limit state probability. The fragility curve for the frame structure is generated by evaluating the limit state probabilities at different levels of peak ground acceleration. A four-story test structure is used for numerical illustration. A five-story building assumed to be located in New York City is also evaluated.

TABLE OF CONTENTS

LIST OF ILLUSTRATIONS

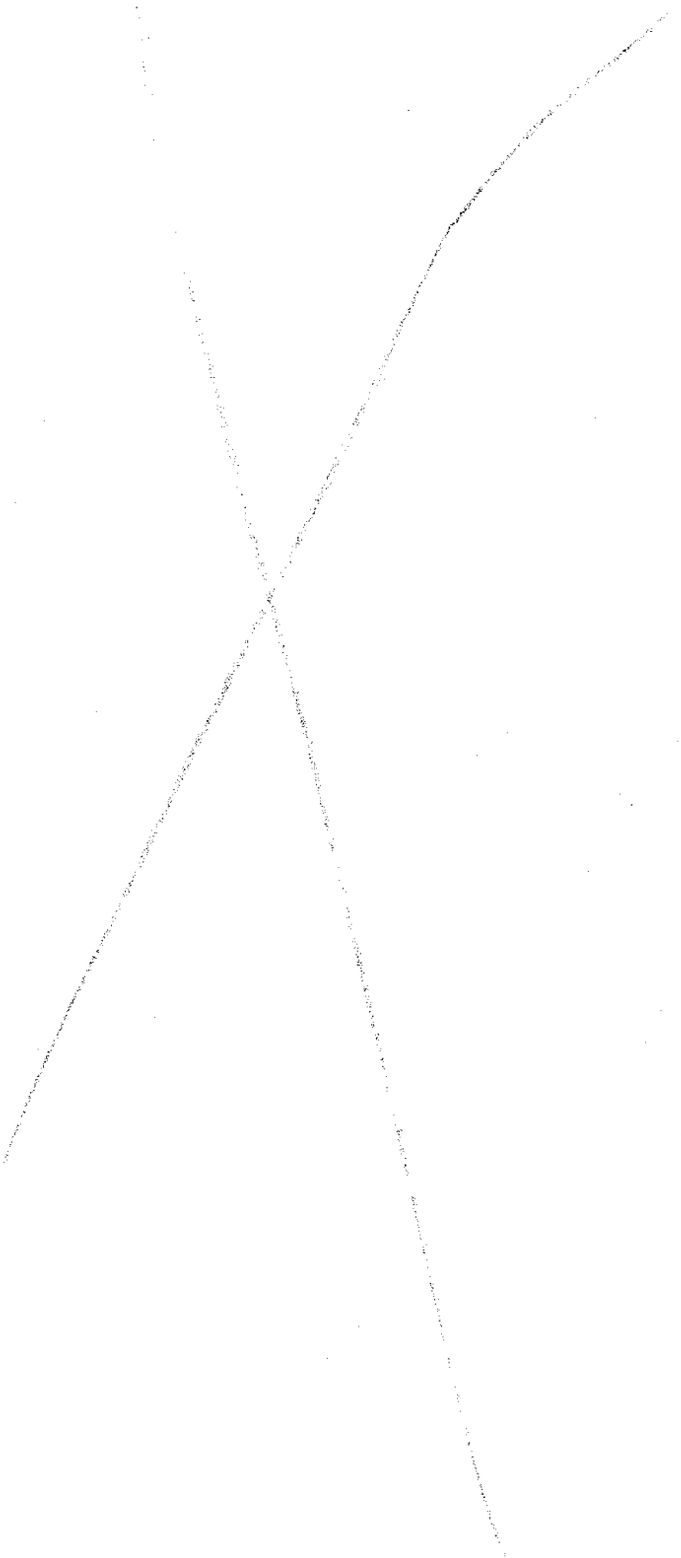

LIST OF TABLES

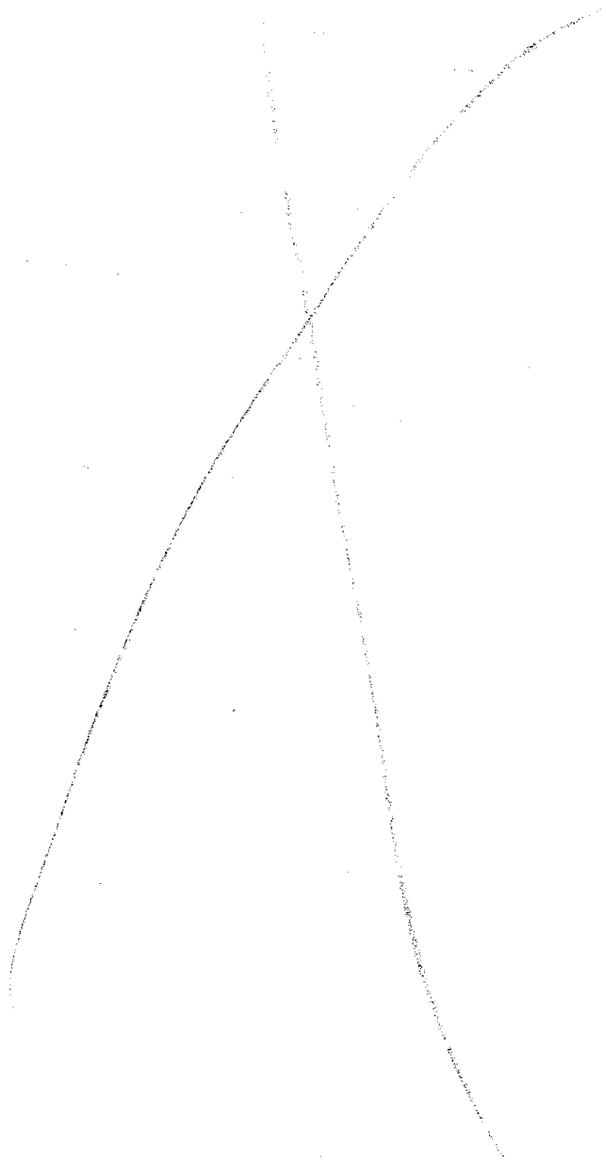

SECTION 1

INTRODUCTION

The enormous destruction caused by a major earthquake is apparent from past experience. For example, Mexico City was struck by a severe earthquake in 1985 [1] that resulted in extensive damage to building structures. As a consequence, heavy economic loss and human casualties occurred. Thus, assessment of structural vulnerability due to earthquakes is a primary concern among the regulatory agencies and engineering professions. The response of structures to earthquakes generally cannot be determined in a definite manner due to the fact that the contributing sources are uncertain to a large extent. For instance, earthquake-induced ground motion cannot be predicted precisely because it involves uncertainties in such factors as source mechanisms of future earthquakes, geological details of the seismic transmission path and local soil conditions. Similarly, mechanical properties of materials used to construct a structure are known to exhibit random variabilities and uncertainties. In addition, the structural response analysis usually involves some degree of modeling idealization further aggravates the situation. Therefore, in order to realistically assess the structural vulnerability under earthquakes, a probabilistic approach is appropriate since uncertainties and randomness involved in the load-structure system can be incorporated.

At a very low level of ground shaking, one can be almost certain that the building would not collapse. Conversely, at an extreme high level of ground shaking, one can reasonably assume that the building would collapse. The likelihood of structural damage due to different levels of earthquakes can be expressed by a fragility curve [2]. For example, the fragility curves for a five-story shear wall building are shown in Fig. 1-1 [3]. As displayed in the figure, the fragility curve describes the probability of a specific type of damage at various levels of ground shaking. The generation and the usage of fragility curves have been discussed in Ref. 2; in addition, comments regarding the generation of a fragility curve were also presented.

This report presents a practical and simplified fragility analysis method for plane reinforced concrete frame structures subject to in-plane earthquake ground accelerations. The following four characteristics are incorporated in this study: (1) random vibration approach is utilized since it yields directly the statistical information about the structural response

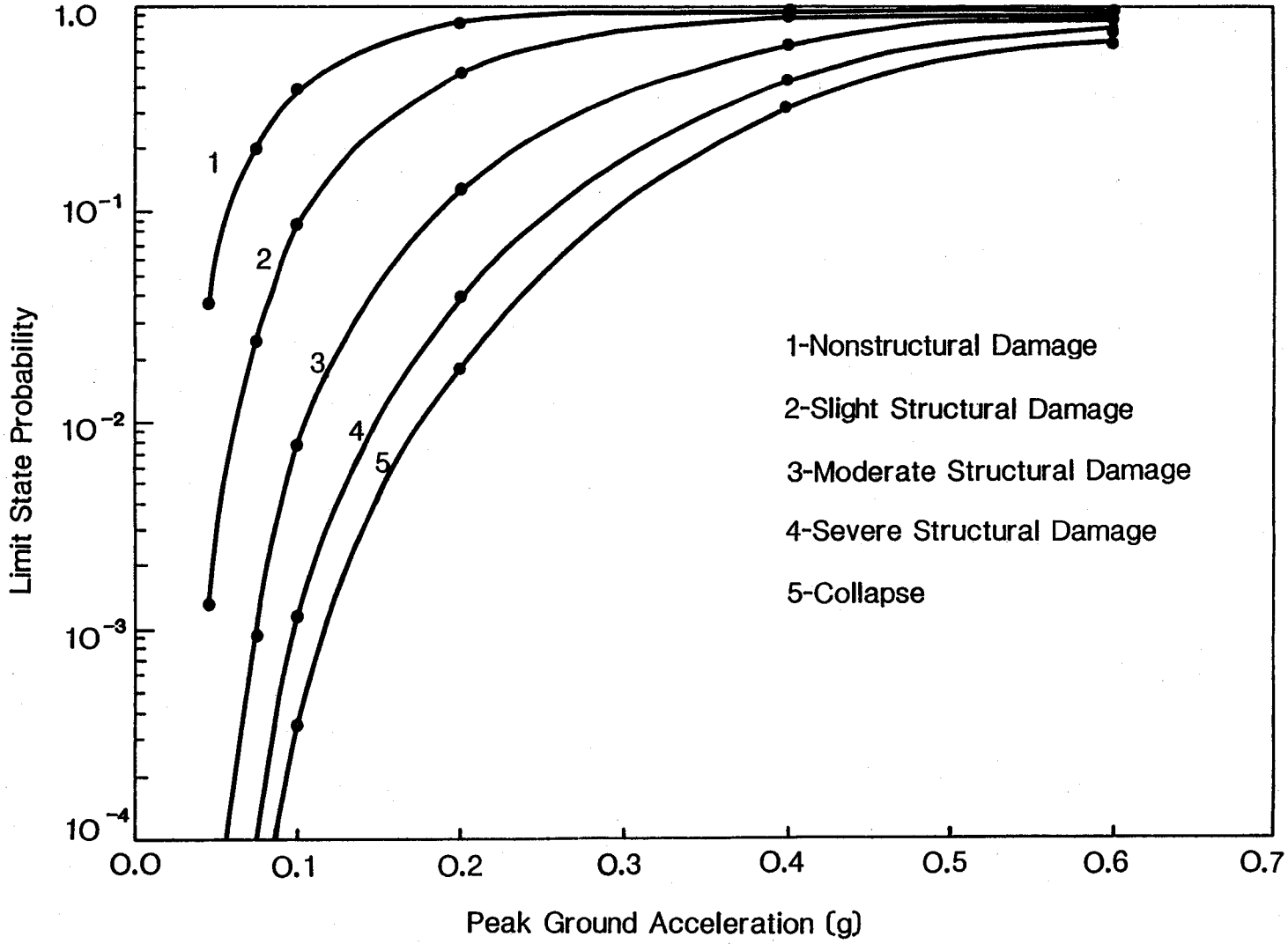

Fig. 1-1 Fragility Curves (Ref. 3)

and allows rapid assessment of the probability of the response exceeding a certain capacity threshold. (2) emphasis is placed on the overall performance of the frame structure instead of on each structural member. It is well-known that the failure of a member does not constitute the failure of the entire structure, especially for a highly redundant frame structure. (3) a simplified limit analysis procedure is used to evaluate the story shear capacity without having to consider all other failure mechanisms. (4) the modeling of the frame structure with a large number of degrees-of-freedom using finite element formulation is, in general, too time consuming and complicated for probabilistic assessment of structural system. In order to reduce the degree of complexity in structural modeling, the frame structure is condensed to a stick model using a condensation technique. Such a structural modeling is more sound both theoretically and technically than the commonly used shear beam model to represent the frame structure, especially for the frame structure with weak beams.

The earthquake ground acceleration considered in this study is represented by a stationary Gaussian random process with mean zero and a Kanai-Tajimi power spectrum. A finite duration of ground acceleration is used to account for the nonstationarity in the ground acceleration. The corresponding structural response, on the basis of linear structural behavior, is also a stationary and Gaussian random process with mean zero. The structural response selected for this study is story shear force, which is used as the basis for evaluating the reliability of the frame structure.

A simplified limit analysis is utilized to determine the failure mechanism and the corresponding structural capacity, in which the mean values of the material properties are utilized to simplify the reliability analysis. The limit state probability for the entire frame structure is assessed in terms of the largest value of the story limit state probabilities, which are determined by comparing the structural response at each story due to an earthquake with the computed structural capacity. The fragility curve of the structure is then constructed by evaluating the frame limit state probabilities at various levels of peak ground accelerations.

This report begins with the dynamic modeling of the plane frame structure in Section 2. The structure is described using the standard structural analysis approach. A stick model is then derived using a condensation technique. The dynamic analysis of the stick model using modal analysis is also presented in Section 2. Random vibration analysis is described in Section 3. The procedure to determine the structural capacity is presented in Section

4, and Section 5 shows the evaluation of the limit state probability and the fragility of the frame structure. In Section 6, a four-story reinforced concrete test structure is used to illustrate the application of this fragility analysis method, followed by a five-story reinforced concrete frame building in Section 7. Finally, Section 8 closes the study with conclusions.

SECTION 2

DYNAMIC ANALYSIS OF PLANE FRAME STRUCTURE

2.1 Modeling of Plane Frame Structure

The structural system analyzed in this study is a plane frame structure. A sketch of a typical frame structure is shown in Fig. 2-1. The structural idealization described in this section basically follows the approach employed by the computer program TABS77 [4]. In addition, TABS77 is utilized to evaluate the dynamic characteristics of the frame structure such as natural frequencies and mode shapes which are subsequently used in the random vibration analysis of the frame structure.

The frame structure is assumed to be fixed at the foundation level. Column centerlines and floor levels are the basic reference lines in the frame description. The plane frame consists of two element types: beam and column elements. The beam element has two degrees-of-freedom (DF), one rotation and one lateral; whereas the column element has three DF's with an additional axial deformation. The floor systems are usually very stiff in their own plane, therefore, it is reasonable to assume that the floor diaphragms are rigid in their own plane and all joints at the same floor level undergo the same lateral displacement. Therefore, the global structural system retains only a rotational and a vertical translational DF for each beam-column joint, and a lateral displacement for each story.

The formulation of column and beam stiffness matrices is standard. Prismatic columns are used with shearing and axial deformations taken into account. The beams need not be prismatic but must be symmetric about their vertical midplane. The shearing deformation of beams may be considered by making the appropriate modification to the stiffness factors. For the formulation of column stiffness, expressing in terms of the deformations shown in Fig. 2-2, the member forces may be defined in matrix form as follows:

$$\begin{Bmatrix} M_i \\ M_j \\ S \end{Bmatrix} = \begin{bmatrix} k_{11} & k_{12} & 0 \\ k_{21} & k_{22} & 0 \\ 0 & 0 & k_{33} \end{bmatrix} \begin{Bmatrix} \phi_i \\ \phi_j \\ \delta \end{Bmatrix} \tag{2.1}$$

or

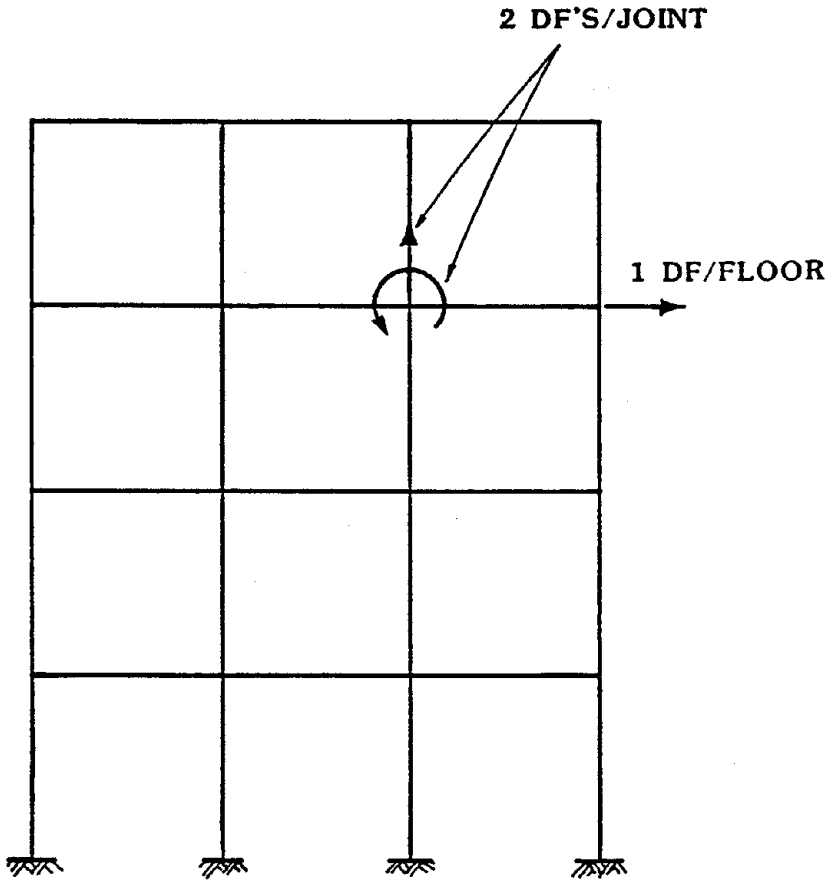

Fig. 2-1 Typical Plane Frame Structure

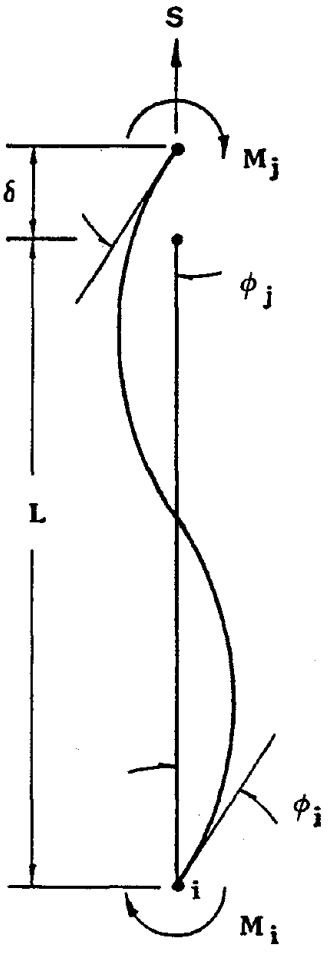

Fig. 2-2 Column Deformations and Member Forces

$$\{S_c\} = [k_c]\{\phi_c\} \tag{2.2}$$

and

$$k_{11} = k_{22} = \frac{2EI}{L}\left(\frac{2+\beta}{1+2\beta}\right) \tag{2.3}$$

$$k_{12} = k_{21} = \frac{2EI}{L}\left(\frac{1-\beta}{1+2\beta}\right) \tag{2.4}$$

$$k_{33} = \frac{AE}{L} \tag{2.5}$$

where,

M_i : moment at joint i
M_j : moment at joint j
S : axial force
ϕ_i : rotation at joint i
ϕ_j : rotation at joint j
δ : axial deformation
β : shear flexibility factor, $\beta = 6EI/(L^2\bar{A}G)$
$\bar{A}$: effective shear area
A : member cross-sectional area
E : Young's modulus
I : moment of inertia
G : shear modulus
L : member length

The transformation between member deformations and frame displacements as shown in Fig. 2-3 is given below:

$$\begin{Bmatrix} \phi_i \\ \phi_j \\ \delta \end{Bmatrix} = \begin{bmatrix} 1 & 1/L & 0 & -1/L & 0 & 0 \\ 0 & 1/L & 1 & -1/L & 0 & 0 \\ 0 & 0 & 0 & 0 & 1 & -1 \end{bmatrix} \begin{Bmatrix} \theta_B \\ u_B \\ \theta_T \\ u_T \\ v_B \\ v_T \end{Bmatrix} \tag{2.6}$$

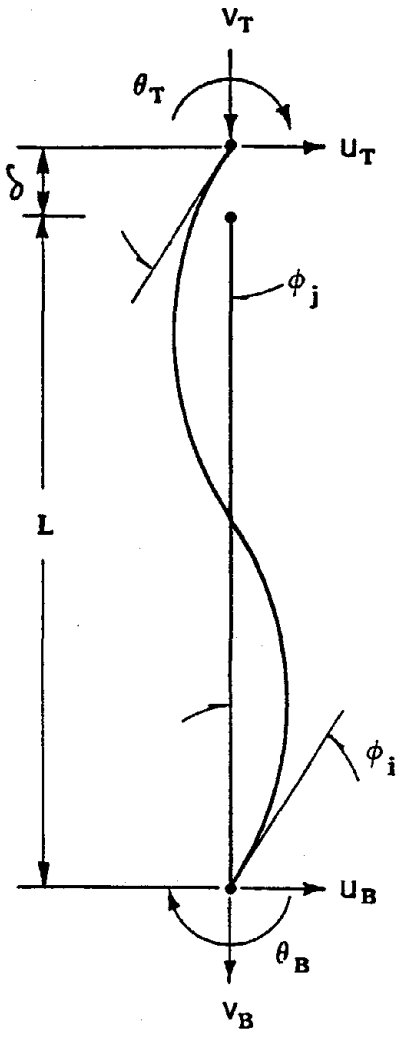

Fig. 2-3 Column Deformations and Joint Displacements

or

$$\{\phi_c\} = [a_c]\{r_c\} \tag{2.7}$$

Following the standard structural analysis theory, the stiffness matrix for an individual column, $[K_c^e]$ is

$$[K_c^e] = [a_c]^T[k_c][a_c] \tag{2.8}$$

The beam stiffness is derived in a very similar fashion with the exception that the axial deformation term is neglected. Therefore, for the beam element, Eq. 2.1 may be written as follows:

$$\begin{Bmatrix} M_i \\ M_j \end{Bmatrix} = \begin{bmatrix} k_{11} & k_{12} \\ k_{21} & k_{22} \end{bmatrix} \begin{Bmatrix} \phi_i \\ \phi_j \end{Bmatrix} \tag{2.9}$$

or

$$\{S_b\} = [k_b]\{\phi_b\} \tag{2.10}$$

With reference to Fig. 2-4, the transformation between beam deformations and frame displacements is

$$\begin{Bmatrix} \phi_i \\ \phi_j \end{Bmatrix} = \begin{bmatrix} 1 & 1/L & 0 & -1/L \\ 0 & 1/L & 1 & -1/L \end{bmatrix} \begin{Bmatrix} \theta_L \\ v_L \\ \theta_R \\ v_R \end{Bmatrix} \tag{2.11}$$

or

$$\{\phi_b\} = [a_b]\{r_b\} \tag{2.12}$$

Using Eqs. 2.10 and 2.12, the beam stiffness matrix $[K_b^e]$ can be derived as

$$[K_b^e] = [a_b]^T[k_b][a_b] \tag{2.13}$$

The overall stiffness matrix for the frame is assembled by the direct stiffness technique. In this study, the deformations within joints are neglected. A condensation technique as shown in Appendix A is carried out within TABS77 to eliminate the joint DF's (rotation and vertical displacements). Thus, the two-dimensional frame structure is reduced to a one-dimensional stick model with only one lateral DF at each floor level as shown in Fig.

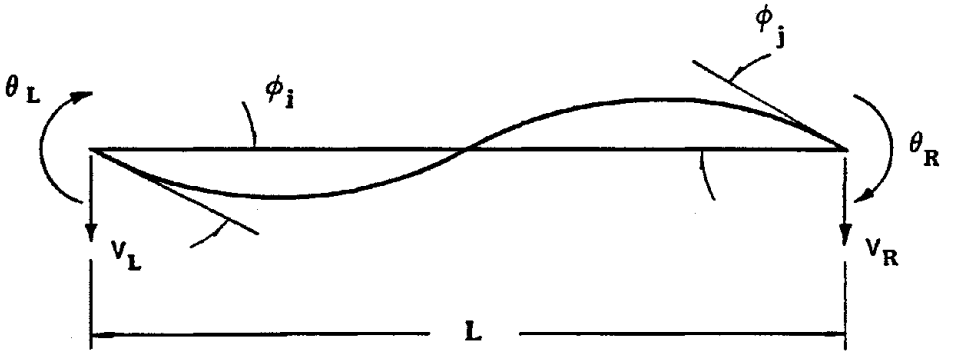

Fig. 2-4 Beam Deformations and Joint Displacements

2-5. This stick model will be used subsequently for the dynamic analysis of the frame structure.

2.2 Modal Analysis

For the frame structure modeled as a stick model as shown in Fig. 2-6, the equations of motion can be derived in terms of the lateral displacement at each story level where the lumped mass is located. The equations of motion of a frame structure subject to an in-plane earthquake ground acceleration $\ddot{u}_g$ are

$$[M]\{\ddot{\Delta}\} + [C]\{\dot{\Delta}\} + [K]\{\Delta\} = -[M]\{\hat{I}\}\ddot{u}_g \tag{2.14}$$

where $[M]$ and $[C]$ are the mass and damping matrices respectively. $[K]$ is the modified stiffness matrix as shown in Eq. A.7. $\{\Delta\}$ is the floor displacement vector relative to the base of the structure, and $\{\hat{I}\}$ is the identity vector for the condensed system. From the free vibration analysis, the natural frequencies and mode shapes can be determined. Under the assumption that the normal modes exist, the floor displacement $\{\Delta\}$ can be expressed as

$$\{\Delta\} = [\Phi]\{q\} \tag{2.15}$$

where,

$[\Phi]$: modal matrix, $[\Phi] = [\{\phi_1\}\{\phi_2\}\ldots\{\phi_n\}]$
n : number of modes considered
$\{q\}$: generalized coordinate vector corresponding to n modes

Making use of the orthogonality conditions of the normal modes with respect to the mass matrix $[M]$ and the stiffness matrix $[K]$, as well as the assumption that the damping matrix $[C]$ can be diagonalized, we can simplify Eq. 2.14 into a set of uncoupled systems

$$\{\ddot{q}\} + [D]\{\dot{q}\} + [\Omega^2]\{q\} = -\{\Gamma\}\ddot{u}_g \tag{2.16}$$

where $[D]$ and $[\Omega^2]$ are the (diagonal) modal damping and frequency matrices with non-zero elements $2\zeta_1\omega_1, 2\zeta_2\omega_2$, ..., $2\zeta_n\omega_n$ and ω_1^2, ω_2^2, ..., ω_n^2, respectively. The vector $\{\Gamma\} = [\Phi]^T[M]\{\hat{I}\}$ is the modal participation vector. The solution of Eq. 2.16 can be expressed in the following integral form:

$$\{q\} = -\int_{-\infty}^{\infty} [h(t-\tau)]\{\Gamma\}\ddot{u}_g(\tau)d\tau \tag{2.17}$$

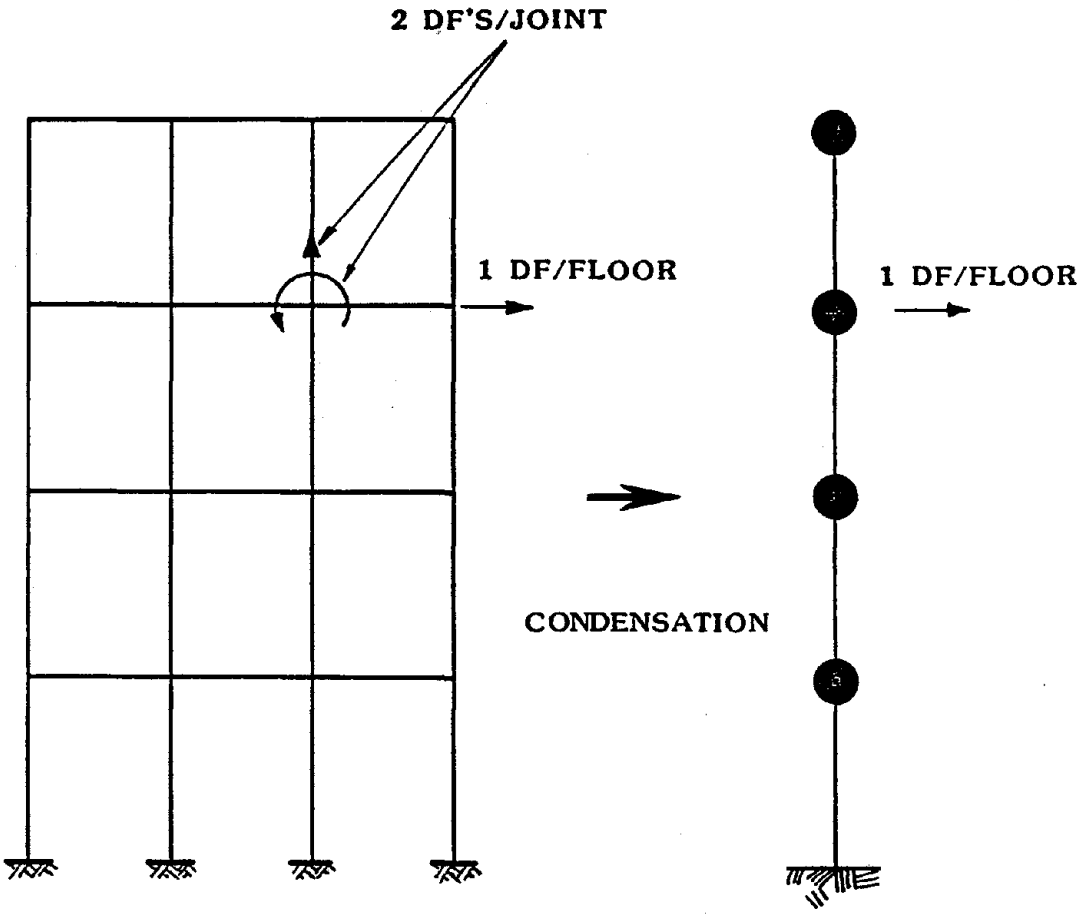

Fig. 2-5 Condensation of Plane Frame Structure

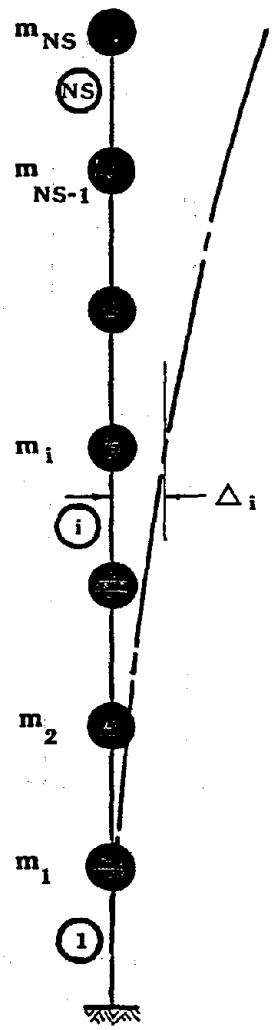

Fig. 2-6 Stick Model of Structure

where $[h(t)]$ is the (diagonal) impulse response function matrix

$$[h(t)] = \begin{bmatrix} h_1(t) & & & 0 \\ & h_2(t) & & \\ & & \ddots & \\ 0 & & & h_n(t) \end{bmatrix} \tag{2.18}$$

and $h_i(t)$ is the impulse response function of the i^{th} mode.

2.3 Story Shear Formulation

The restoring force vector $\{f\}$ can be expressed by using the relative floor displacements $\{\Delta\}$ as

$$\{f\} = [K]\{\Delta\} \tag{2.19}$$

Since $\{\Delta\} = [\Phi]\{q\}$ (Eq. 2.15), Eq. 2.19 expressed in terms of the generalized coordinates $\{q\}$ is

$$\{f\} = [K][\Phi]\{q\} \tag{2.20}$$

Following the relationship of eigen-value problem, i.e.

$$[K][\Phi] = [M][\Phi][\Omega^2] \tag{2.21}$$

the restoring force vector $\{f\}$ becomes

$$\{f\} = [M][\Phi][\Omega^2]\{q\} \tag{2.22}$$

From the equilibrium of the free body diagram shown in Fig. 2-7, the story shear force at the i^{th} story Q_i is equal to the sum of the restoring forces above that story:

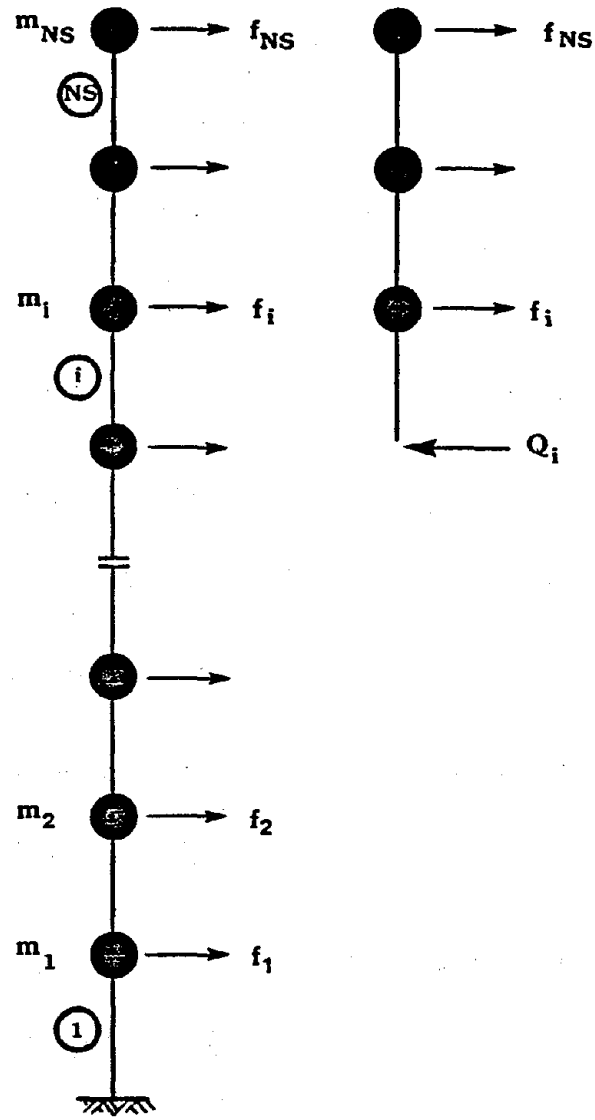

Fig. 2-7 Story Shear Force

$$
\begin{aligned}
Q_{NS} &= f_{NS} \\
Q_{NS-1} &= f_{NS} + f_{NS-1} \\
&\vdots \\
Q_i &= f_{NS} + f_{NS-1} \cdots + f_i \\
&\vdots \\
Q_2 &= f_{NS} + f_{NS-1} + \cdots + f_2 \\
Q_1 &= f_{NS} + f_{NS-1} + \cdots + f_2 + f_1
\end{aligned}
\tag{2.23}
$$

where NS is the total number of masses. As shown in Fig. 2-7, the mass and restoring force of the stick model are numbered from bottom to top in an ascending order; for instance, m_1 and f_1 correspond to the mass and restoring force at the first story, respectively. In matrix form, Eq. 2.23 can be written as

$$
\begin{Bmatrix} Q_1 \\ Q_2 \\ \vdots \\ Q_{NS-1} \\ Q_{NS} \end{Bmatrix} =
\begin{bmatrix} 1 & & & \mathbf{1} \\ & 1 & & \\ & & \ddots & \\ & \mathbf{0} & & 1 \end{bmatrix}
\begin{Bmatrix} f_1 \\ f_2 \\ \vdots \\ f_{NS-1} \\ f_{NS} \end{Bmatrix}
$$

or

$$
\{Q\} = [T^*]\{f\} \tag{2.24}
$$

where $[T^*]$ is the transformation matrix. Combining Eq. 2.22 with Eq. 2.24, the story shear force vector $\{Q\}$ can be expressed as

$$
\{Q\} = [A']\{q\} \tag{2.25}
$$

where

$$
[A'] = [T^*][M][\Phi][\Omega^2] \tag{2.26}
$$

SECTION 3

RANDOM VIBRATION ANALYSIS

3.1 Response Spectral Analysis

Under the stationary assumption the cross-correlation matrix $[R_{qq}(t_0)]$ of $\{q\}$ is defined as

$$[R_{qq}(t_0)] = E[\{q(t)\}\{q(t+t_0)\}^T] \tag{3.1}$$

Using the following well-known Wiener-Khintchine (W-K) transform [5]:

$$[S_{qq}(\omega)] = \frac{1}{2\pi}\int_{-\infty}^{\infty}[R_{qq}(t_o)]e^{-i\omega t_o}dt_0 \tag{3.2}$$

and

$$[R_{qq}(t_0)] = \int_{-\infty}^{\infty}[S_{qq}(\omega)]e^{i\omega t_o}d\omega \tag{3.3}$$

We can transform Eq. 3.1 from the time domain into the frequency domain. It can be shown that the power spectral density function of $\{q\}$, i.e. $[S_{qq}(\omega)]$, is

$$[S_{qq}(\omega)] = [H(\omega)]\{\Gamma\}S_{gg}(\omega)\{\Gamma\}^T[H^*(\omega)] \tag{3.4}$$

where $S_{gg}(\omega)$ is the power spectral density function of the horizontal ground acceleration; $[H(\omega)]$ is the frequency response matrix and $[H^*(\omega)]$ is its complex conjugate matrix. The frequency response matrix $[H(\omega)]$ is

$$[H(\omega)] = \begin{bmatrix} H_1(\omega) & & & 0 \\ & \ddots & & \\ & & H_i(\omega) & \\ & & & \ddots \\ 0 & & & H_n(\omega) \end{bmatrix} \tag{3.5}$$

in which $H_i(\omega)$ is the i^{th} frequency response function:

$$H_i(\omega) = \frac{1}{({\omega_i}^2 - \omega^2) + 2i\zeta_i\omega_i\omega} \tag{3.6}$$

The elements of $[S_{qq}(\omega)]$ are

$$S_{qq_{ii}}(\omega) = \left|H_i(\omega)\right|^2 \Gamma_i{}^2 S_{gg}(\omega) \qquad \text{for } i = j \tag{3.7}$$

and

$$S_{qq_{ij}}(\omega) = H_i(\omega) H_j^*(\omega) \Gamma_i \Gamma_j S_{gg}(\omega) \qquad \text{for } i \neq j \tag{3.8}$$

where i and j denote the i^{th} and j^{th} modes, respectively.

3.2 Earthquake Ground Acceleration

The earthquake ground acceleration is assumed to act in the plane of the structure and along the horizontal direction. The earthquake ground acceleration is represented by a stationary Gaussian process with mean zero and an appropriate power spectral density function. In reality an earthquake ground acceleration is non-stationary. To account for this non-stationarity, a finite duration of strong ground motion is used.

In this study, a (two-sided) spectral density function suggested by Kanai and Tajimi is utilized [6]. The Kanai-Tajimi power spectrum has the following form:

$$S_{gg}(\omega) = S_0 \frac{1 + 4\zeta_g{}^2 \left(\frac{\omega}{\omega_g}\right)^2}{[1 - \left(\frac{\omega}{\omega_g}\right)^2]^2 + 4\zeta_g{}^2 \left(\frac{\omega}{\omega_g}\right)^2} \tag{3.9}$$

Parameters ω_g and ζ_g are the dominant ground frequency and the critical damping, respectively, which depend on the site soil conditions [7]. S_0 is a parameter describing the amplitude of the spectrum and related to the peak ground acceleration. The peak ground acceleration A_1, given an earthquake, is assumed to be [8]

$$A_1 = p_g \sigma_g \tag{3.10}$$

where σ_g is the standard deviation of the ground acceleration evaluated by integrating the Kanai-Tajimi spectral density function with respect to ω. p_g is the peak factor and taken as 3.0 in this study [8]. The standard deviation σ_g can be written as follows:

$$\sigma_g = \left[\pi \omega_g \left(\frac{1}{2\zeta_g} + 2\zeta_g\right)\right]^{1/2} S_0^{1/2} \tag{3.11}$$

Therefore, S_0 can be written as

$$S_0 = \frac{A_1^2}{p_g^2 \left[\pi \omega_g \left(\frac{1}{2\zeta_g} + 2\zeta_g\right)\right]} \tag{3.12}$$

3.3 Spectral Story Shear Response

From Eq. 2.25 the cross-correlation matrix of $\{Q(t)\}$, i.e. $[R_{QQ}(t_0)]$, can be derived as

$$[R_{QQ}(t_0)] = [A'][R_{qq}(t_0)][A']^T \tag{3.13}$$

Using the W-K transform, the power spectral density function of $\{Q\}$, $[S_{QQ}(\omega)]$, is

$$[S_{QQ}(\omega)] = [A'][S_{qq}(\omega)][A']^T \tag{3.14}$$

From the stochastic process theory, the covariance matrix of $\{Q(t)\}$, $[V_{QQ}]$, can be expressed as follows:

$$[V_{QQ}] = \int_{-\infty}^{\infty} [S_{QQ}(\omega)] d\omega \tag{3.15}$$

In addition, the covariance matrix of $\{\dot{Q}(t)\}$, i.e. $[V_{\dot{Q}\dot{Q}}]$, is

$$[V_{\dot{Q}\dot{Q}}] = \int_{-\infty}^{\infty} \omega^2 [S_{QQ}(\omega)] d\omega \tag{3.16}$$

The covariance matrices as shown in Eqs. 3.15 and 3.16 are the statistical descriptions of the story shear responses. They will be used later to evaluate the limit state probability of the frame structure.

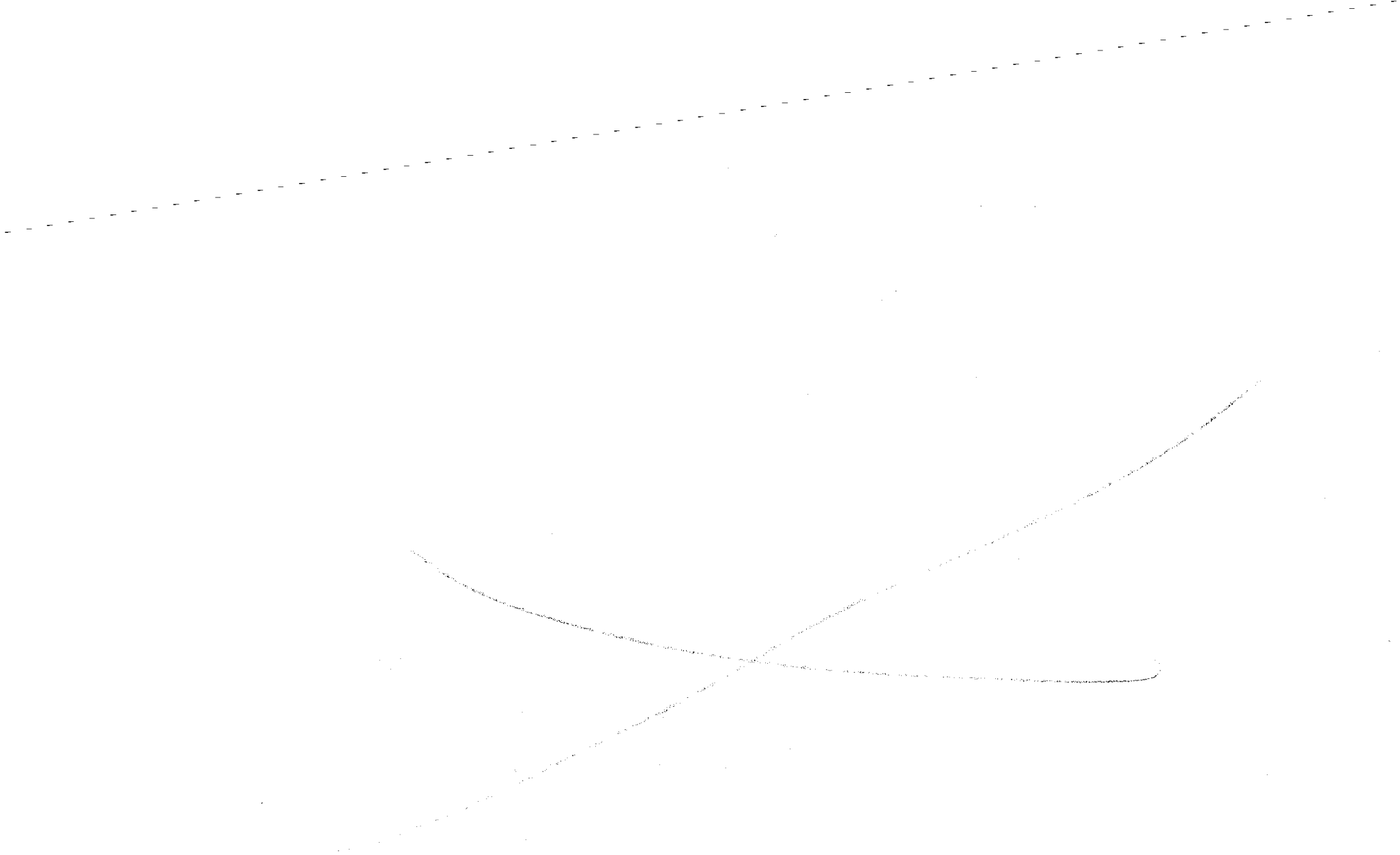

SECTION 4

LIMIT STATE AND STRUCTURAL CAPACITY

4.1 Limit State

A limit state is defined as a state of undesirable structural behavior. To ensure the normal function of a structure, the structural response should stay within the limit state throughout its entire service life. The limit state considered in this study is the collapse of the frame structure. In order to derive this collapse limit state, the ultimate flexural and shear strengths of beams and columns are evaluated according to the ACI Code 318-83 [9] for the reinforced concrete structures. These quantities are then utilized in a simplified limit analysis method proposed by Aoyama [10] to determine the ultimate story shear capacities of the frame structure at the formation of a collapse mechanism.

In this study, the structural response is evaluated linearly. In order to be compatible with this linear response, the ultimate structural capacity is modified to the equivalent linear capacity. This is accomplished through the use of a conversion factor F as follows:

$$Q_\ell = F \times Q_n \tag{4.1}$$

where Q_ℓ is the equivalent linear shear capacity and Q_n is the nonlinear shear capacity. The factor F has been found to be a function of the ductility ratio μ which reflects the degree of deformability of a structure. Thus, F is called the ductility index. For a single degree-of-freedom system with elastic-perfectly plastic behavior, the ductility index may be determined by the well-known Newmark's formula:

$$F = \sqrt{2\mu - 1} \tag{4.2}$$

which is based on the assumption that the strain energy accumulated in a linear system is equivalent to the strain energy of an elastic-perfectly plastic system. However, the behavior of a concrete structure may vary considerably from an elastic-perfectly plastic system when subject to a cyclic loading such as earthquake ground motion. Thus, the appropriate F value is best determined from the evaluation of damage data from past earthquakes. The F values suggested by Hawkins [11] shown in Table 4-I is adopted in this study. These

Table 4-I Recommended F_i Values (Ref. 11)

Mark	Member Type	F_i*
1.	Column with clear height-to-depth ratio less than 2.0 and shear capacity less than flexural capacity (brittle failure).	0.8
2.	Column with shear capacity less than flexural capacity but $H/d > 2.0$.	1.0
3.	Column with flexural capacity less than shear capacity but inadequate hoops and high axial stress.	1.5
4.	Column as in 3 and with hoops satisfying code requirements for shear.	2.5
5.	Column as in 3 and with hoops satisfying special confinement requirements adjacent to connections.	3.5

*F_i values for columns framing panels with brick infill should be multiplied by 0.9.

F values are similar to those suggested by Aoyama [10], which were compiled from the earthquake performance of frame structures in Japan. It is assumed that the F values shown in Table 4-I are applicable to each story shear force of a multi-degree-of-freedom system. For each story, Eq. 4.1 can be written as follows:

$$Q_{\ell i} = F_i \times Q_{ni} \tag{4.3}$$

where,

$Q_{\ell i}$: equivalent linear shear capacity at story i
F_i: ductility index at story i
Q_{ni}: nonlinear shear capacity at story i

Once the nonlinear shear capacity Q_{ni} is determined from the limit analysis, the equivalent linear shear capacity $Q_{\ell i}$ for each story can also be determined.

4.2 Ultimate Strengths of Beams and Columns

The ultimate flexural and shear strengths of beams and columns are evaluated in accordance with the formulas in ACI Code 318-83 [9]. For a doubly reinforced rectangular beam, the resistance moment about the center of the cross section M_R is shown in Eq. 4.4. It is noted that the moment causing compression on the top of beam is defined as positive, and vice-versa.

$$M_R = 0.85 f'_c ab \left(\frac{h}{2} - \frac{a}{2}\right) + A'_s f'_s \left(\frac{h}{2} - d'\right) + A_s f_y \left(\frac{h}{2} - d''\right) \tag{4.4}$$

where,

f'_c: compressive strength of concrete
f_y: yield stress of steel
A'_s and A_s: areas of compressive and tensile reinforcement, respectively
a: depth of rectangular stress block
b: width of cross-section
d' and d'': distances from extreme compression fiber to centroid of compression steel and to centroid of tension steel, respectively
f'_s: the compressive reinforcement stress under loads.

The ultimate shear capacity of a beam V_R is

$$V_R = V_C + V_S \tag{4.5}$$

where V_C and V_S are the strengths provided by concrete and shear reinforcement (vertical stirrups), respectively. V_C and V_S are expressed as

$$V_C = 2\sqrt{f_c'}bd \tag{4.6}$$

$$V_S = \frac{A_v f_y d}{s} \tag{4.7}$$

where d is the effective depth of a beam. s is the spacing between the shear reinforcement and A_v is the total cross-sectional area of shear reinforcement within spacing s.

The ultimate flexural and shear capacities for columns are defined in a similar manner as those for beams except that the column capacities are affected by the presence and the magnitude of axial force. For column, the moment that causes compression on the left-hand face of the column is defined as positive and vice-versa. In reality, the magnitude of axial force on a column are resulted from a combination of gravity load and earthquakes. In other words, the axial force will fluctuate around that caused by gravity load. In this study, the column capacity is determined by assuming that the axial force on a column is due to gravity load to simplify the analysis. This assumption is valid, in particular, for low-rise structures.

4.3 Ultimate Story Shear Capacity

The flexural and shear strengths of beams and columns are utilized in the limit analysis procedure suggested by Aoyama [10] to determine the collapse mechanism of the frame structure and the corresponding story shear capacities. A collapse mechanism is associated with the formation of plastic hinges at the ends of clear spans of beam and column members. The limit analysis procedure is outlined as follows:

(1) The positive and negative ultimate moments as well as the shear strengths at all possible hinge locations are first computed. For each member, the shear strength due to flexure V_{RF} is obtained by dividing the sum of the ultimate moments by the clear span. The shear strength due to shear V_{RS} is taken as the smaller of the two values computed at both hinges.

(2) For each member, comparison is made between V_{RF} and V_{RS}. In the case where V_{RS} is smaller, the flexural moments at both ends of the member are reduced proportionally so that the resulting V_{RF} value from the new moments is equal to V_{RS}. If V_{RF} is smaller than V_{RS}, then M_R's at both ends of the member remain unchanged. A moment distribution diagram can then be obtained for the entire frame structure.

(3) The joint moment capacities at the intersections of beam and column centerlines are obtained by linearly extrapolating from the moments at the ends of the clear span. At each joint, the sum of beam moments and the sum of column moments are compared to determine the actual location of the plastic hinges. If the sum of the beam moments is smaller, then, the plastic hinges are formed at the ends of beams and half of this sum is substituted for the upper and lower column moments. On the other hand, if the sum of the beam moments is larger, then, the plastic hinges are formed at the ends of column and half of the sum of the column moments is substituted for the left and right beam moments.

(4) The shear capacity of each column is determined by dividing the summation of end moments by the column length. The story shear capacity is obtained by summing the shear capacities of all the columns at each story level [11]. This is a good approximation if the capacities and geometries for columns in a given floor level do not differ significantly from one to another. However, if the differences are significant, it is necessary to consider compatibility of deformations at failure to determine the story shear capacity. It is noted that the story shear capacity determined in this way represents the capacity resulting from either shear or flexural failure mechanism.

(5) The ductility index F for each story is determined once the failure mode of that story is known. The ultimate story shear capacity obtained for each floor level is multiplied by the corresponding story ductility index to determine the equivalent linear story shear capacity.

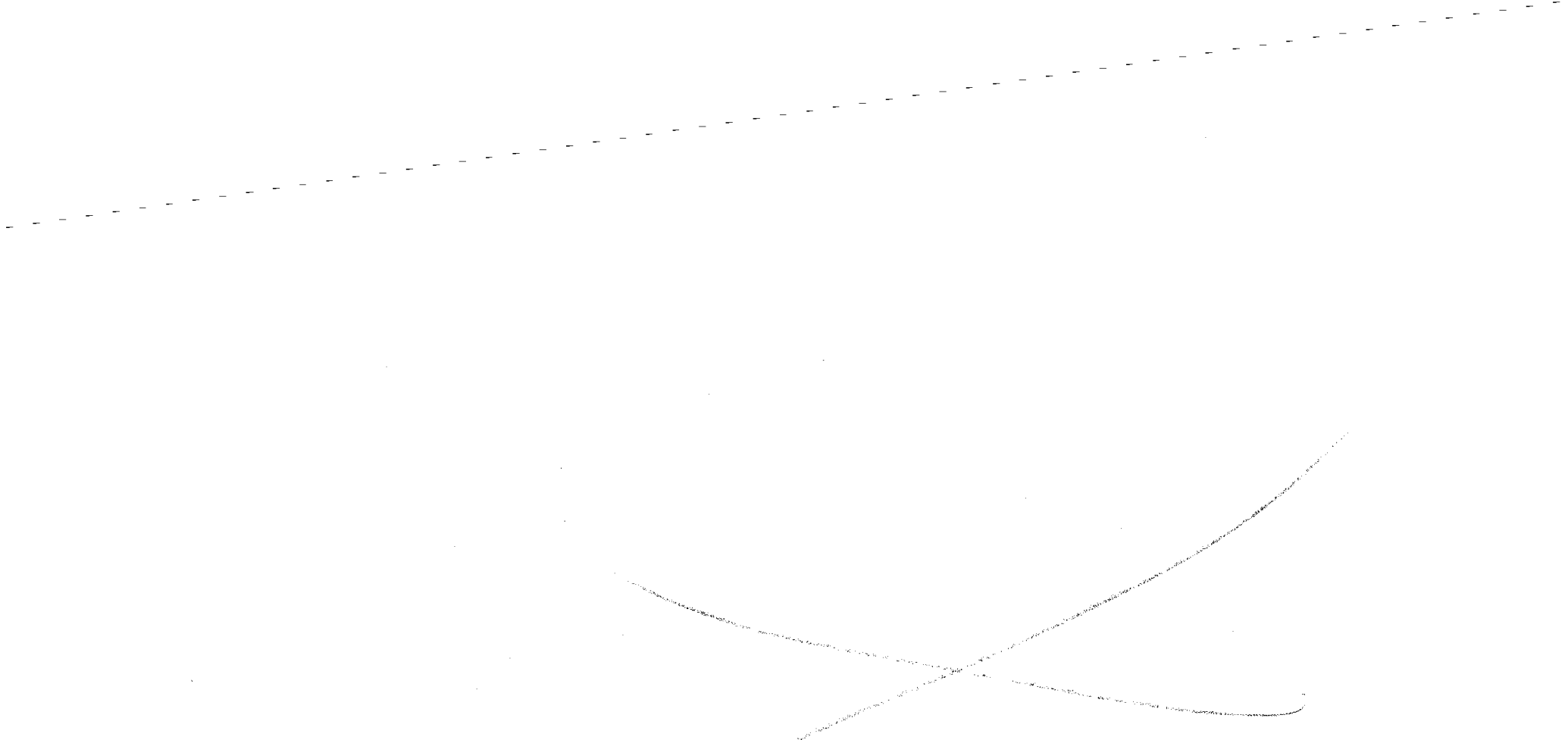

SECTION 5

RELIABILITY ANALYSIS

The aim of the reliability analysis is to evaluate the limit state probabilities for each story and for the entire frame structure given the occurrence of an earthquake. The limit state probability is the probability that the structural response due to an earthquake $Q(t)$ exceeds the capacity Q_ℓ. If the structural response Q stays within the bound represented by $+Q_\ell$ and $-Q_\ell$ as shown in Fig. 5-1, then the structure is considered safe. After a certain time T_f, there exists a probability that $Q(t)$ may outcross $+Q_\ell$ or $-Q_\ell$. This random time to failure T_f known as the first crossing time is directly related to the probability of failure P_f. It is assumed that the out-crossings of the capacity threshold occur so rarely that the out-crossings can be considered as statistically independent events, and the instant of crossing constitutes a Poisson process. For a Poisson process, the probability of no crossing in the duration of an earthquake μ_{dE} is related to the expected rate of crossing v_b as follows [12, 13]

$$P(T_f \geq \mu_{dE}) = exp(-v_b \mu_{dE}) \tag{5.1}$$

Thus, the limit state probability P_f, i.e., the probability of at least one crossing is

$$P_f = 1 - exp(-v_b \mu_{dE}) \tag{5.2}$$

For a stationary Gaussian process with mean zero, v_b in the case of double crossing can be found through the crossing analysis as [12, 13]

$$v_b = \frac{1}{\pi} \frac{\sigma_{\dot{Q}}}{\sigma_Q} exp\left(\frac{-Q_\ell^2}{2{\sigma_Q}^2}\right) \tag{5.3}$$

For the evaluation of the limit state probability of the i^{th} story, i.e. the i^{th} story limit state probability, $P_{f,i}$, the structural response is represented by the story shear force due to an earthquake $Q_i(t)$ and the structural capacity is represented by the equivalent linear story shear $Q_{\ell i}$. From Eqs. 5.2 and 5.3, the limit state probability of the i^{th} story can be expressed as

$$P_{f,i} = 1 - exp\left[-\frac{1}{\pi} \frac{\sigma_{\dot{Q}i}}{\sigma_{Qi}} \mu_{dE} exp\left(\frac{-{Q_{\ell i}}^2}{2{\sigma_{Qi}}^2}\right)\right] \tag{5.4}$$

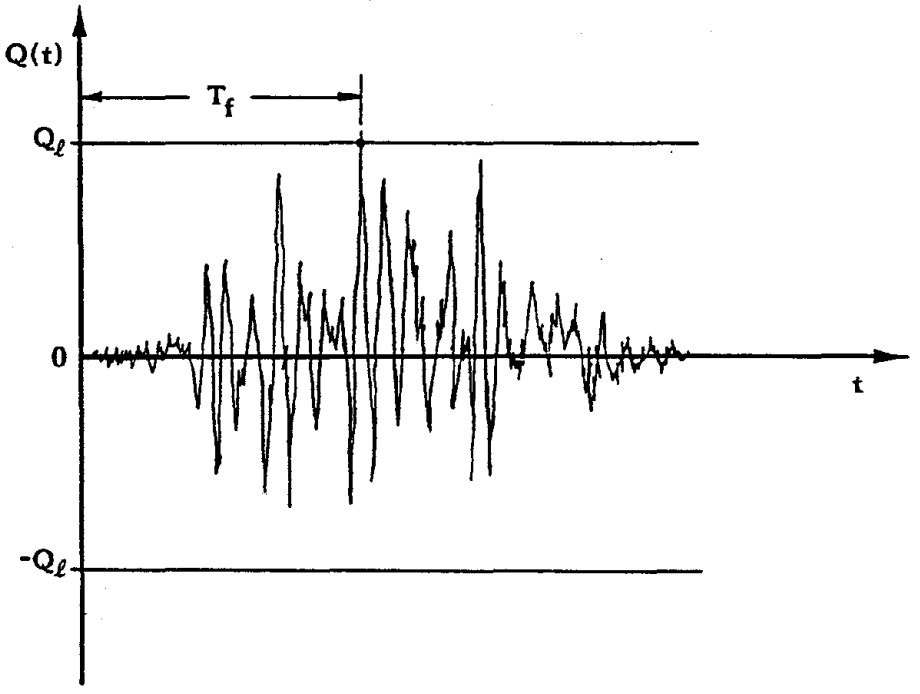

Fig. 5-1 Random Time of Crossing

The standard deviations, σ_{Q_i} and $\sigma_{\dot{Q}_i}$ in Eq. 5.4 are obtained from the diagonal terms of their respective covariance matrices in Eqs. 3.15 and 3.16. Furthermore, the limit state probability of the entire frame structure PF is represented by the largest story limit state probability.

$$PF = max P_{f,i} \tag{5.5}$$

For different peak ground acceleration (PGA) levels, the limit state probabilities of the frame structure can be computed using Eq. 5.5. Then, the fragility curve (PF vs. PGA) can be generated for the frame structure.

SECTION 6

FOUR-STORY TEST STRUCTURE

The fragility analysis methodology developed in this study is first applied to a four-story test structure [14]. The four-story test structure is one of the two identical structures constructed in 1965-1966 at the Nevada Test Site. The design seismic loads was estimated based on seismic requirements of the 1961 Uniform Building Code (UBC) with seismic zone 3. The test structure was designed according to the 1963 ACI building code. A series of non-destructive and destructive dynamic vibration tests were carried out to investigate the dynamic behavior of this test structure. Several reports and technical papers were published on these test studies [14, 15]. Fig. 6-1 shows the plan and elevation of the test structure. The frame along the longitudinal direction is considered in this study. Fig. 6-2 shows an idealization of this frame. The cross-sectional data for each member of the test structure are tabulated in Table 6-I.

For dynamic analysis, the lumped mass at each story level is computed as shown in Table 6-II. The natural frequencies and modal participation factors determined from TABS77 are tabulated in Table 6-III, while the mode shapes are listed in Table 6-IV. In this study quasi-linear response analysis instead of nonlinear analysis is performed; thus a damping ratio equal to 7 percent of critical is used as recommended for a reinforced concrete structure under strong ground acceleration [16].

The earthquake ground acceleration is represented by a stationary Gaussian process with mean zero and a Kanai-Tajimi power spectrum as described in Section 3. The soil condition on which the test structure was constructed is assumed to be stiff soil, thus, the values of ω_g and ζ_g in Eq. 3.9 are taken to be 5π rad/sec and 0.6 respectively [7]. The Kanai-Tajimi power spectrum using these values is shown in Fig. 6-3. The mean duration of the strong earthquake acceleration is assumed to be 10 seconds.

During an earthquake event the frame structure will vibrate to the left and right in the longitudinal direction due to the reversal of earthquake ground acceleration. Thus, the capacity of the frame structure should be evaluated for both directions. However, the test structure considered herein is symmetric. In this case, the structure needs to be evaluated only in one direction, e.g. towards the right.

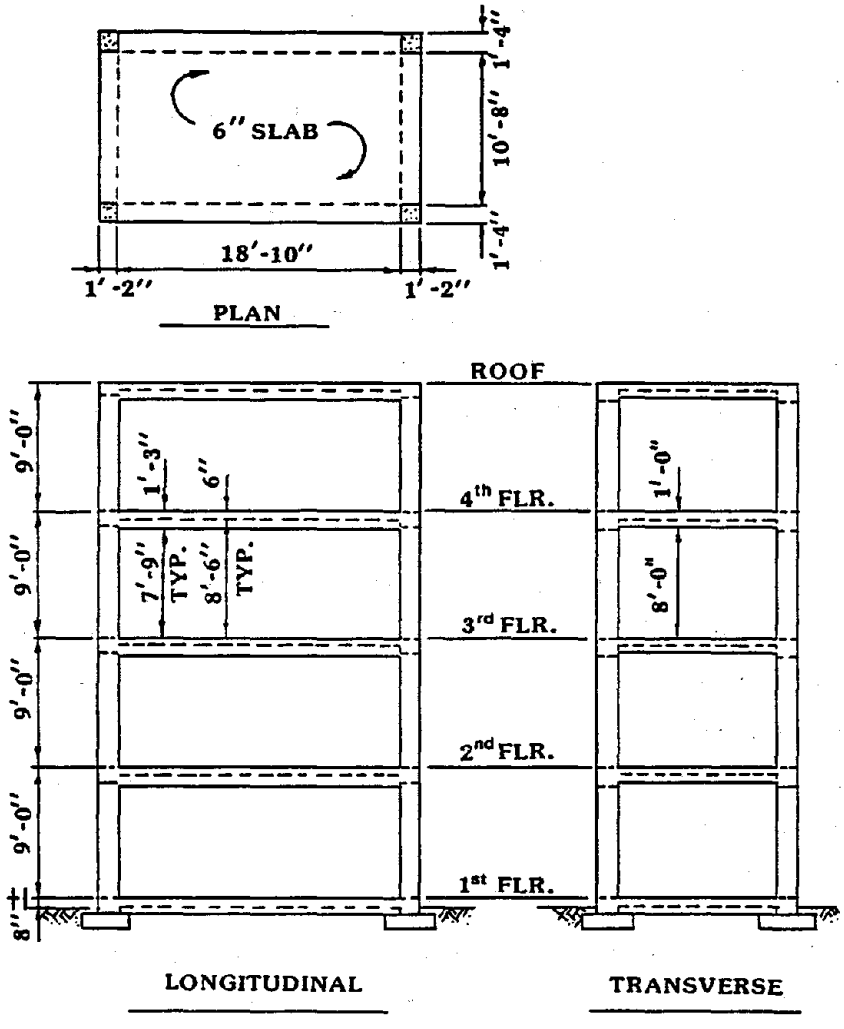

Fig. 6-1 Four-Story Test Structure

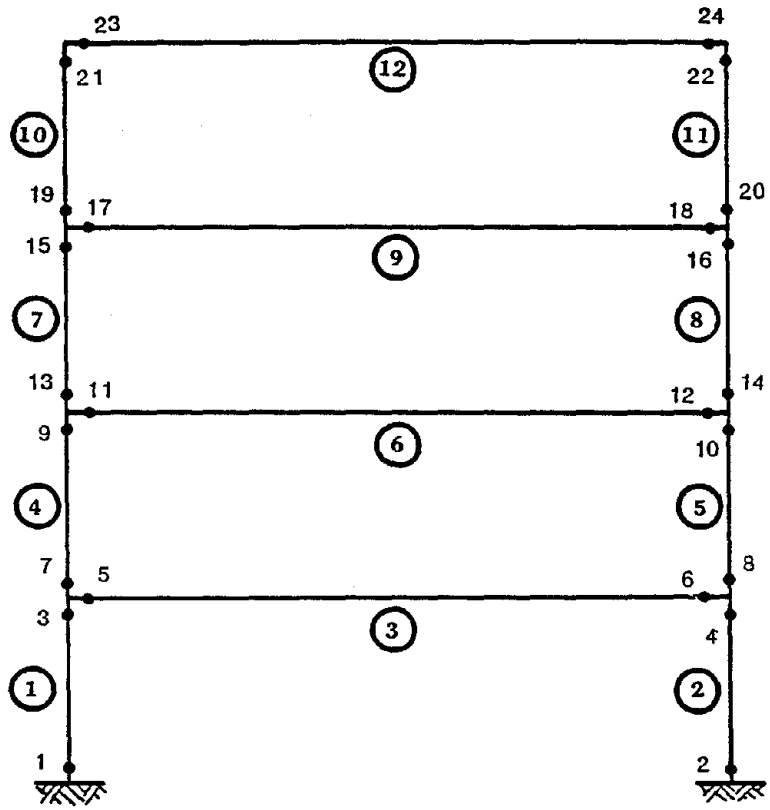

Fig. 6-2 Possible Plastic Hinges (Test Structure)

Table 6-I Member Cross Sectional Data (Test Structure)

Member	h	b	A'_s	A_s	d'	d''	A_v
1	14.0	16.0	3.00	3.00	2.94	2.94	0.22
2	14.0	16.0	3.00	3.00	2.94	2.94	0.22
3	15.0	16.0	3.00	2.37	2.94	2.88	0.22
4	14.0	16.0	3.00	3.00	2.94	2.94	0.22
5	14.0	16.0	3.00	3.00	2.94	2.94	0.22
6	15.0	16.0	2.79	2.37	2.92	2.88	0.22
7	14.0	16.0	3.00	3.00	2.94	2.94	0.22
8	14.0	16.0	3.00	3.00	2.94	2.94	0.22
9	15.0	16.0	2.37	1.80	2.88	2.81	0.22
10	14.0	16.0	3.00	3.00	2.94	2.94	0.22
11	14.0	16.0	3.00	3.00	2.94	2.94	0.22
12	15.0	16.0	2.00	1.80	2.94	2.81	0.22

Unit: inch

Table 6-II Story Mass (Test Structure)

Node No.	m_i(kips–sec^2/in)
1	0.047
2	0.047
3	0.047
4	0.042

Table 6-III Natural Frequencies and Modal Participation Factor (Test Structure)

Mode No.	Natural Frequencies (rad/sec)	Modal Participation Factors
1	14.71	0.389
2	48.33	-0.145
3	90.82	0.091
4	132.58	-0.051

Table 6-IV Mode Shapes (Test Structure)

	Mode No.			
Node No.	1	2	3	4
1	0.72	-2.12	3.09	-2.59
2	1.83	-3.02	-0.01	2.97
3	2.76	-0.53	-2.89	-2.25
4	3.31	2.88	1.94	0.89

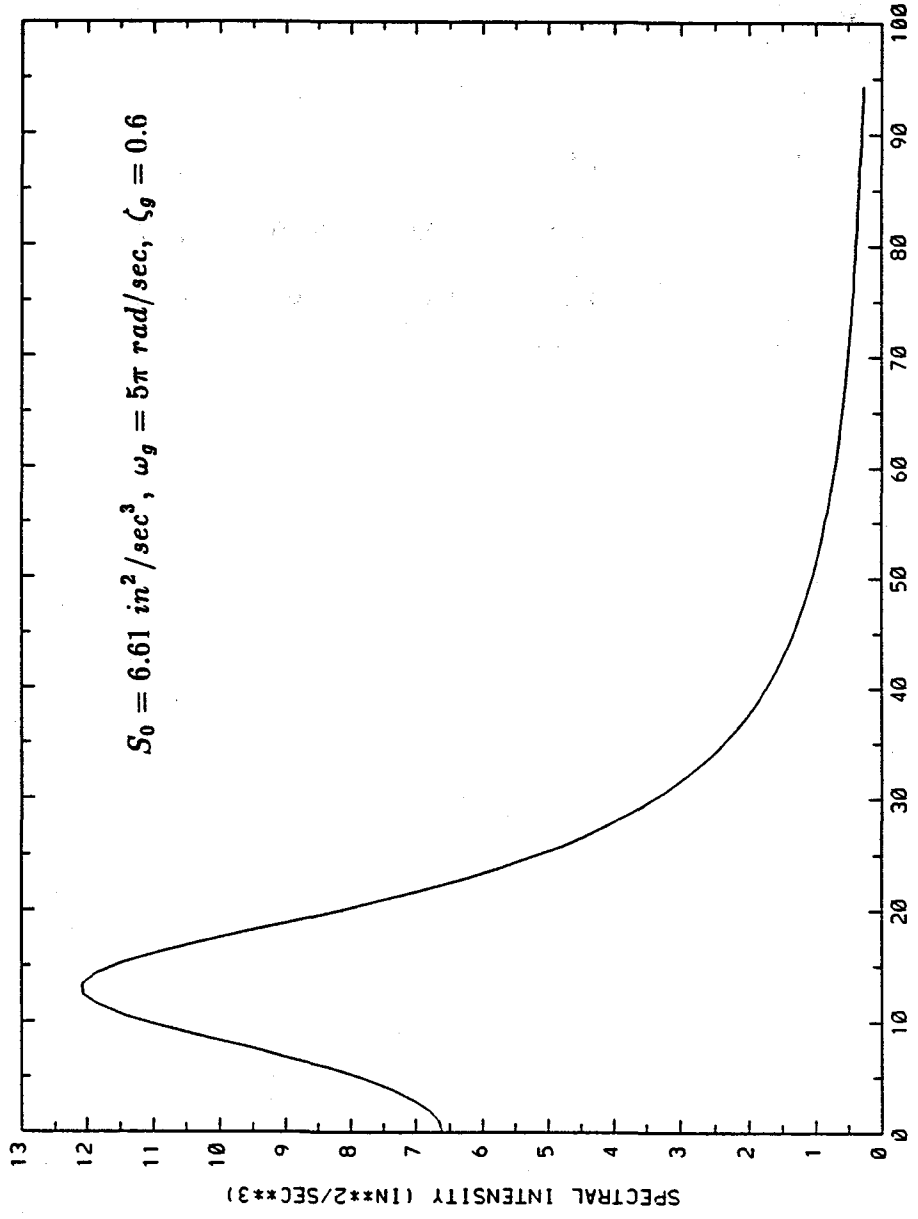

Fig. 6-3 Kanai-Tajimi Power Spectrum

For the strength computation, the geometry of the test structure is assumed to be deterministic and the design values are used. On the other hand, the mean values of the material strengths are utilized to account for the increase of actual strength. For concrete with f'_c of 4500 psi, the mean value is 5809 psi [17]. The unit weight of reinforced concrete is taken as 150 pcf; Young's modulus is computed according to ACI Code. For reinforcing steel with f_y of 50,000 psi, the mean value is 67,100 psi [18], and Young's modulus is 29.0×10^6 psi.

The flexural and shear strengths for all the members at the possible plastic hinge locations as shown in Fig. 6-2 are computed using the strength formulas in ACI Code 318-83. The strength values at these locations are summarized in Table 6-V. The comparison of the V_{RS} values computed from the shear formulas with the V_{RF} values derived from the end moments is shown in Table 6-VI for all the members. From this table, it can be seen that all the members have shear strengths V_{RS} larger than V_{RF}. This indicates that the frame will first undergo flexural yielding. A moment distribution for the frame structure due to flexure is shown in Fig. 6-4. The moments at the ends of clear spans are extrapolated to joints. At each joint, the sum of beam moments and the sum of column moments are compared. In this case, the sum of beam moments are smaller at all the joints. This indicates that the plastic hinges will form at the ends of all beams instead of at the ends of columns. The plastic hinges of all beams together with the formation of hinges at the lower ends of first story columns constitute a failure mechanism. The sum of beam moment at each joint is then distributed equally to the columns framing into that joint. A new moment distribution associated with this failure mechanism is obtained as shown in Fig. 6-5. Also shown in Fig. 6-5 is the shear capacity of each column obtained by summing the end moments and then dividing by the length of the column. The shear capacity Q_{ni} at each story is obtained by summing the shear capacities of all the columns of that story and is shown in Table 6-VII. Since the flexural capacities of all the columns are less than the shear capacities with shear reinforcements satisfying the code requirements, the ductility indices F_i for all the stories are 2.5 as indicated in Table 4-I. Table 6-VII also shows the equivalent linear story shear capacities $Q_{\ell i}$ which are determined by multiplying the ultimate story shear capacity Q_{ni} with the corresponding F_i value.

The story limit state probabilities for the frame structure can be evaluated once the equivalent linear story shear capacities are established. For a specified PGA value (PGA ranging from 0.2 g to 1.4 g), the covariance matrices in Eqs. 3.15 and 3.16 are first evaluated

Table 6-V Flexural and Shear Strengths (Test Structure)

Story	Plastic Hinge Location	M_R^+(ft–kips)	M_R^-(ft–kips)	V_{RS}(kips)
1	1,2	175.85	175.85	83.42
	3,4	175.17	175.17	83.31
	5,6	148.58	180.72	88.76
2	7,8	172.92	172.92	82.91
	9,10	172.27	172.27	82.80
	11,12	148.47	169.98	88.90
3	13,14	169.96	169.96	82.41
	15,16	169.30	169.30	82.30
	17,18	118.50	147.98	89.20
4	19,20	166.98	166.98	81.90
	21,22	166.36	166.36	81.79
	23,24	118.64	127.31	88.76

Table 6-VI Comparison of Shear Strengths Due to Flexure and Shear (Test Structure)

Story	Member	M_R^+(ft–kips)	M_R^-(ft–kips)	V_{RF}(kips)	V_{RS}(kips)
1	1,2	175.17	175.85	41.91	83.31
	3	148.58	180.72	17.49	88.76
2	4,5	172.27	172.92	44.54	82.80
	6	148.47	169.98	16.91	88.90
3	7,8	169.30	169.96	43.78	82.30
	9	118.50	147.98	14.15	89.20
4	10,11	166.36	166.98	43.01	81.79
	12	118.64	127.31	13.06	88.76

Note: $V_{RF} = (M_R^+ + M_R^-)$/clear span

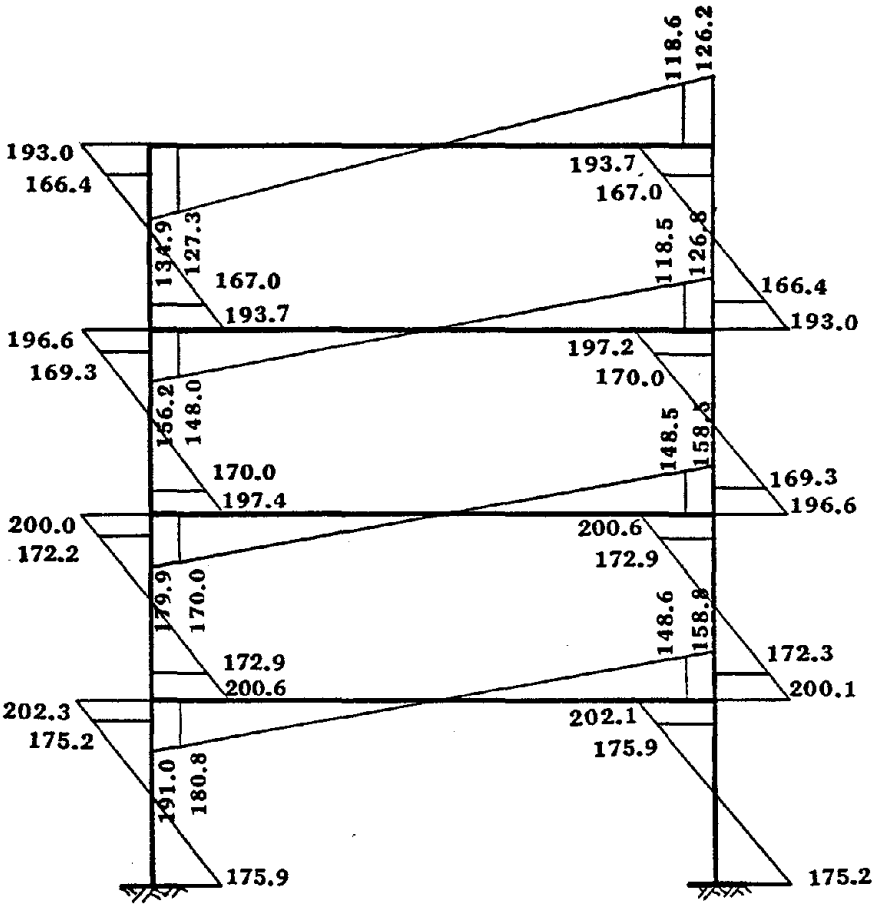

Fig. 6-4 Ultimate Moments at Plastic Hinges and Joints (Test Structure)

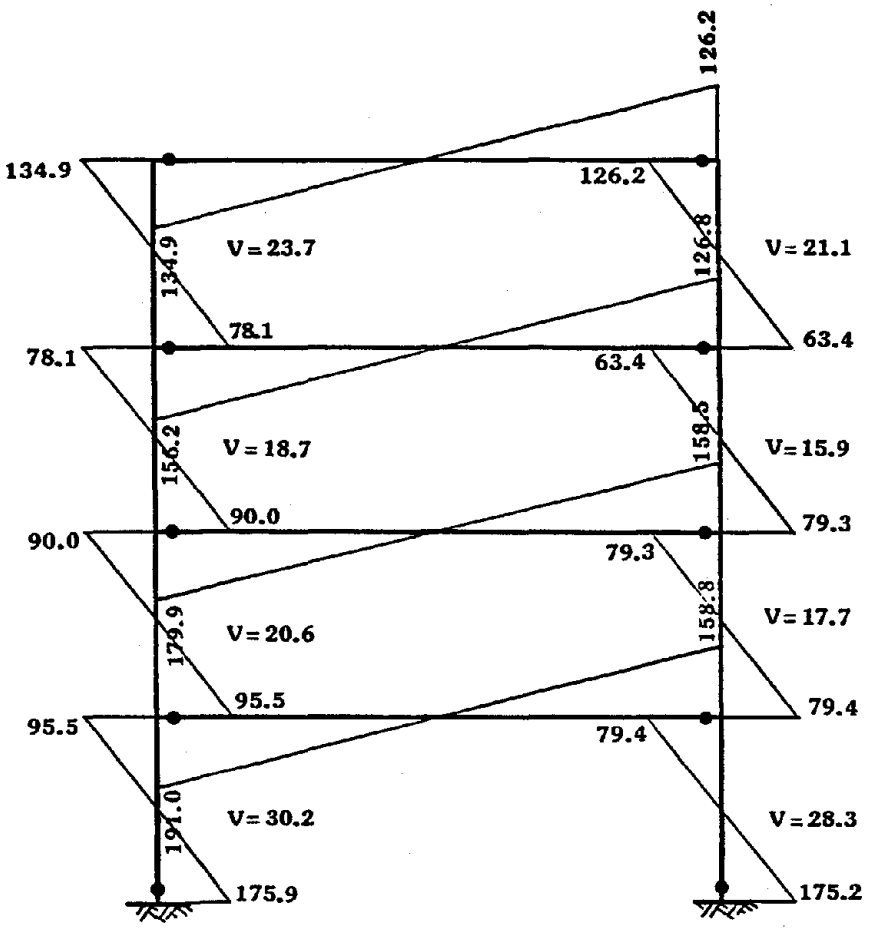

Fig. 6-5 Failure Mechanism and Moment Distribution (Test Structure)

Table 6-VII Ultimate and Equivalent Linear Shear Capacities (Test Structure)

Story	F_i	Q_{ni}(kips)	$Q_{\ell i}$(kips)
4	2.5	44.8	112.0
3	2.5	34.6	86.5
2	2.5	38.3	95.8
1	2.5	58.5	146.3

to obtain the standard deviations σ_{Qi} and $\sigma_{\dot{Q}i}$ for each story. Then the story limit state probabilities for each story can be computed using Eq. 5.4 as summarized in Table 6-VIII. The limit state probability for the entire frame structure PF is taken as the maximum story limit state probability and tabulated in Table 6-IX. Using the data from Table 6-IX, the fragility curve for the frame structure is constructed as shown in Fig. 6-6. From the fragility curve in Fig. 6-6, it can be seen that the limit state probability increases as the PGA level becomes larger. This trend is expected as the earthquake gets more severe the chance of building collapse increases.

The story limit state probability is the highest in the second story followed by the third story (see Table 6-VIII). This indicates that the second story is the most likely to fail leading to the collapse of the entire frame. This is consistent with the observed damage pattern during the destructive vibration tests on this structure [14]. Extensive damage was observed on the second and third floors during the high-amplitude motion, when a maximum roof acceleration of about 0.75 g was reached. The damage was found to be in the form of x-cracking at the beam-column joints. If the destructive test were to be conducted to the point of collapse of the structure, the second and third stories would be more likely to fail as damages have already occurred in those stories.

Table 6-VIII Story Limit State Probability (Test Structure)

	$P_{f,i}$			
PGA (G)	1st. Story	2nd. Story	3rd. Story	4th Story
0.20	0.0	0.0	0.0	0.0
0.30	0.0	0.0	9.01×10^{-12}	0.0
0.40	1.92×10^{-12}	3.28×10^{-6}	2.98×10^{-9}	0.0
0.50	1.26×10^{-7}	1.23×10^{-3}	1.41×10^{-5}	0.0
0.60	5.20×10^{-5}	0.03	1.40×10^{-3}	0.0
0.70	1.97×10^{-3}	0.19	0.02	0.0
0.80	0.02	0.53	0.13	1.73×10^{-14}
0.90	0.10	0.83	0.37	3.11×10^{-11}
1.00	0.28	0.96	0.68	6.64×10^{-9}
1.10	0.54	0.99	0.88	3.51×10^{-7}
1.20	0.78	1.00	0.97	7.17×10^{-6}
1.30	0.92	1.00	0.99	7.50×10^{-5}
1.40	0.98	1.00	1.00	4.83×10^{-4}

Table 6-IX Fragility Data (Test Structure)

PGA (G)	PF
0.20	0.0
0.30	0.0
0.40	3.28×10^{-6}
0.50	1.23×10^{-3}
0.60	0.03
0.70	0.19
0.80	0.53
0.90	0.83
1.00	0.96
1.10	0.99
1.20	1.00
1.30	1.00
1.40	1.00

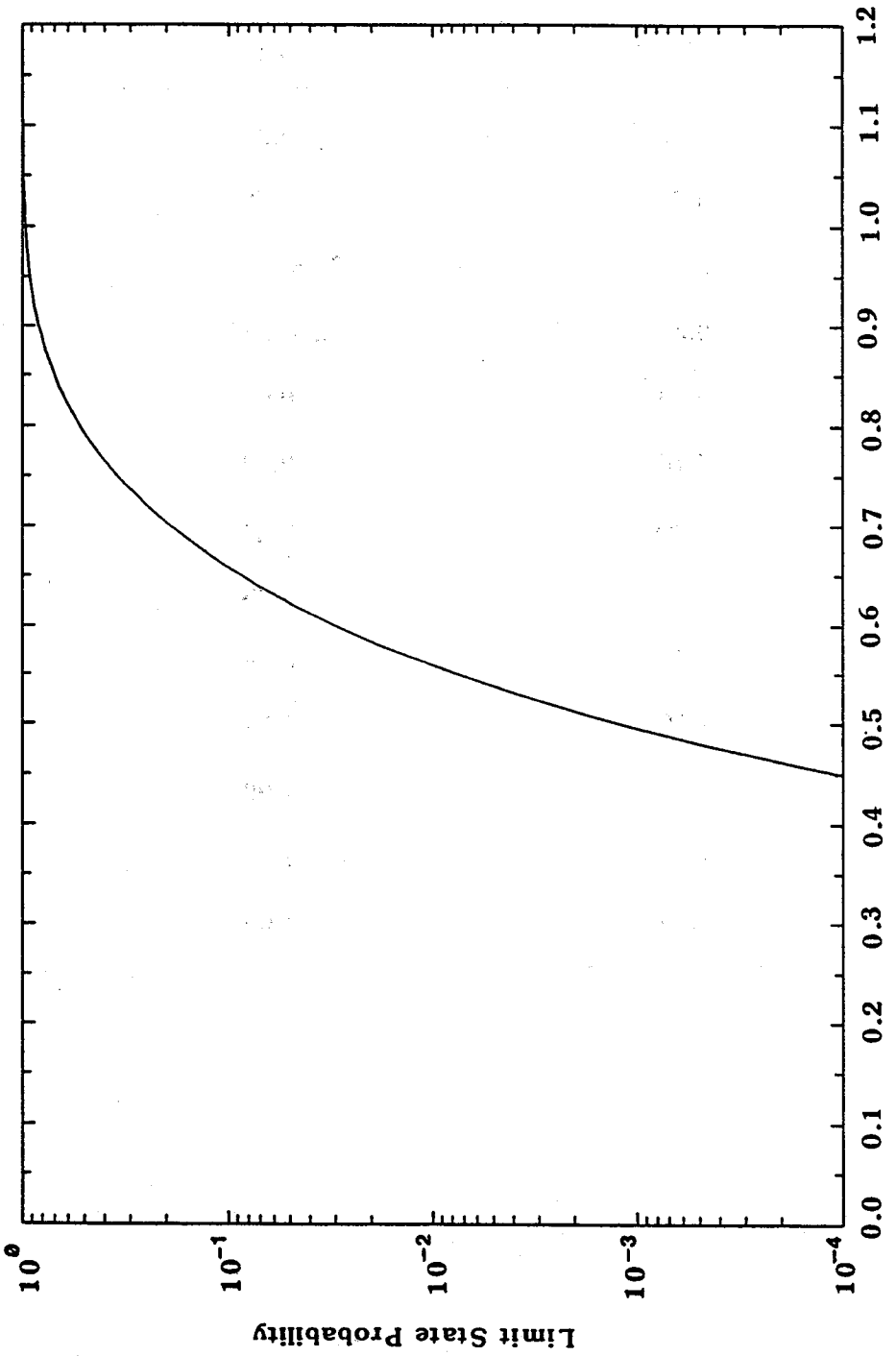

Fig. 6-6 Fragility Curve (Test Structure)

SECTION 7

FIVE-STORY FRAME BUILDING

A five-story reinforced concrete frame building assumed to be located in New York City is also used to demonstrate the fragility analysis methodology. Fig. 7-1 shows a typical floor plan and section of the building. In this study, seismic fragility analysis is performed for an interior frame in the north-south direction. The detail of the design is shown in Appendix B and a brief summary of the design is outlined below.

The frame building is designed according to the provisions of ANSI A58.1-1982 standard [19] and ACI 318-83 code [9]. Three types of loads, i.e., dead, live, and earthquake loads are considered to act on the building. The design seismic base shear is determined by the formula specified in ANSI-A58.1 with seismic zone 2 and soil type S_2. This design base shear is distributed over the height of the building, and then the equivalent static seismic load at each floor level is determined accordingly. The frame structure is designed to provide sufficient resisting capacity against the load effects (axial force, shear force, moment, etc.) due to the combinations of various loads. The beams and columns each have constant cross sections for the entire building. The cross section of beams is 16 in. $\times$ 18 in., while 16 in. $\times$ 16 in. is used for columns. The reinforcement details of beams and columns are shown in Fig. 7-2.

This five-story building designed according to the building code results in a weak beam and strong column system. It is of interest, for purpose of comparison, to investigate the case of strong beam and weak column. For convenience, all the beams of the five-story building are artificially increased to 16 in. $\times$ 24 in.; while the main reinforcement is increased to 3-No. 9 at the top and bottom of the beam. The first five-story building is denoted as Case I, whereas the modified building is termed as Case II for identification purposes. Case I and II are subject to the same earthquake excitations.

For dynamic analysis, the lumped mass at each story level is computed. Then the natural frequencies, mode shapes, and modal participation factors of the stick model are determined from TABS77. The results for both cases are shown in Appendix C. Like the four-story test structure, a critical damping of 7 percent is used. The site condition is assumed to be rock; thus, the values of ω_g and ζ_g in the Kanai-Tajimi power spectrum are

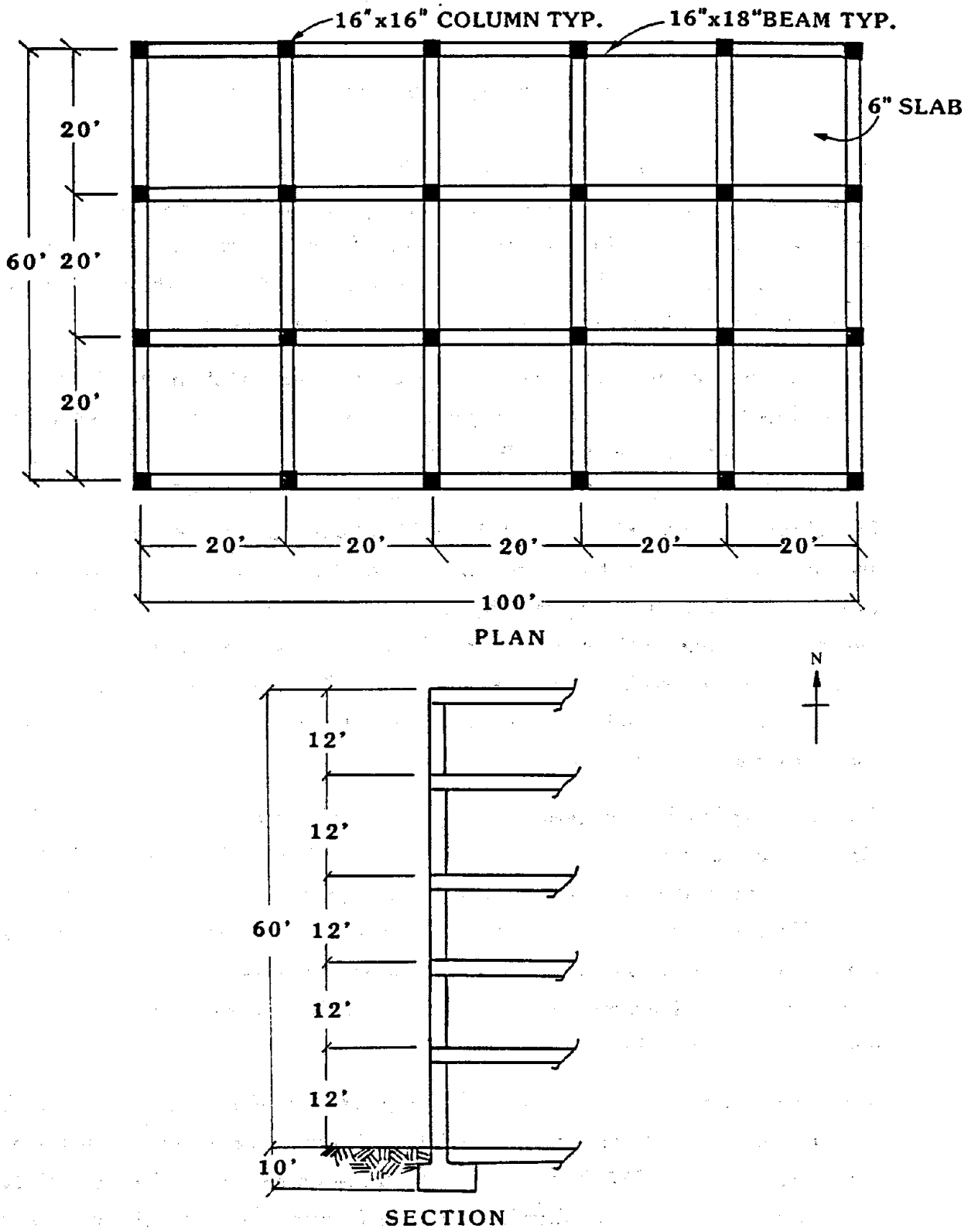

Fig. 7-1 Five-Story Frame Building

2-#7 (Roof Beam)

3-#7 (3rd -4th Floor Beam)

4-#7 (1st -2nd Floor Beam)

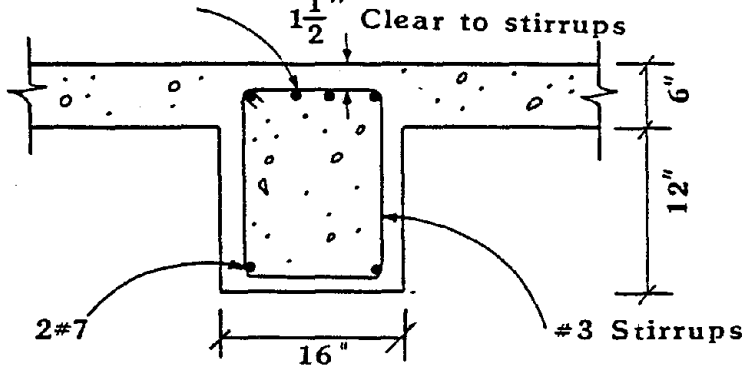

BEAM

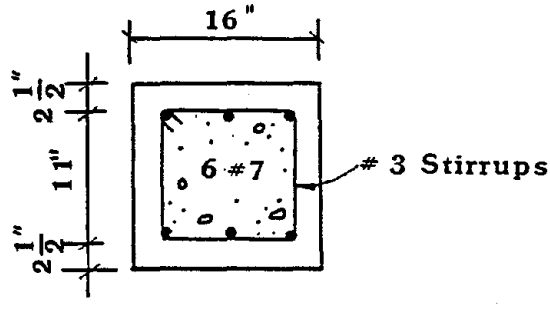

COLUMN

Fig. 7-2 Reinforcing Details of Beams and Columns (Five-Story Building)

taken to be 8π rad/sec and 0.6 respectively [7]. The mean duration of the strong motion is also assumed to be 10 seconds.

In the capacity evaluation of this frame structure, the following mean values of the material strengths are used. For concrete with f'_c of 4000 psi, the mean value is 5299 psi [17]; the unit weight of reinforced concrete is 155 pcf and Young's modulus is computed according to ACI Code. For steel with f_y of 60,000 psi, the mean value is 71,000 psi [17] and Young's modulus is 29.0 $\times 10^6$ psi.

7.1 Case I

The flexural and shear strengths for all the members at the possible plastic hinge locations as shown in Fig. 7-3 are computed and tabulated in Table 7-I. Comparison of V_{RS} with V_{RF} for all the members are shown in Table 7-II. As can be seen from Table 7-II, all the members have shear strengths V_{RS} larger than V_{RF}; thus, the frame will first undergo flexural yielding. Fig. 7-4 shows the moment distribution diagram due to flexure with the moments at the ends of clear spans and the extrapolated moments at the joints. For each joint, the sum of beam moments and sum of column moments are compared, the smaller of which dictates the formation of plastic hinge. By redistributing the moments at each joint, a new moment distribution with the associated failure mechanism is obtained as shown in Fig. 7-5. The ultimate story shear capacity Q_{ni} and equivalent linear shear capacity Q_{ti} for each story are shown in Table 7-III. The equivalent linear capacity is obtained from multiplying ultimate shear capacity by the ductility index. In this case, the ductility index is 2.5 for all the stories, since the flexural capacities of all the columns of the frame are less than the shear capacities with shear reinforcements satisfying the code requirements.

The story limit state probabilities for the frame structure are evaluated for PGA values ranging from 0.10 g to 1.0 g and tabulated in Table 7-IV. It can be seen from this Table that the second story has the largest limit state probability. The limit state probabilities for the entire frame structure, i.e. the fragility data, are tabulated in Table 7-V and plotted in Fig. 7-6. In this study, the fragility curve is plotted in semi-logarithmic scale to clearly display the tail of the fragility curve.

7.2 Case II

The member capacities at all the possible plastic hinges are computed and summarized in Table 7-VI. Comparison of shear strengths due to flexure and shear in Table 7-VII

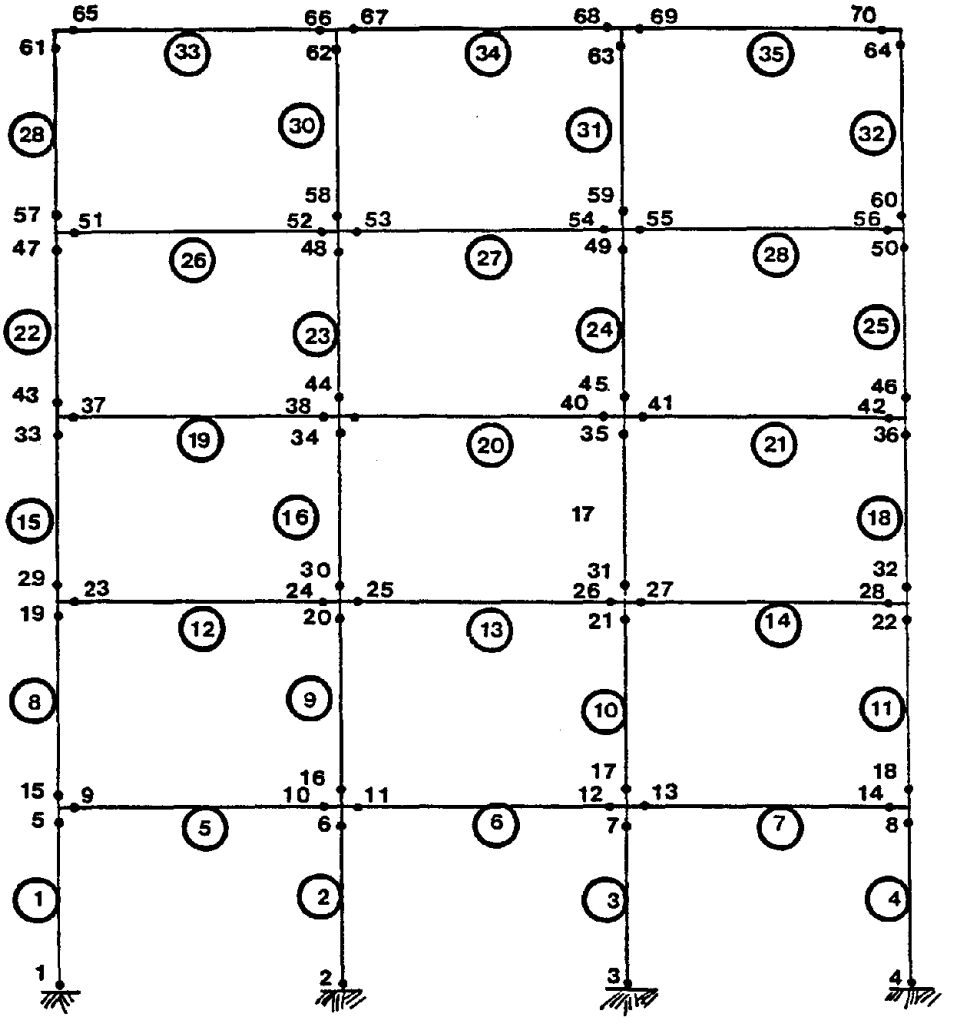

Fig. 7-3 Possible Plastic Hinges (Five-Story Building)

Table 7-I Flexural and Shear Strengths (Case I)

Story	Plastic Hinge Location	M_R^+(ft–kips)	M_R^-(ft–kips)	V_{RS}(kips)
1	1,4	193.32	193.32	69.33
	2,3	232.75	232.75	75.33
	5,8	192.05	192.05	69.13
	6,7	231.69	231.69	75.15
	9,10,11,12,13,14	109.46	203.21	68.39
2	15,18	182.25	182.25	67.79
	16,17	215.37	215.37	72.56
	19,22	180.95	180.95	67.61
	20,21	214.20	214.20	72.39
	23,24,25,26,27,28	109.46	203.21	68.39
3	29,32	170.77	170.77	66.23
	30,31	196.72	196.72	69.82
	33,36	169.45	169.45	66.06
	34,35	195.48	195.48	69.64
	37,38,39,40,41,42	109.19	156.22	68.39
4	43,46	159.03	159.03	64.67
	44,45	176.96	176.96	67.07
	47,50	157.64	157.64	64.50
	48,49	175.66	175.66	66.90
	51,52,53,54,55,56	109.19	156.22	68.39
5	57,60	146.99	146.99	63.11
	58,59	156.44	156.44	64.34
	61,64	145.63	145.63	62.93
	62,63	155.13	155.13	64.16
	65,66,67,68,69,70	108.78	108.78	68.39

Table 7-II Comparison of Shear Strengths Due to Flexure and Shear (Case I)

Story	Member	M_R^+(ft–kips)	M_R^-(ft–kips)	V_{RF}(kips)	V_{RS}(kips)
	1,4	192.05	193.32	36.70	69.13
1	2,3	231.69	232.75	44.23	75.15
	5,6,7	109.46	203.21	16.57	68.39
	8,11	180.95	182.25	34.59	67.61
2	9,10	214.20	215.37	40.91	72.39
	12,13,14	109.46	203.21	16.57	68.39
	15,18	169.45	170.77	32.40	66.06
3	16,17	195.48	196.72	37.35	69.82
	19,20,21	109.19	156.22	14.22	68.39
	22,25	157.64	159.03	30.16	64.50
4	23,24	175.64	176.96	33.58	66.90
	26,27,28	109.19	156.22	14.22	68.39
	29,32	145.63	146.99	27.87	62.93
5	30,31	155.13	156.44	29.67	64.16
	33,34,35	108.78	108.78	11.65	68.39

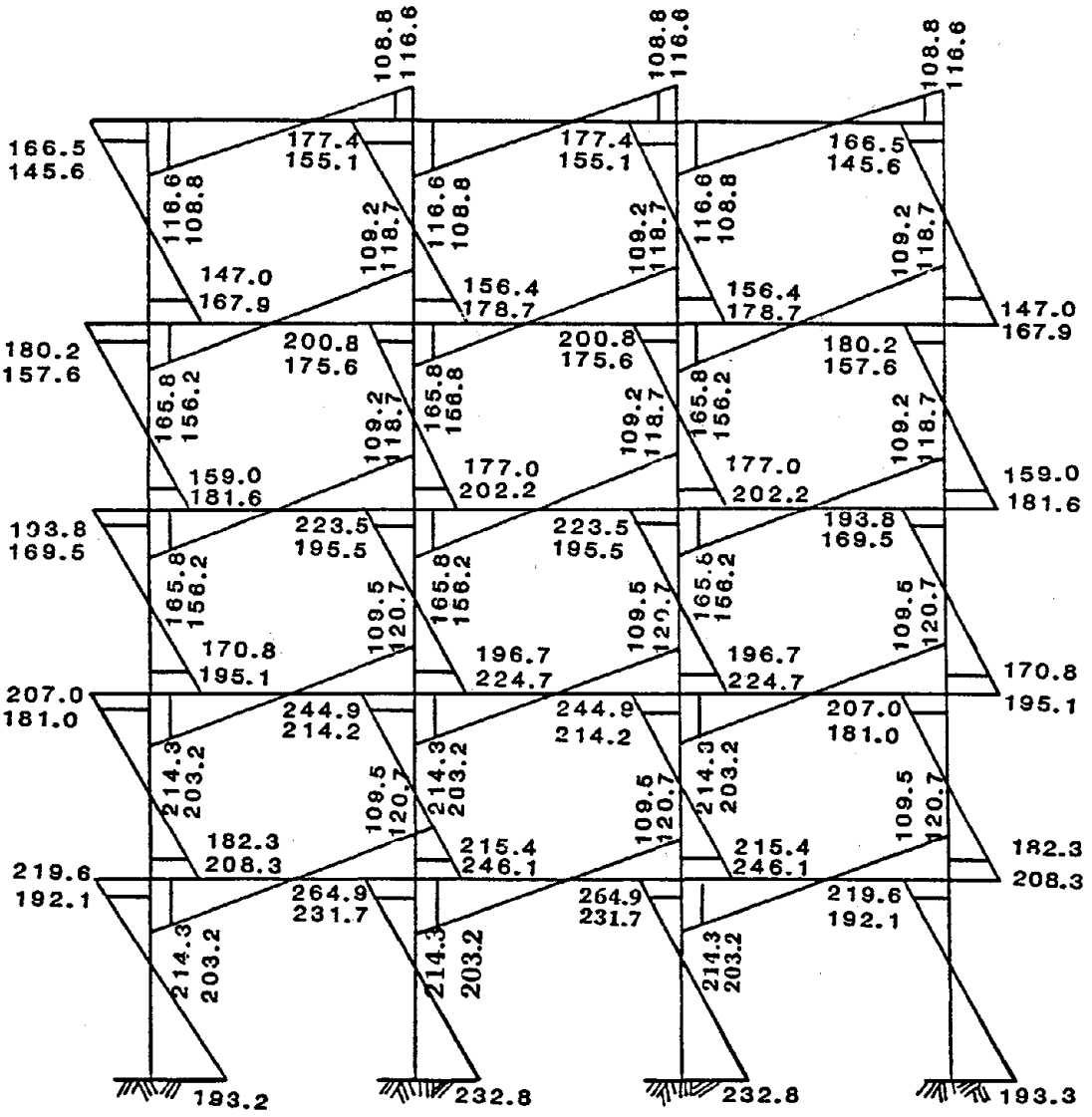

Fig. 7-4 Ultimate Moments at Plastic Hinges and Joints (Case I)

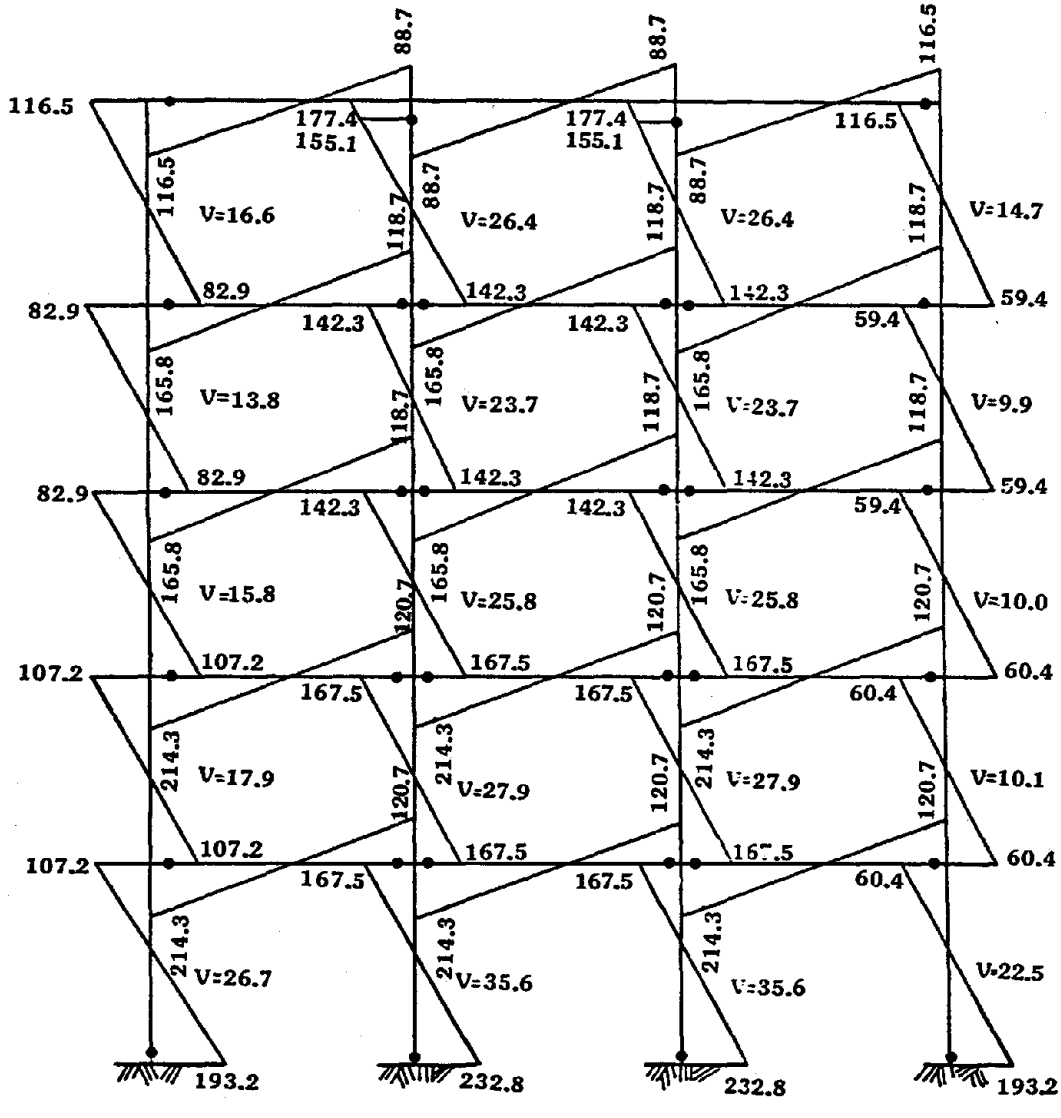

Fig. 7-5 Failure Mechanism and Moment Distribution (Case1)

Table 7-III Ultimate and Equivalent Linear Shear Capacities (Case I)

Story	F_i	Q_{ni}(kips)	$Q_{\ell i}$(kips)
5	2.5	84.1	210.3
4	2.5	71.1	177.8
3	2.5	77.4	193.5
2	2.5	83.8	209.5
1	2.5	120.4	301.0

Table 7-IV Story Limit State Probability (Case I)

	$P_{f,i}$				
PGA (G)	1st. Story	2nd. Story	3rd. Story	4th Story	5th Story
0.10	0.0	0.0	0.0	0.0	0.0
0.20	3.66×10^{-15}	1.43×10^{-8}	2.69×10^{-10}	6.33×10^{-15}	0.0
0.30	2.37×10^{-6}	1.91×10^{-3}	3.40×10^{-4}	3.38×10^{-6}	0.0
0.40	2.86×10^{-3}	0.11	0.05	3.83×10^{-3}	3.11×10^{-15}
0.50	0.07	0.55	0.36	0.09	2.14×10^{-9}
0.60	0.37	0.90	0.79	0.44	3.15×10^{-6}
0.70	0.74	0.99	0.96	0.82	2.56×10^{-4}
0.80	0.93	1.00	1.00	0.96	4.44×10^{-3}
0.90	0.99	1.00	1.00	1.00	0.03
1.00	1.00	1.00	1.00	1.00	0.12

Table 7-V Fragility Data (Case I)

PGA (G)	PF
0.10	0.0
0.20	1.43×10^{-8}
0.30	1.91×10^{-3}
0.40	0.11
0.50	0.55
0.60	0.90
0.70	0.99
0.80	1.00
0.90	1.00
1.00	1.00

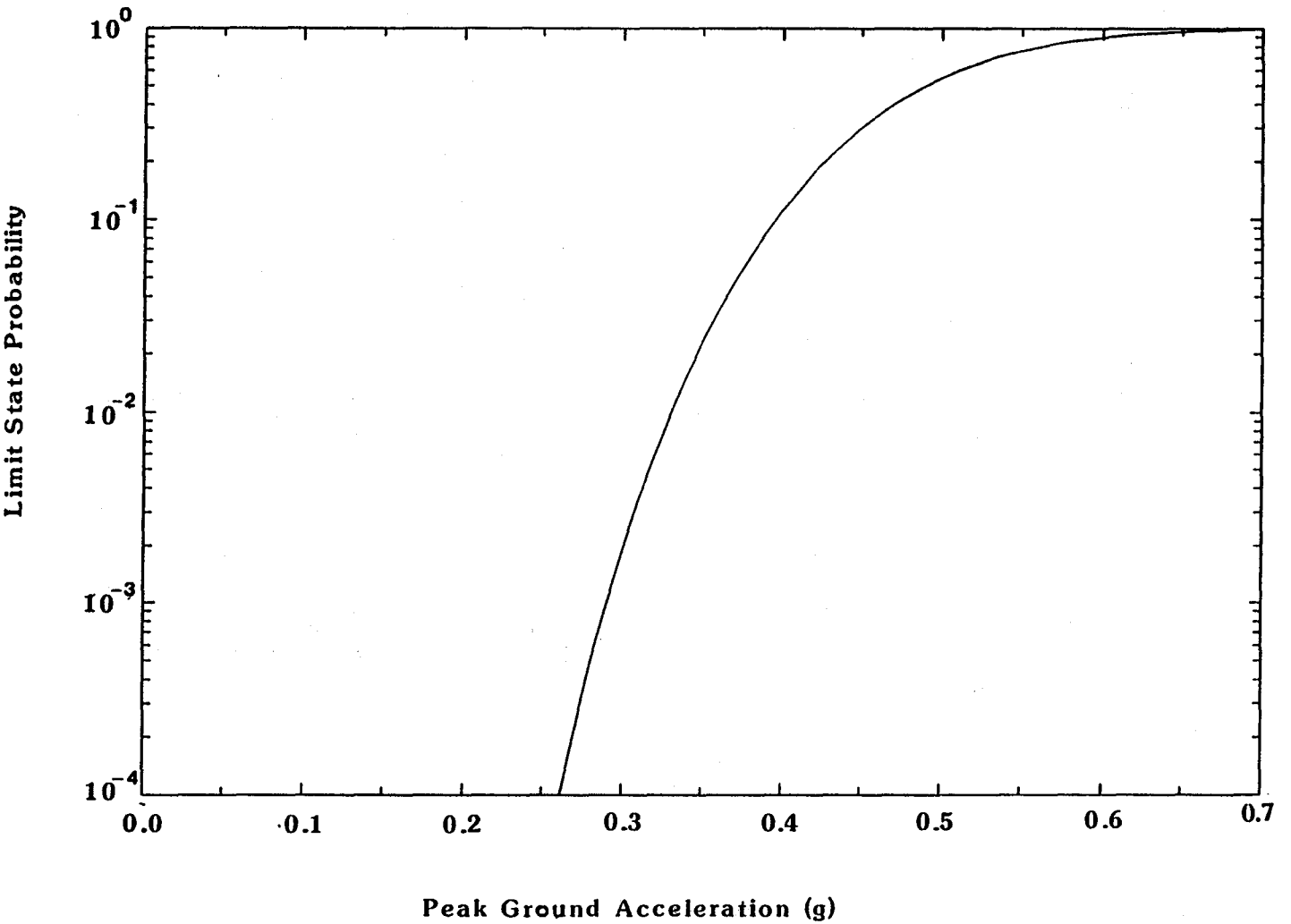

Fig. 7-6 Fragility Curve (Case I)

Table 7-VI Flexural and Shear Strengths (Case II)

Story	Plastic Hinge Location	M_R^+(ft–kips)	M_R^-(ft–kips)	V_{RS}(kips)
	1,4	195.84	195.84	69.69
	2,3	237.49	237.49	76.12
1	5,8	194.63	194.63	69.52
	6,7	236.49	236.49	75.95
	9,10,11,12,13,14	423.39	423.39	94.86
	15,18	184.37	184.37	68.08
	16,17	219.45	219.45	73.19
2	19,22	183.09	183.09	67.91
	20,21	218.39	218.39	73.02
	23,24,25,26,27,28	423.39	423.39	94.86
	29,32	172.42	172.42	66.46
	30,31	199.99	199.99	70.29
3	33,36	171.16	171.16	66.29
	34,35	198.82	198.82	70.12
	37,38,39,40,41,42	423.39	423.39	94.86
	43,46	160.15	160.15	64.82
	44,45	179.31	179.31	67.39
4	47,50	158.87	158.87	64.65
	48,49	178.03	178.03	67.22
	51,52,53,54,55,56	423.39	423.39	94.86
	57,60	147.52	147.52	63.17
	58,59	157.69	157.69	64.50
5	61,64	146.23	146.23	63.00
	62,63	156.44	156.44	64.33
	65,66,67,68,69,70	423.39	423.39	94.86

Table 7-VII Comparison of Shear Strengths Due to Flexure and Shear (Case II)

Story	Member	M_R^+(ft-kips)	M_R^-(ft-kips)	V_{RF}(kips)	V_{RS}(kips)
	1,4	194.63	195.84	37.19	69.52
1	2,3	236.49	237.49	45.14	75.95
	5,6,7	423.39	423.39	45.36	94.86
	8,11	183.09	184.37	35.00	67.91
2	9,10	218.39	219.45	41.70	73.02
	12,13,14	423.39	423.39	45.36	94.86
	15,18	171.16	172.42	32.72	66.29
3	16,17	198.82	199.99	37.98	70.12
	19,20,21	423.39	423.39	45.36	94.86
	22,25	158.87	160.15	30.38	64.65
4	23,24	178.03	179.31	34.03	67.22
	26,27,28	423.39	423.39	45.36	94.86
	29,32	146.23	147.52	27.98	63.00
5	30,31	156.44	157.69	29.92	64.33
	33,34,35	423.39	423.39	45.36	94.86

shows that all the members are governed by flexural strength. The same procedure is used to determine the failure mechanism. Fig. 7-7 shows the ultimate moments at plastic hinges and joints; while Fig. 7-8 shows the moment distribution associated with the failure mechanism, as well as the individual column capacity.

As can be seen from Fig. 7-8, the plastic hinges are formed at the ends of all the columns as a result of the stronger beams. The ultimate story shear capacities Q_{ni} obtained from this failure mechanism are tabulated in Table 7-VIII. The F factor is determined to be 2.5 for all stories as the failure of the frame is controlled by flexure. The equivalent story shear capacities $Q_{\ell i}$ are also shown in Table 7-VIII. The limit state probability of this frame is evaluated and shown in Table 7-IX for PGA levels ranging from 0.10g to 1.20 g. From Table 7-IX, it is apparent that the first story has the largest limit state probability, indicating that the first story is a weak story. This is expected because the beams are stronger than the columns, and the earthquake produces the largest demand on the first story columns, while all the columns have the same dimensions and reinforcement details. Thus, the first story columns are the weakest elements in the entire frame. The fragility data, taken as the largest story limit state probability, is shown in Table 7-X. From this data, the fragility curve is constructed as shown in Fig. 7-9.

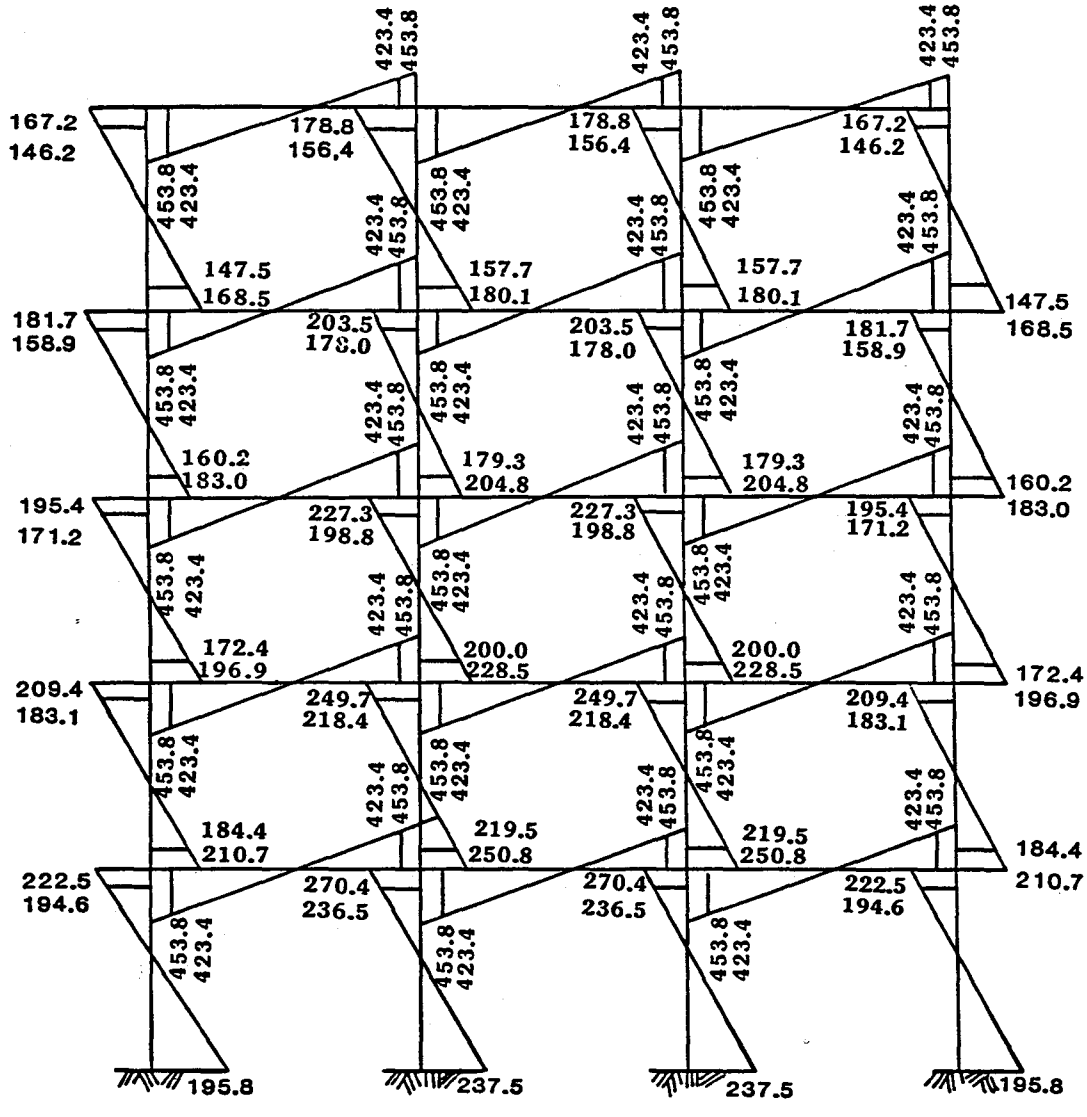

Fig. 7-7 Ultimate Moments at Plastic Hinges and Joints (Case II)

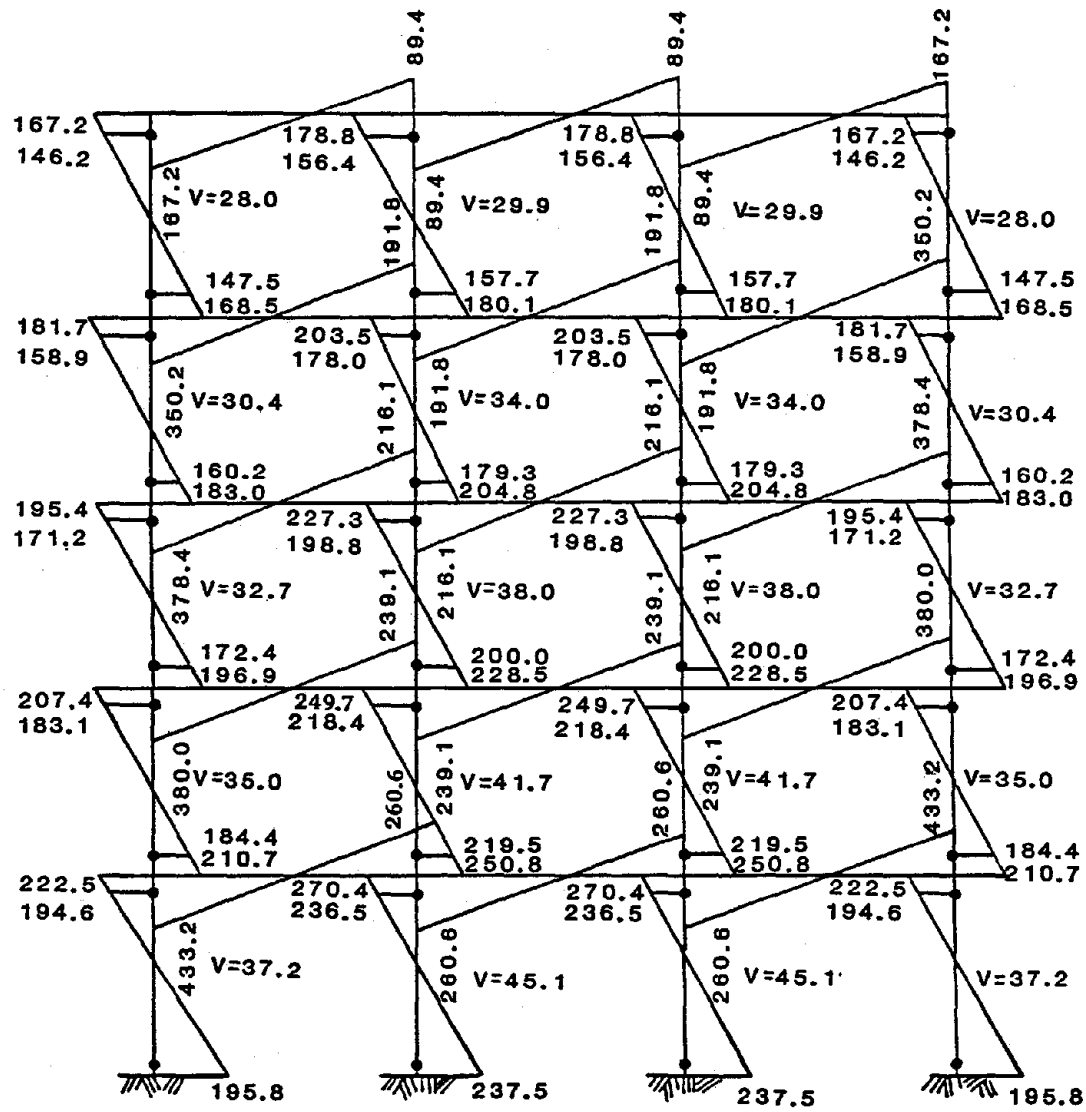

Fig. 7-8 Failure Mechanism and Moment Distribution (Case II)

Table 7-VIII Ultimate and Equivalent Linear Shear Capacities (Case II)

Story	F_i	Q_{ni}(kips)	$Q_{\ell i}$(kips)
5	2.5	115.8	289.5
4	2.5	128.8	257.6
3	2.5	140.8	352.0
2	2.5	153.4	383.5
1	2.5	164.6	411.5

Table 7-IX Story Limit State Probability (Case II)

	$P_{f,i}$				
PGA (G)	1st. Story	2nd. Story	3rd. Story	4th Story	5th Story
0.10	0.0	0.0	0.0	0.0	0.0
0.20	0.0	0.0	0.0	0.0	0.0
0.30	2.02×10^{-8}	6.70×10^{-9}	1.30×10^{-10}	1.32×10^{-9}	0.0
0.40	2.01×10^{-4}	1.05×10^{-4}	1.17×10^{-5}	4.79×10^{-5}	0.0
0.50	0.01	9.09×10^{-3}	2.31×10^{-3}	6.17×10^{-3}	8.92×10^{-14}
0.60	0.13	0.10	0.04	0.08	2.86×10^{-9}
0.70	0.44	0.36	0.21	0.35	1.49×10^{-6}
0.80	0.76	0.69	0.51	0.70	8.66×10^{-5}
0.90	0.93	0.89	0.78	0.91	1.40×10^{-3}
1.00	0.98	0.97	0.93	0.98	0.01
1.10	1.00	0.99	0.98	1.00	0.04
1.20	1.00	1.00	1.00	1.00	0.13

Table 7-X Fragility Data (Case II)

PGA (G)	PF
0.10	0.0
0.20	0.0
0.30	2.02×10^{-8}
0.40	2.01×10^{-4}
0.50	0.01
0.60	0.13
0.70	0.44
0.80	0.76
0.90	0.93
1.00	0.98
1.10	1.00
1.20	1.00

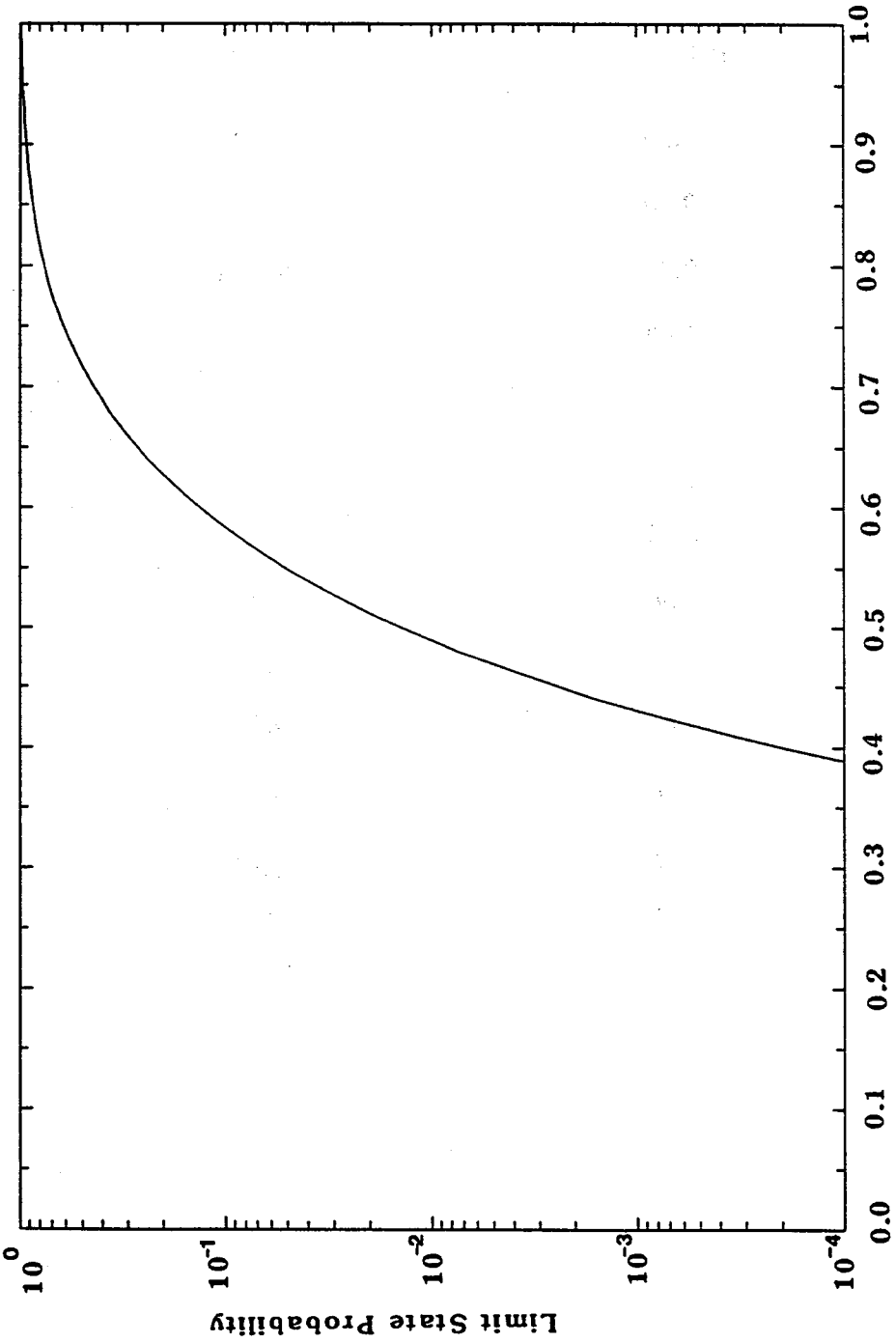

Fig. 7-9 Fragility Curve (Case II)

SECTION 8

CONCLUSIONS

This report presents a fragility analysis method for plane reinforced concrete frame structures subject to in-plane ground accelerations. This fragility analysis method has been developed with the emphasis placed on the simplicity and practicality of the entire analysis procedure. In order to simplify the degree of complexity in modeling the frame structure, the stick model which is derived from a condensation technique is employed. Such a structural modeling is more sound both theoretically and technically than the commonly used shear beam model to represent the original frame structure. The random vibration analysis is utilized so that the statistical information on the response can be determined directly without having to carry out Monte Carlo simulation with multiple time history analyses. A simplified limit analysis is used to determine the failure mechanism and the corresponding story shear capacities without considering all other possible failure mechanisms. However, it is noted that such a limit analysis can only be used to determine the limit state corresponding to the collapse of structure. For other limit states, such as moderate damage of structures, a different approach is needed to compute the structural capacity. Furthermore, the fragility curve constructed by the proposed method represents the best-estimate curve, since only the randomness of earthquakes is included in the analysis. To include the total uncertainty in the fragility analysis as shown in Ref. 3, additional effort needs to be made.

The fragility analysis method developed in this study can be applied immediately to existing reinforced concrete structures. This method may be applied to steel frame structures with minor modification in the capacity evaluation of steel frames. The proposed method may also be extended for the flat-plate structures. The limit state probability obtained from the analysis can be integrated with the seismic hazard curve in order to determine the lifetime limit state probability of the frame structure. Furthermore, the fragility curves can be used with the inventory of structures and cost of damage to estimate the economic and societal risk given the occurrence of an earthquake. Such a risk assessment is essential and important for emergency preparedness planning.

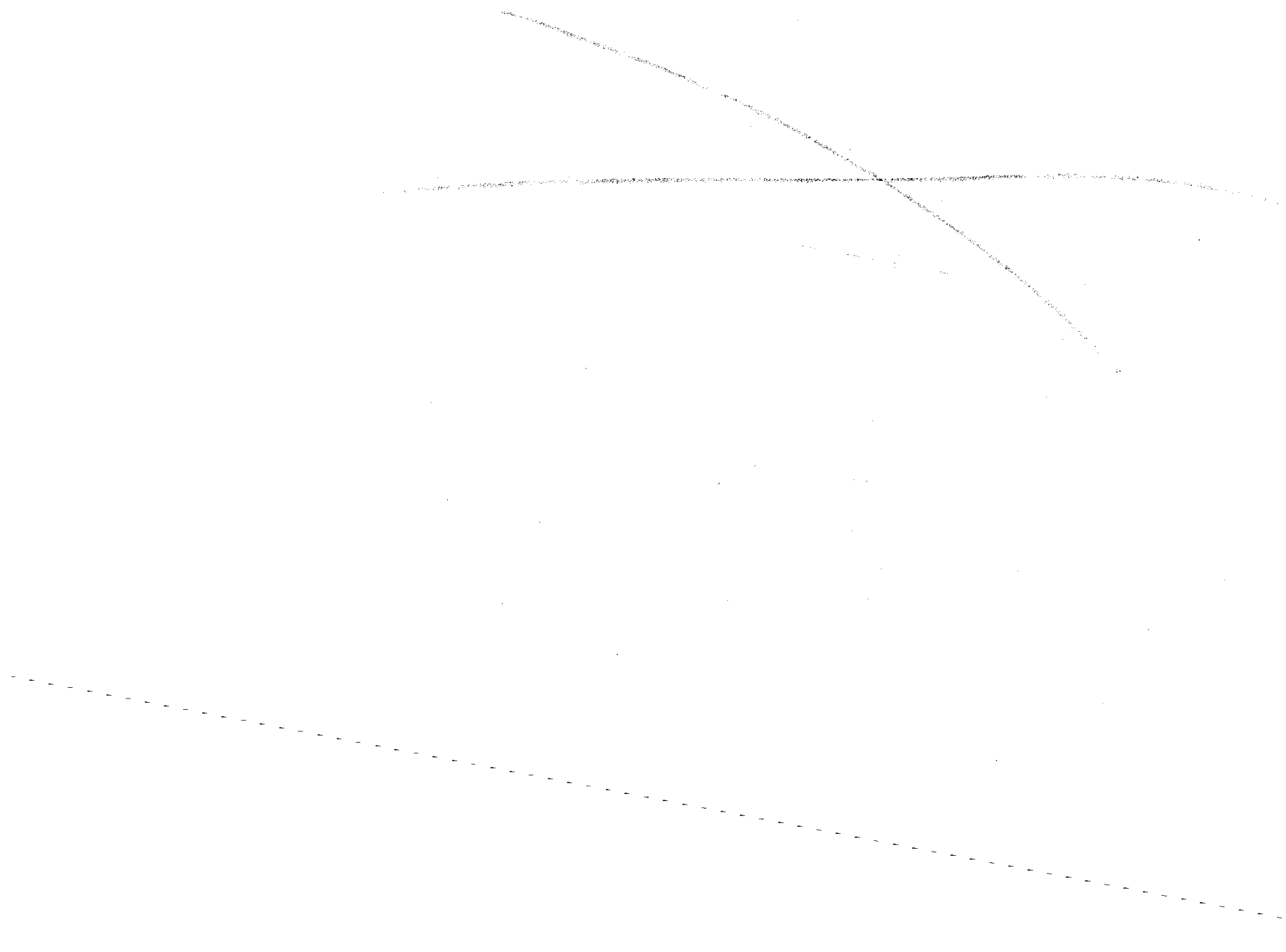

SECTION 9

REFERENCES

1. Rosenblueth, E. and Meli, R., "The 1985 Earthquake: Causes and Effects in Mexico City," Concrete International, May 1986, pp. 23-34.
2. Hwang, H., "Seismic Probabilistic Risk Assessment and Seismic Margins Studies for Nuclear Power Plants," Technical Report NCEER-87-0011, National Center for Earthquake Engineering Research, SUNY, Buffalo, New York, June 1987.
3. Jaw, J.-W. and Hwang, H., "Seismic Fragility Analysis of Shear Wall Structures", NCEER-88-0009, National Center for Earthquake Engineering Research, SUNY, Buffalo, New York, April 1988.
4. Wilson, E.L., Dovey. H.H., and Habibullah, A., "Three Dimensional Analysis of Building Systems, TABS77," EERC 72-8, Earthquake Engineering Research Center, University of California, Berkeley, April 1979.
5. Lin, Y.K., *Probabilistic Theory of Structural Dynamics*, Robert E. Krieger Publishing Co., 1967.
6. Tajimi, H., "A Statistical Method of Determining the Maximum Response of a Building Structure During an Earthquake", Proceedings of the 2nd World Conference on Earthquake Engineering, Tokyo and Kyoto, Japan, Vol. II, July 1960.
7. Ellingwood, B. and Batts, M., "Characterization of Earthquake Forces for Probability Based Design of Nuclear Structures", NUREG/CR-2945, U.S. Nuclear Regulatory Commission, Washington, D.C., September 1982.
8. Shinozuka, M., Hwang, H., and Reich, M., "Reliability Assessment of Reinforced Concrete Containment Structures," Nuclear Engineering and Design, Vol. 80, 1984, pp. 247-267.
9. American Concrete Institute, *Building Code Requirements for Reinforced Concrete*, ACI 318-83, Detroit, Michigan, 1983.
10. Aoyama, H., "A Method in the Evaluation of the Seismic Capacity of Existing Reinforced Concrete Buildings in Japan," Bulletin of the New Zealand National Society for Earthquake Engineering, Vol. 14, No. 3, September 1981, pp. 105-130.
11. Hawkins, N.M., "Seismic Evaluation Procedure for Existing Structures," American Concrete Institute Seminar Course Manual, SCM-14, 1986.

12. Newland, D.E., *Random Vibrations and Spectral Analysis*, Longman, 1975.
13. Yang, C.Y., *Random Vibration of Structures*, John Wiley and Sons, 1986.
14. Chen, C.K., Czarnecki, R.M., and Scholl, R.E., "Vibrations Test of a 4-Story Concrete Test Structure," JAB-99-119, URS/John A. Blume and Associates, Engineers, San Francisco, California, January 1976.
15. Freeman, S.A., "Concrete Test Structures: Second Progress Report on Structural Response," JAB-99-50, John A. Blume and Associates Research Division, San Francisco, California, 1971.
16. U.S. Atomic Energy Commission, "Damping values for Seismic Design of Nuclear Power Plants," Regulatory Guide 1.61, Washington, D.C., 1973.
17. Ellingwood, B. and Hwang, H., "Probabilistic Descriptions of Resistance of Safety-related Structures in Nuclear Power Plants," Nuclear Engineering and Design, Vol. 88, 1985, pp. 169-178.
18. Mirza, S.A. and MacGregor, J.G., "Variability of Mechanical Properties of Reinforcing Bars," Journal of Structural Division, American Society of Civil Engineers, No. 105, May 1979, pp. 921-937.
19. American National Standard Institute, *Minimum Design Loads for Buildings and other Structures*, ANSI A58-1-1982, New York, 1982.

APPENDIX A
CONDENSATION OF STIFFNESS MATRIX

A condensation technique is used to eliminate the two DF's (rotation and vertical displacement) at all the beam-column joints and retains the single DF (lateral displacement) at each floor level. The equations of motion due to the horizontal ground motion $\ddot{u}_g$ for the frame structure, neglecting the rotational inertia at the beam-column joints and the damping effect, are given by

$$\begin{bmatrix} [0] & [0] \\ [0] & [M] \end{bmatrix} \begin{Bmatrix} \{\ddot{\delta}\} \\ \{\ddot{\Delta}\} \end{Bmatrix} + \begin{bmatrix} [K_{\delta\delta}] & [K_{\delta\Delta}] \\ [K_{\Delta\delta}] & [K_{\Delta\Delta}] \end{bmatrix} \begin{Bmatrix} \{\delta\} \\ \{\Delta\} \end{Bmatrix} = - \begin{bmatrix} [0] & [0] \\ [0] & [M] \end{bmatrix} \begin{Bmatrix} \{0\} \\ \{\hat{I}\} \end{Bmatrix} \ddot{u}_g \quad (A.1)$$

where $\{\delta\}$ is the vector corresponding to the rotational and translational DF's of the beam-column joints to be reduced and $\{\Delta\}$ is the vector consisting of the remaining lateral floor displacement. The mass matrix $[M]$ is

$$[M] = \begin{bmatrix} m_1 & & & & \\ & \ddots & & & \\ & & m_i & & \\ & & & \ddots & \\ & & & & m_{NS} \end{bmatrix} \quad (A.2)$$

where, m_i is the lumped mass at node i and NS is the number of mass. $\{\hat{I}\}$ is the identity vector consisting of NS unit elements. The global stiffness matrix, which is shown in four partitions in Eq. A.1, is assembled using the element stiffness. Eq. A.1 can be rewritten as follows:

$$[K_{\delta\delta}]\{\delta\} + [K_{\delta\Delta}]\{\Delta\} = \{0\} \quad (A.3)$$

$$[M]\{\ddot{\Delta}\} + [K_{\Delta\delta}]\{\delta\} + [K_{\Delta\Delta}]\{\Delta\} = -[M]\{\hat{I}\}\ddot{u}_g \quad (A.4)$$

From Eq. A.3, the vector $\{\delta\}$ can be expressed in terms of the displacements $\{\Delta\}$,

$$\{\delta\} = -[K_{\delta\delta}]^{-1}[K_{\delta\Delta}]\{\Delta\} \quad (A.5)$$

Using Eq. A.5, Eq. A.4 can be expressed in terms of $\{\Delta\}$ in the following form:

$$[M]\{\ddot{\Delta}\} + [K]\{\Delta\} = -[M]\{\hat{I}\}\ddot{u}_g \qquad (A.6)$$

where $[K]$ is the modified stiffness matrix given by

$$[K] = [K_{\Delta\Delta}] - [K_{\Delta\delta}][K_{\delta\delta}]^{-1}[K_{\delta\Delta}] \qquad (A.7)$$

It is noted that $[K]$ is symmetric for linear structural systems.

APPENDIX B

DESIGN OF FIVE-STORY FRAME BUILDING

B.1 Description of Building

The five-story frame building selected for this study is assumed to be located in New York City. A typical plan and section of the building is shown in Fig. B-1. The columns have constant cross section throughout the building and the beams and slabs also have the same dimensions at all floor levels. This study focuses on the design of a typical interior frame in the north-south direction. The modeling of this interior frame is shown in Fig. B-2 with the bases of the lowest story columns assumed to be fixed.

B.2 Determination of Slab Thickness

The minimum slab thickness can readily be determined with the aid of a design chart as shown in Fig. B-3. Entering the vaue of clear span ℓ_n = 18.67 ft. into the chart, the minimum thickness value h_{min} is equal to about 5.7 in. for the two-way slab with square panel. Therefore, a slab thickness of 6 in. is selected.

B.3 Frame Analysis

The sizes of columns and beams are selected as 16 in. × 16 in. and 16 in. × 18 in., respectively. The dead loads due to the weights of the members, and the live loads due to occupancy are listed as follows:

a) Dead Load

6″ Slab	: $6/12 \times 155$	= 77.5 psf
Column	: $16 \times 16 \times 155/144$	= 275.6 plf
Beam	: $16 \times (18 - 6) \times 155/144$	= 206.7 plf
Ext. Wall	:	= 15.0 psf

b) Live Load

Roof	= 20 psf
Floor	= 50 psf (including 10 psf for partitions)

The frame is analyzed for dead and live (full and pattern) loads using TABS77 computer program. The full live load is found to be more critical. The member forces for

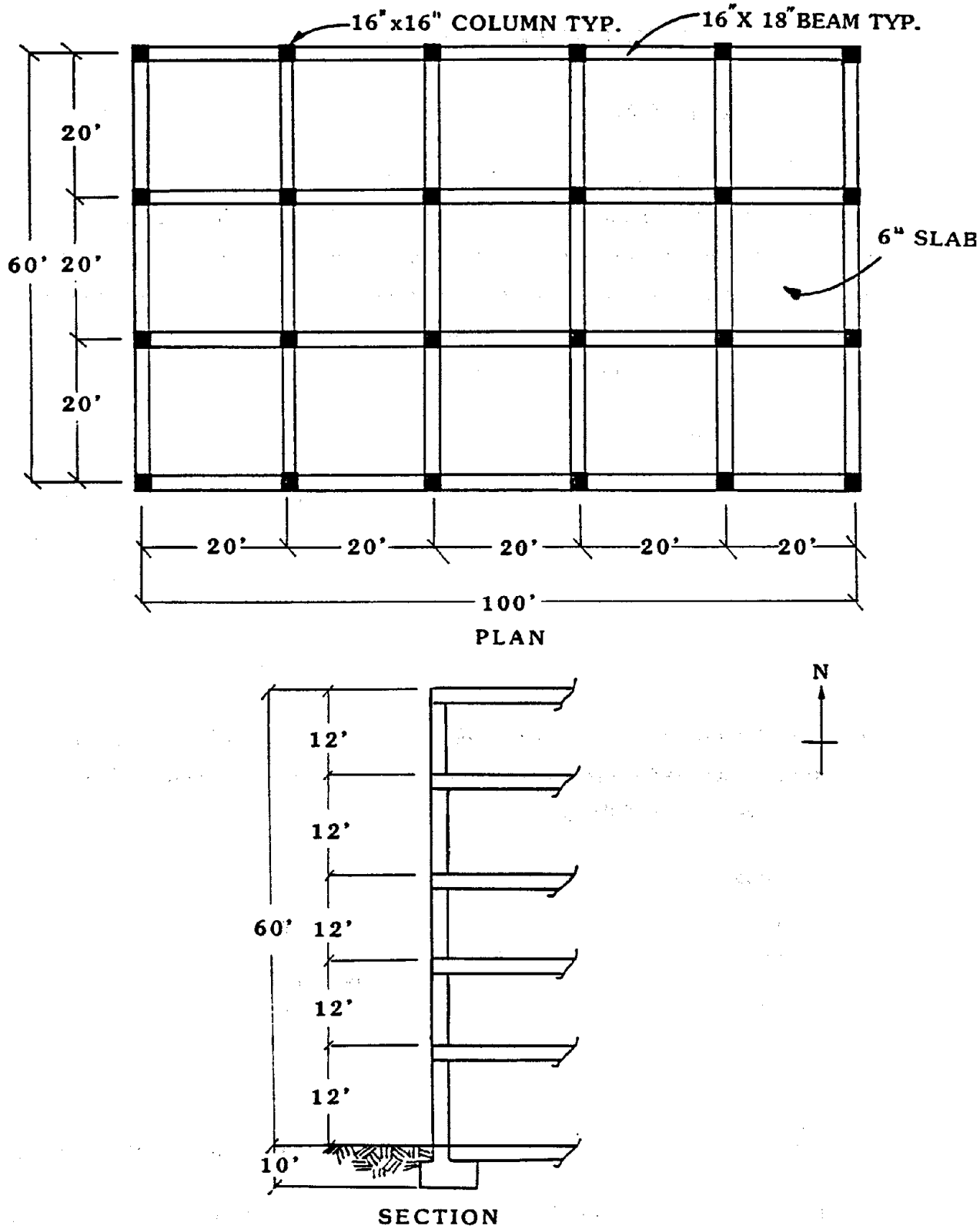

Fig. B-1 Five-Story Frame Structure

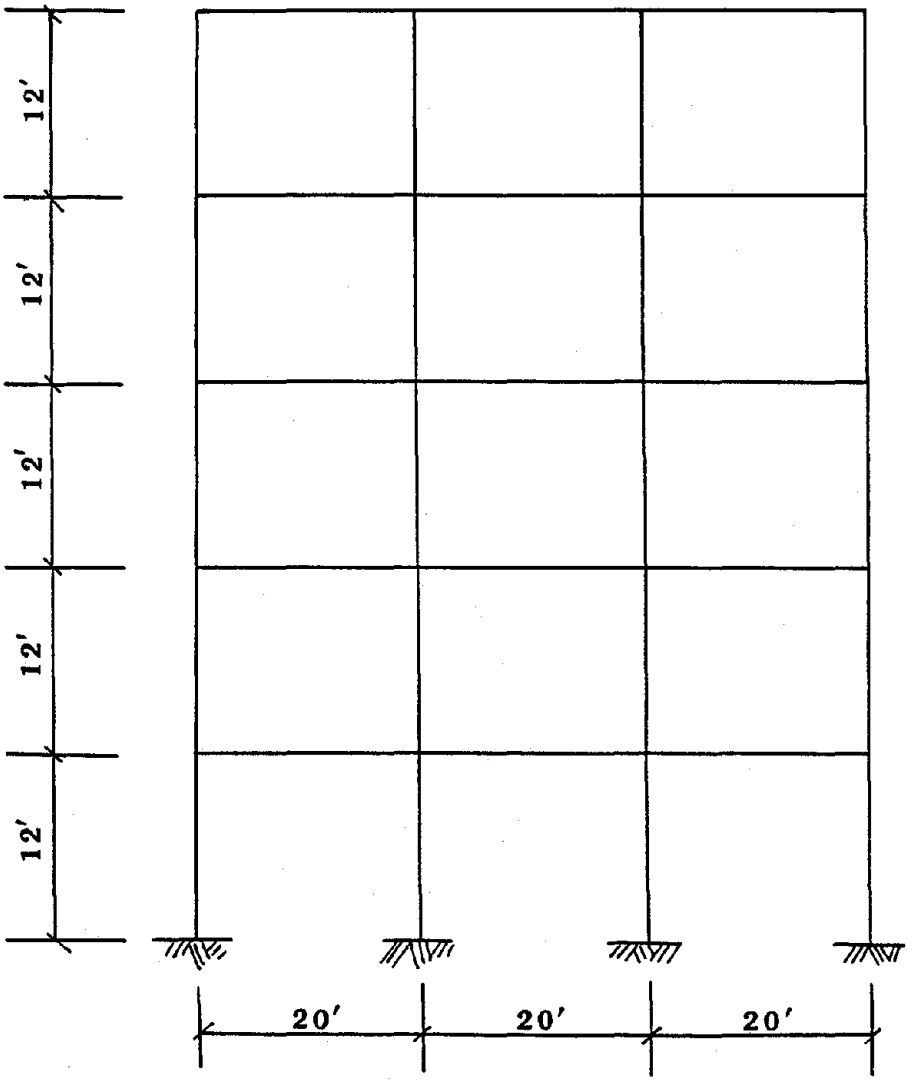

Fig. B-2 Frame Modeling

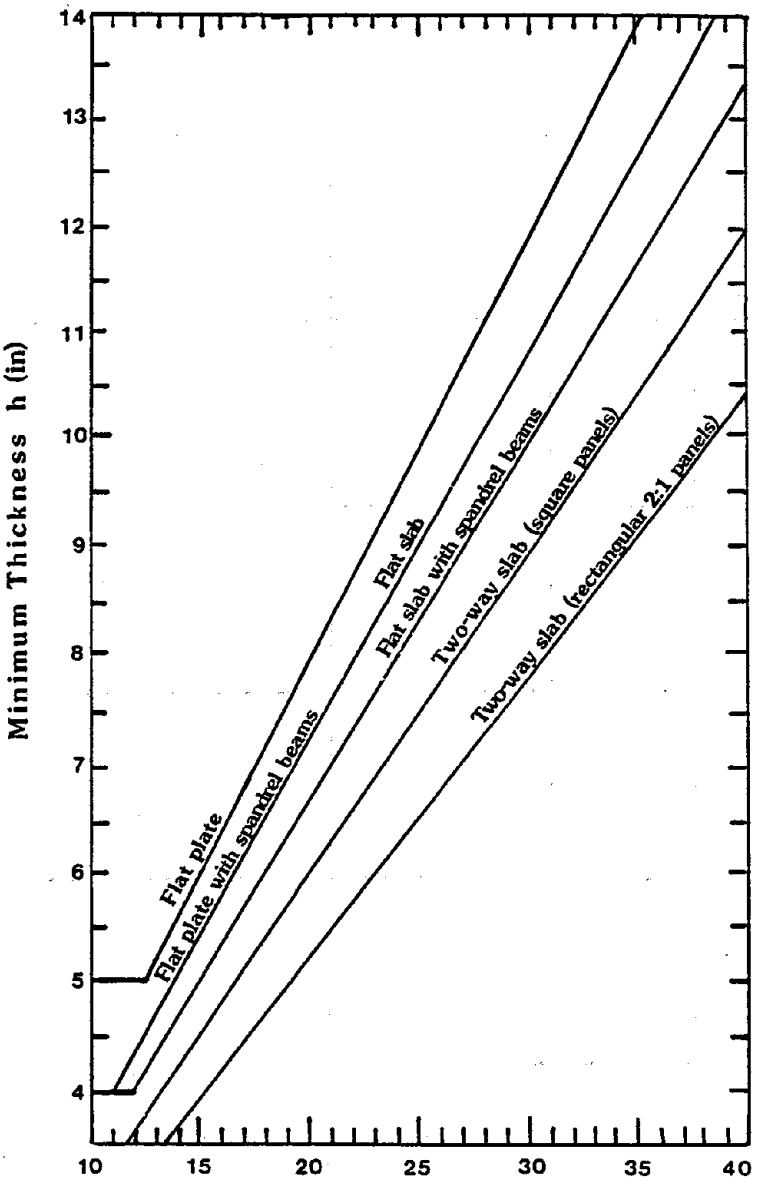

Fig. B-3 Minimum Slab Thickness for Two-Way Slab Systems (Ref. B-1)

the beams at the first, third, and roof level, as well as for the first-story column due to dead and full live loads are shown in Figs. B-4 and B-5, respectively.

c) Wind Load

The wind velocity pressure q_z specified in ANSI A58.1-1982 is

$$q_z = 0.00256 K_z (IV)^2 \qquad (B.1)$$

where V is the basic wind speed at a reference height of 33 ft for exposure C. From the map of basic wind speeds in ANSI A58.1-1982, $V = 80$ mph in New York City for a return period of 50 years. The importance factor I is chosen to be 1.05 (Category I at hurricane ocean line). The velocity pressure coefficient K_z varies with height. For exposure B considered here, K_z and q_z are listed in Table B-I.

The design wind pressure p_z is determined by the following formula:

$$p_z = q_z G_h C_{p(W)} - q_h G_h C_{p(L)} \qquad (B.2)$$

where G_h is the gust response factor at a height of h ft. For exposure B at 60 ft, $G_h = 1.39$. q_h is the wind pressure for leeward wall and roof evaluated at mean roof height. $C_{p(W)}$ and $C_{p(L)}$ are the wall pressure coefficients for the windward and leeward walls, respectively. In this case, $C_{p(W)} = 0.8$ and $C_{p(L)} = -0.5$. The design wind pressure p_z is also shown in Table B-I and plotted in Fig. B-6. For design convenience, the design wind pressure is converted into a concentrated lateral load at each floor level, as shown in Fig. B-6. The loads on each floor level are computed as follows:

$$H_1 = 22.20(100 \times 6.0) = 13320 = 13.32 \text{ kips}$$
$$H_2 = 22.20(100 \times 4.0) + 21.9(100 \times 8.0) = 25832 = 25.83 \text{ kips}$$
$$H_3 = 21.19(100 \times 12.0) = 25428 = 25.43 \text{ kips}$$
$$H_4 = 18.58(100 \times 12.0) = 22296 = 22.30 \text{ kips}$$
$$H_5 = 18.58(100 \times 3.0) + 15.97(100 \times 9.0) = 19947 = 19.95 \text{ kips}$$

The above lateral loads due to wind are divided equally among the six frames in the N-S direction. Fig. B-7 shows the lateral loads on a frame.

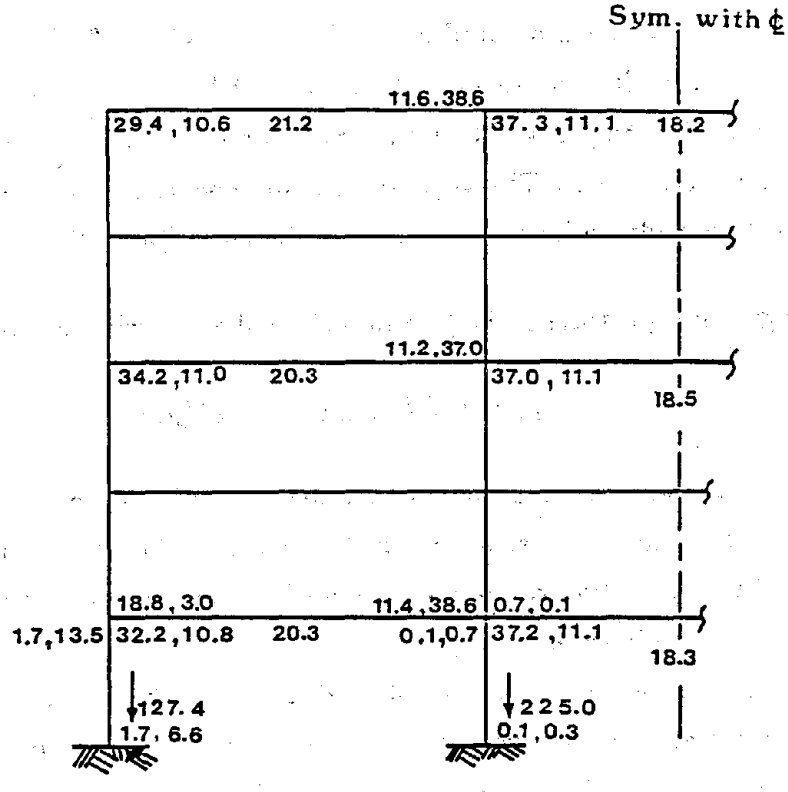

V,M (Bm.L)	M,V (Col. B)
V,M (Col.T)	M,V (Bm.R)

V = kips
M = ft-kips

Fig. B-4 Moment, Shear and Axial Forces due to Dead Load

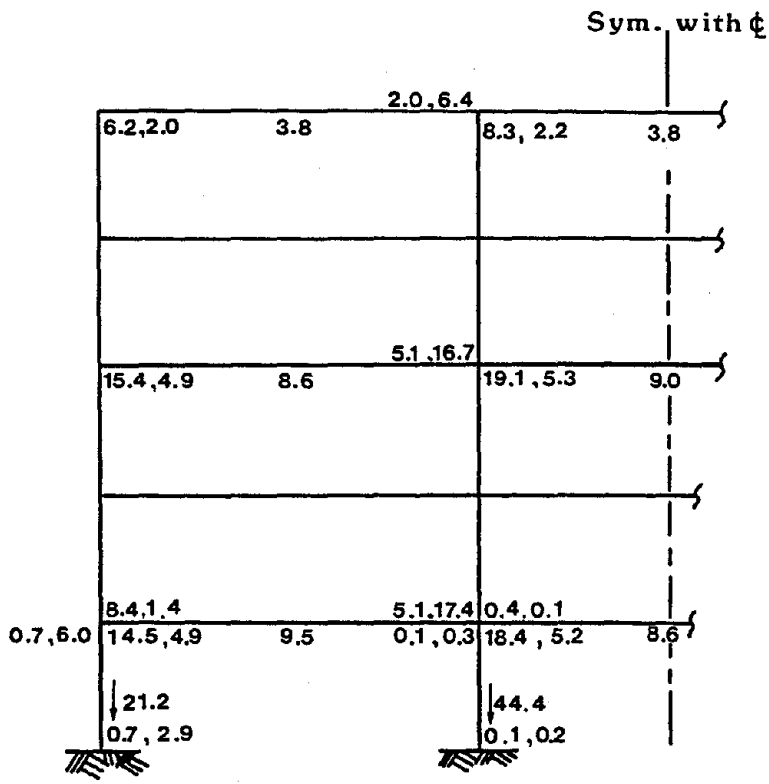

V,M (Bm. L)	M,V (Col.B)
V,M (Col.T)	M,V (Bm.R)

V: kips

M: ft-kips

Fig. B-5 Moment, Shear and Axial Forces due to Live Load.

Table B-I Design Wind Pressure

Height (ft)	K_z	q_z (psf)	p_z (psf)
0 – 15	0.37	6.683	15.97
15 – 30	0.50	9.032	18.58
30 – 50	0.63	11.38	21.19
50 – 60	0.68	12.28	22.20

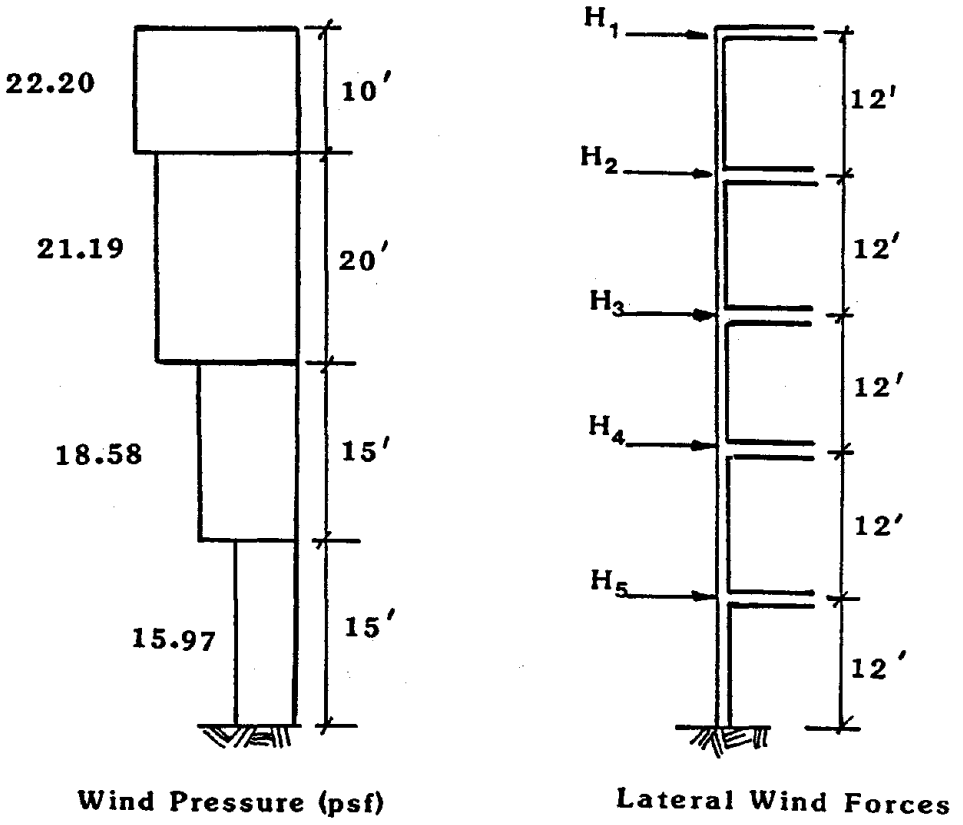

Fig. B-6 Wind Forces

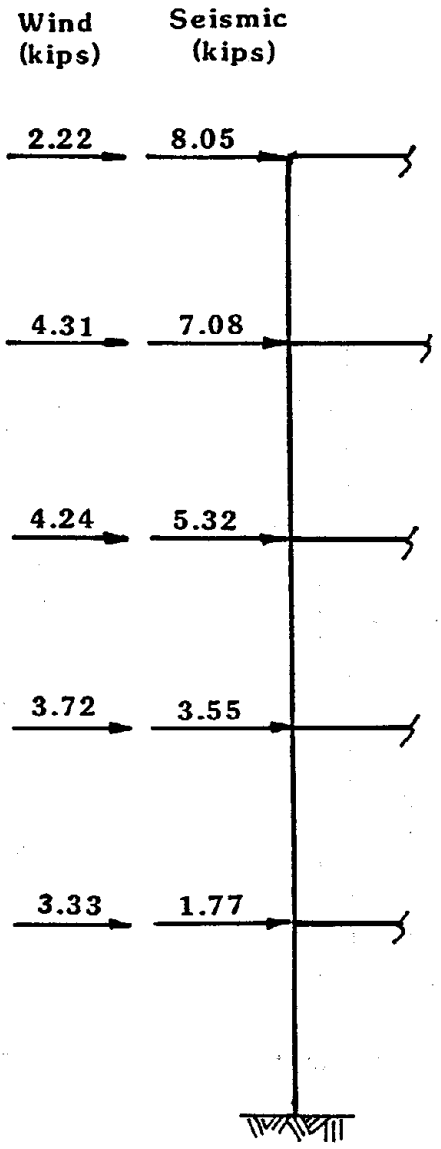

Fig. B-7 Wind and Seismic Loads on a Frame

d) Seismic Load

The design base shear Q due to earthquake specified in ANSI A58.1-1982 is

$$Q = ZIKCSW \tag{B.3}$$

where Q = total shear force at the base, Z = zone factor, I = importance factor, K = building system factor, C = numerical coefficient, S = soil factor and W = total dead load of the building.

New York City is located in seismic zone 2 according to the map for seismic zones in ANSI A58.1-1982. Therefore, Z is equal to 3/8. The importance factor I and building system factor K are taken as 1.0. The value of C is determined by

$$C = \frac{1}{15\sqrt{T}} \tag{B.4}$$

in which T is the fundamental period of the building in seconds and is computed by the following formula:

$$T = C_T h_n^{3/4} \tag{B.5}$$

where C_T is equal to 0.025 for concrete frame and h_n is the building height from the base. For the building under consideration, h_n = 60 ft, thus, T is 0.539 sec and C is equal to 0.091. In this study, the soil type S_2 is used and the soil factor S is 1.2. Thus, CS is equal to 0.11, which is less than the upper limit of 0.14 specified by ANSI A58.1-1982. The dead load of the building W is calculated in Table B-II. Therefore, the total seismic base shear Q determined by Eq. B.3 is

$$Q = 3/8 \times 1.0 \times 1.0 \times 0.11 \times 3743.4 = 154.6 \ kips$$

The base shear is distributed over the height of the structure by using the following formula:

$$F_x = \frac{(Q - F_t)W_x h_x}{\sum_{i=1}^{n} W_i h_i} \tag{B.6}$$

where

F_x = Lateral force applied at level x

F_t = Additional concentrated lateral force at top of structure

Table B-II Calculation of Total Dead Load

Item	Calculation	Weight (kips)
Roof		
Slab	$77.5 \times 100 \times 60$	$= 465$
Column	$275.6(6.0 \times 24)$	$= 39.7$
Beam	$206.7(20 - \frac{16}{12}) \times 38$	$= 146.6$
Ext. Walls	$15 \times 6.0 \times 320$	$= 28.8$
Subtotal		$= 680.1$
2^{nd} - 5^{th} FL.		
Slab	$77.5 \times 100 \times 60$	$= 465$
Column	$275.6 \times 12.0 \times 24$	$= 79.5$
Beam	$206.7(20 - \frac{16}{12}) \times 38$	$= 146.6$
Ext. Walls	$15 \times 12.0 \times 320$	$= 57.6$
Subtotal		$= 748.1$
1^{st} FL.		
Column	$276 \times 6.0 \times 34$	$= 39.7$
Ext. Walls	$15 \times 6.0 \times 320$	$= 28.8$
Subtotal		$= 68.5$
Total Dead Load W		$= 3743.4$

h_x, h_i = Height from the base to levels x or i, respectively

W_x, W_i = Weight located or assigned to level x or i, respectively

n = Number of stories

According to ANSI A58.1-1982, F_t may be considered as zero when T is 0.7 second or less. In this case, $T = 0.539$ sec., thus, $F_t = 0$. The calculation of F_x is shown in Table B-III. The lateral seismic force on each story level is divided equally among the six frames in the N-S direction. The lateral forces acting on a single frame is shown in Fig. B-7. The lateral load analysis is performed only for the seismic load because the seismic load is more critical than the wind load as can be seen from Fig. B-7. Using the computer program TABS 77, the member forces for the beams at the first, third, and roof level as well as for the first story column due to seismic load are shown in Fig. B-8.

B.4 Design of Frame Structure

The beam and column are designed according to the following design formulas specified in ACI Code 318-83:

$$\phi R_n \geq \begin{cases} 1.4D + 1.7L & \text{(B.7a)} \\ 0.75(1.4D + 1.7L + 1.7W) & \text{(B.7b)} \\ 0.9D + 1.3W & \text{(B.7c)} \\ 0.75(1.4D + 1.7L + 1.87E) & \text{(B.7d)} \\ 0.9D + 1.43E & \text{(B.7e)} \end{cases}$$

where D = dead load effect, L = live load effect, W = load effect due to wind (not to be confused with the W used for dead weight in Eq. B.3), E = load effect due to earthquake, ϕ = strength reduction factor and R_n = nominal capacity. Since the wind load is not critical; therefore, only the dead, live, and seismic load effects are considered in the design. The most critical factored moment and shear force from the load combinations (Eq. B.7) due to the three load effects for the beams at the first, third, and roof level are shown in Fig. B-9. The factored moment, shear, and axial forces for the first story column are shown in Table B-IV.

Table B-III Lateral Seismic Force

Level	$W_x(kips)$	$h_x(ft)$	$W_x h_x$	$F_x(kips)$
Roof	680.1	60	40806	48.3
5	748.7	48	35937.6	42.5
4	748.7	36	26953.2	31.9
3	748.7	24	17968.8	21.3
2	748.7	12	8984.4	10.6
Total			130650	154.6

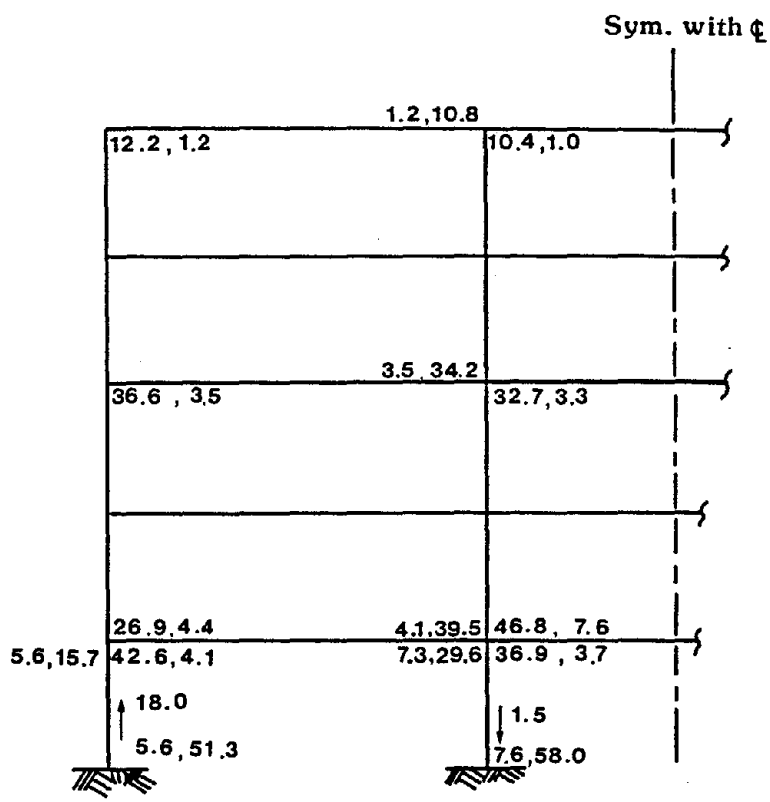

V,M (Bm L)	M,V (Col. B)
V,M (Col.T)	M,V (Bm.R)

V = kips
M = ft-kips

Fig. B-8 Moment, Shear and Axial Forces due to Seismic Load

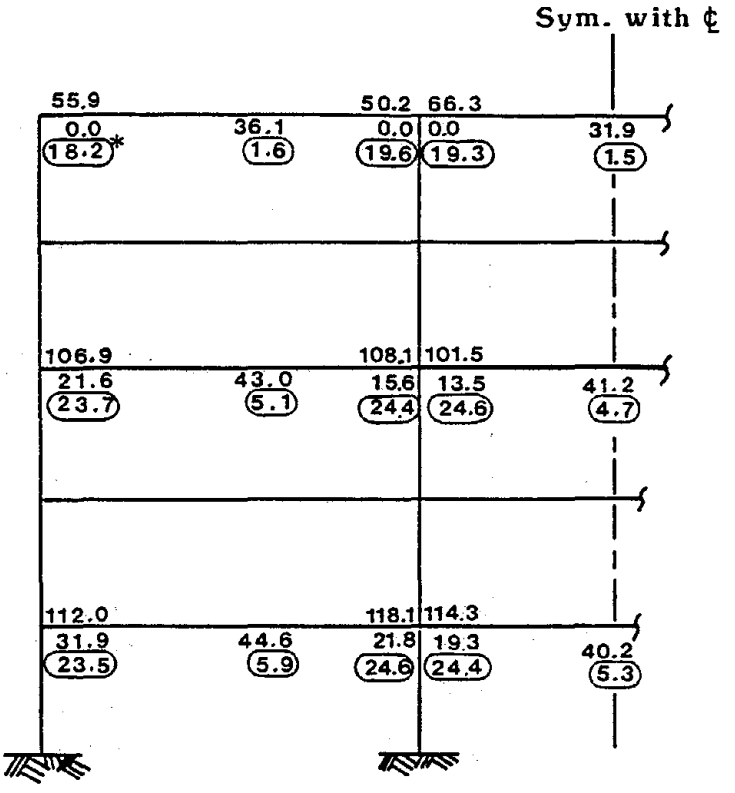

*Note: Factored Shear Force

Mu (Bm. L)	Mu (Bm. R)
Mu (Bm. L)	Mu (Bm. R)

V = kips

M = ft-kips

Fig. B-9 Factored Moment and Shear Forces for Beams

Table B-IV Factored Moment, Shear and Axial Forces for First Story Columns

Eq.	Ext. Col.			Int. Col.		
	M_u (ft-kips)	V_u (kips)	P_u (kips)	M_u (ft-kips)	V_u (kips)	P_u (kips)
B.7a	29.1	3.6	214.2	35.1*	0.3	390.5
B.7d	93.8	10.6	185.9	107.7	10.9	295.0
B.7e	85.5	9.5	140.4	83.2	10.5	204.6

*Note: This factored moment M_u is governed by the minimum eccentricity of (0.6 + 0.03h) (ACI 10.11.5.4)

B.4.1 Design of Beams

The design of first story beam is presented below. The upper story beams are designed following the same procedure.

a) Determine Required Flexural Reinforcement

i) Negative Reinforcement at Support (Top Bars)

The largest factored moment M_u at support in Fig. B-9 for the first story beams is 118.1 ft-kips. Refering to the force diagram in Fig. B-10 and equating the compressive force C to the tensile force T and neglecting the effect of any compressive reinforcement we have

$$0.85 f'_c b a = A_s f_y \qquad (B.8)$$

or

$$a = \frac{A_s f_y}{0.85 f'_c b} = \frac{60 A_s}{(0.85)(4)(16)} = 1.103 A_s \qquad (B.9)$$

The reinforcing area A_s can be determined by

$$M_u = \phi A_s f_y (d - a/2) \qquad (B.10)$$

Substituting $M_u = 118.1$ ft-kips and 'a' from Eq. B.9 into Eq. B.10 and solving for A_s, we have $A_s = 1.81$ in^2. Therefore, use 4-No. 7 ($A_s = 2.40$ in^2).

ii) Check Reinforcement Ratio

$$\rho = \frac{A_s}{bd} = \frac{2.40}{(16)(15.5)} = 0.0097 \qquad (B.11)$$

which is larger than the minimum reinforcement ratio $\rho_{min} = 200/f_y$ required by ACI 10.5.1.

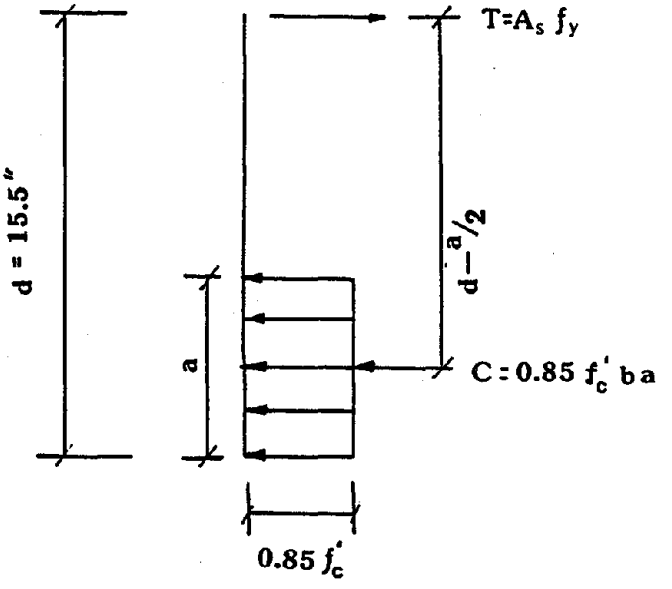

Fig. B-10 Internal Forces

iii) Positive Reinforcement at Center Span (Bottom Bars)

The largest positive moment in Fig. B-9 at mid-span is 44.6 ft-kips. Using Eqs. B.8 to B.10, the reinforcing area A_s is obtained as 0.65 in^2. Thus, providing 2-No. 7 (A_s = 1.20 in^2) is more than adequate. The reinforcement ratio ρ = 1.20/(16)(15.5) = 0.0048 is more than the minimum requirement.

b) Determine Shear Reinforcement

From Fig. B-9 the largest factored shear force at column centerline is 24.6 kips. This factored shear is reduced to 20.3 kips at the critical section of 'd' distance from the face of the column. The shear strength ϕV_c provided by concrete is

$$\phi V_c = \phi 2\sqrt{f'_c} b_w d \qquad (B.12)$$

$$= 0.85(2)\sqrt{4000}(16)(15.5)/1000$$

$$= 26.7 \ kips$$

Since V_u is larger than $0.5\phi V_c$, but is less than

$$\phi V_c = \phi(50 b_w d) = 37.2 \ kips \qquad (B.13)$$

Therefore, minimum shear reinforcement is required per ACI 11.5.5.3. Using No. 3 vertical stirrups at a spacing of 7.5 in ($d/2$ = 7.8 in) is adequate. The same reinforcing details are used for the second story beams. The reinforcement selected for the third story beams are used for the beams at the fourth story, while the roof beams are designed accordingly. Details of the beams are shown in Fig. B-11.

B.4.2 Design of Columns

The design of the first story interior column is presented below and the same procedure is used for the exterior column.

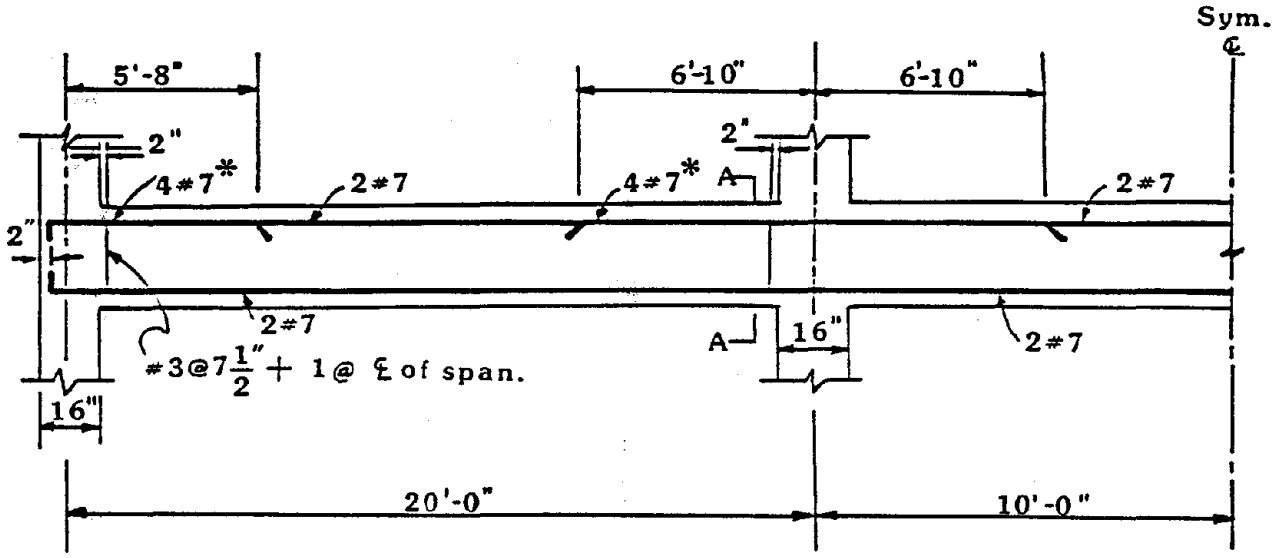

* Note: Use 4-#7 for 1st to 2nd Floor Beam
3-#7 for 3rd to 4th Floor Beam
2-#7 for Roof Beam

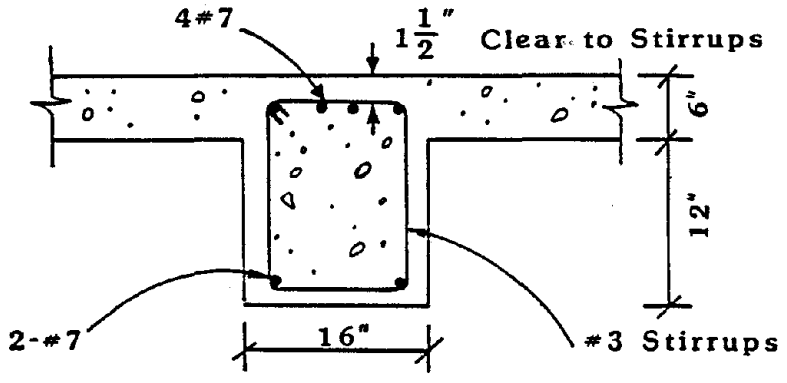

SECTION A-A

Fig. B-11 Beam Reinforcing Details

a) Column Slenderness Consideration

ACI 10.11.4.2-10.11.4.3 states that if the slenderness ratio $k\ell_u/r$ is greater than 22, then slenderness effect needs to be considered. The effective length factor k can be assumed to be 1.2 for the unbraced columns (ACI 10.11.2.2). The unsupported length of column $\ell_u = 12 \times 12 - 18 = 126$ in. and the radius of gyration, $r = 0.3h$ or 4.8 in. Therefore, the slenderness ratio is

$$\frac{k\ell_u}{r} = \frac{1.2 \times 126}{4.8} = 31.5 \qquad (B.14)$$

which is larger than 22; therefore, slenderness effect must be considered.

b) Determine the Longitudinal Reinforcement

The design column chart of Ref. B.1 is used for selecting the longitudinal reinforcement for the interior column using the factored moment and axial forces in Table B-IV. The load combination of Eq. B.7d is found to be the most critical load combination effects and 4-No. 7 is slected. This bar number is increased to 6-No. 7 in order to include the effects of column slenderness. The trial selection is then checked as a column with moment M_u magnified by the magnification δ_a to account for the secondary moments due to the column slenderness. δ_a can be expressed in the following equation [Ref. B.1]

$$\delta_a = \frac{1}{1 - \left[\frac{P_u}{(415+200\rho_t)h^2}\right]\left(\frac{k\ell_u}{h}\right)^2} \qquad (B.15)$$

where the reinforcement percentage, ρ_t for 6-No. 7 is 1.4 percent and P_u is taken as the maximum factored axial load in Table B-IV. Therefore, δ_a is

$$\delta_a = \frac{1}{1 - \left[\frac{390.5}{(415+200\times1.4)(16)^2}\right]\left(\frac{1.2\times126}{16}\right)^2}$$

$$= 1.25$$

The new load combination due to slenderness effects is $P_u = 295.0$ kips and $M_u = 1.25(107.7) = 134.6$ ft-kips. Entering these values into the column chart of Ref. B.1,

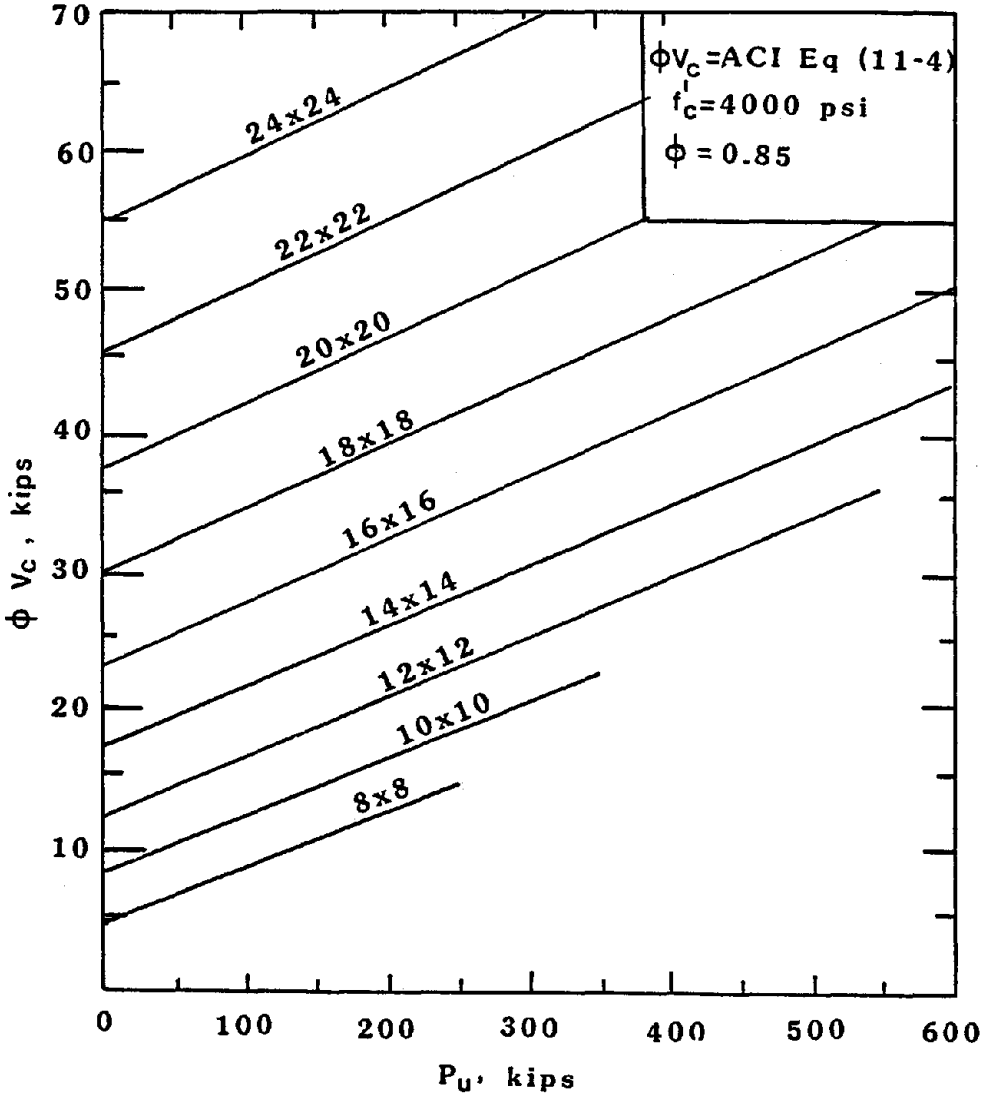

Fig. B-12 Column Shear Strength ϕV_c(Ref. B.1)

6-No. 7 bars are adequate. The same bar arrangement is also selected for the exterior column.

c) Determine the Shear Reinforcement

The chart in Fig. B-12 provides an easy way to check shear strength provided by concrete ϕV_c. The largest factored shear forces of the exterior and interior columns in Table B-IV should be used to check the column shear strength. From Table B-IV the largest factor column shear forces for exterior and interior columns are 10.6 kips and 10.9 kips respectively. Entering the corresponding factored axial forces for both exterior and interior columns and reading the values of ϕV_c from Fig. B-12 for both columns, we obtain ϕV_c equal to 32 kips and 37 kips for exterior and interior column, respectively. These values are relatively larger than the corresponding shear forces V_u. Therefore, the column shear strength is adequate and No. 3 stirrups with a spacing less than or equal to the following (ACI 7.10.5) are used

$$s_{max} = \begin{cases} 16d_b \text{ (col. bar dia.)} \\ \leq 48d_b \text{ (stirrup dia.)} \\ \leq \text{least col. dimension} \end{cases} \qquad (B.16)$$

$$= \begin{cases} 16(.875) = 14 \text{ in. (governs)} \\ \leq 48(.375) = 18 \text{ in.} \\ \leq 16 \text{ in.} \end{cases}$$

For a distance of 30 in. from both ends of the column, a spacing of 7 in. is used, while 11 in. interval is provided for the remaining length of the column. The details of a first story column is shown in Fig. B-13. For simplicity, the same bar arrangement is assumed for all the upper story columns.

References:

B.1 Simplified Design, Reinforced Concrete Buildings of Moderate Size and Height, edited by Neville, G.B., Portland Cement Association, 1984.

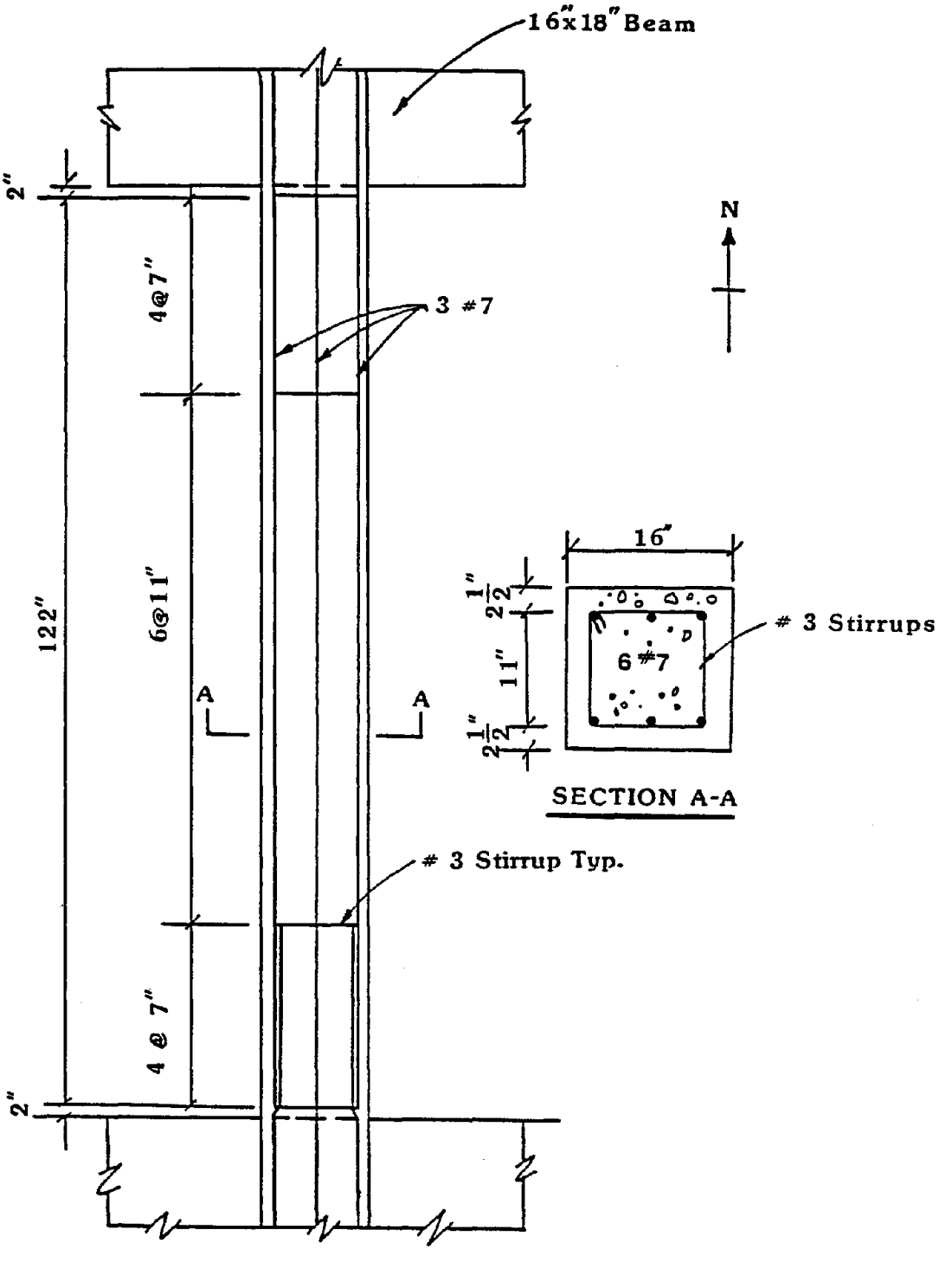

Fig. B-13 Column Reinforcing Details

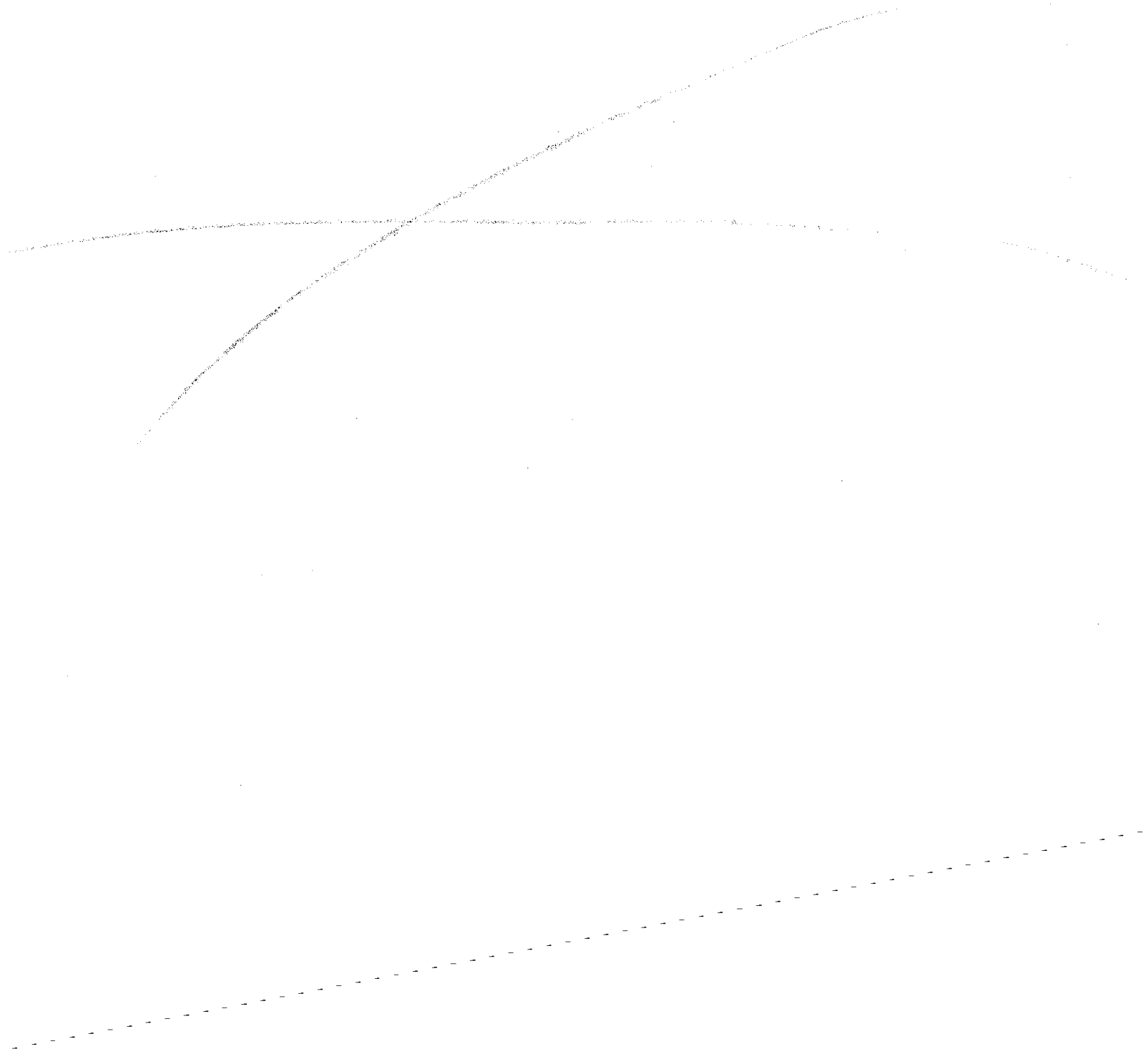

APPENDIX C

DYNAMIC CHARACTERISTICS OF FIVE-STORY FRAME BUILDING

The following are the dynamic characteristics, such as story mass, natural frequencies, mode shapes, and modal participation factors of the five-story frame building for Case I and Case II as computed by TABS77.

Table C-I Story Mass (Case I)

Node No.	m_i(kips–sec^2/in)
1	0.323
2	0.323
3	0.323
4	0.323
5	0.293

Table C-II Natural Frequencies and Modal Participation Factors (Case I)

Mode No.	Natural Frequencies (rad/sec)	Modal Participation Factors
1	6.26	1.153
2	19.38	0.402
3	33.81	-0.245
4	48.48	-0.163
5	60.23	0.087

Table C-III Mode Shapes (Case I)

	Mode No.				
Node No.	1	2	3	4	5
1	0.23	0.65	-0.98	-1.06	0.73
2	0.54	1.08	-0.54	0.60	-1.00
3	0.80	0.69	0.87	0.48	0.99
4	1.00	-0.25	0.66	-1.04	-0.71
5	1.11	-1.03	-0.85	0.57	0.28

Table C-IV Story Mass (Case II)

Node No.	m_i(kips–sec^2/in)
1	0.355
2	0.355
3	0.355
4	0.355
5	0.325

Table C-V Natural Frequencies and Modal Participation Factors (Case II)

Mode No.	Natural Frequencies (rad/sec)	Modal Participation Factors
1	7.09	1.221
2	21.38	-0.413
3	35.72	0.238
4	48.73	-0.149
5	58.26	0.075

Table C-VI Mode Shapes (Case II)

	Mode No.				
Node No.	1	2	3	4	5
1	0.24	-0.68	0.97	-0.98	0.63
2	0.53	-1.03	0.42	0.66	-0.93
3	0.77	-0.61	-0.88	0.37	0.97
4	0.95	0.27	-0.58	-1.00	-0.72
5	1.04	0.97	0.81	0.57	0.29

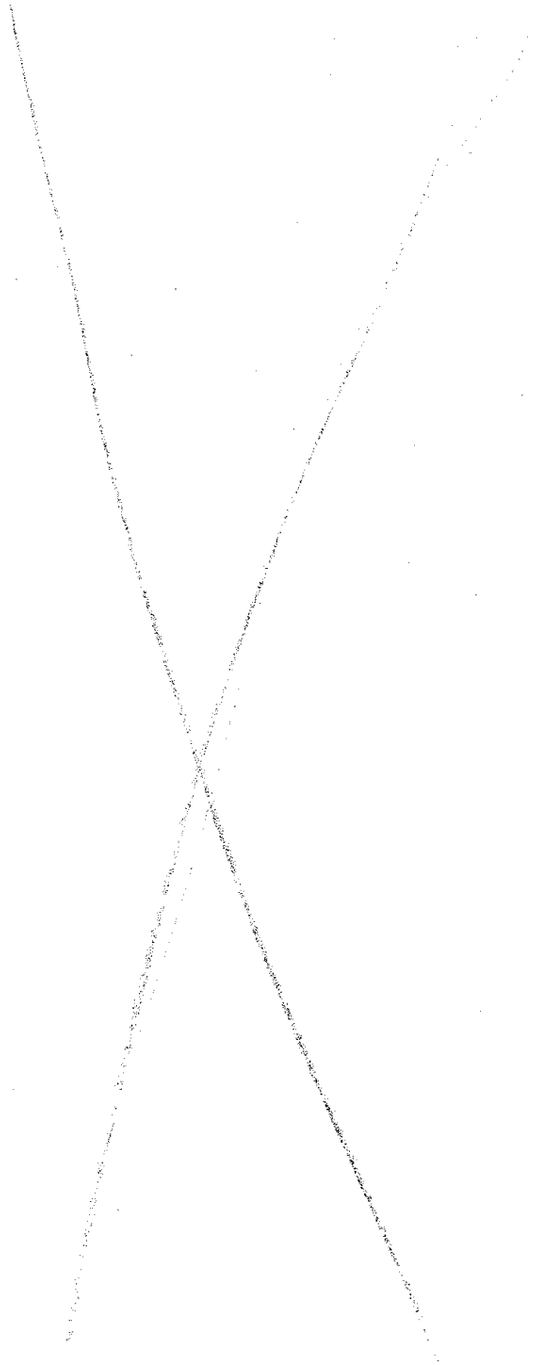

NATIONAL CENTER FOR EARTHQUAKE ENGINEERING RESEARCH
LIST OF PUBLISHED TECHNICAL REPORTS

The National Center for Earthquake Engineering Research (NCEER) publishes technical reports on a variety of subjects related to earthquake engineering written by authors funded through NCEER. These reports are available from both NCEER's Publications Department and the National Technical Information Service (NTIS). Requests for reports should be directed to the Publications Department, National Center for Earthquake Engineering Research, State University of New York at Buffalo, Red Jacket Quadrangle, Buffalo, New York 14261. Reports can also be requested through NTIS, 5285 Port Royal Road, Springfield, Virginia 22161. NTIS accession numbers are shown in parenthesis, if available.

NCEER-87-0001 "First-Year Program in Research, Education and Technology Transfer," 3/5/87, (PB88-134275/AS).

NCEER-87-0002 "Experimental Evaluation of Instantaneous Optimal Algorithms for Structural Control," by R.C. Lin, T.T. Soong and A.M. Reinhorn, 4/20/87, (PB88-134341/AS).

NCEER-87-0003 "Experimentation Using the Earthquake Simulation Facilities at University at Buffalo," by A.M. Reinhorn and R.L. Ketter, to be published.

NCEER-87-0004 "The System Characteristics and Performance of a Shaking Table," by J.S. Hwang, K.C. Chang and G.C. Lee, 6/1/87, (PB88-134259/AS).

NCEER-87-0005 "A Finite Element Formulation for Nonlinear Viscoplastic Material Using a Q Model," by O. Gyebi and G. Dasgupta, 11/2/87, (PB88-213764/AS).

NCEER-87-0006 "Symbolic Manipulation Program (SMP) - Algebraic Codes for Two and Three Dimensional Finite Element Formulations," by X. Lee and G. Dasgupta, 11/9/87, (PB88-219522/AS).

NCEER-87-0007 "Instantaneous Optimal Control Laws for Tall Buildings Under Seismic Excitations," by J.N. Yang, A. Akbarpour and P. Ghaemmaghami, 6/10/87, (PB88-134333/AS).

NCEER-87-0008 "IDARC: Inelastic Damage Analysis of Reinforced Concrete-Frame Shear-Wall Structures," by Y.J. Park, A.M. Reinhorn and S.K. Kunnath, 7/20/87, (PB88-134325/AS).

NCEER-87-0009 "Liquefaction Potential for New York State: A Preliminary Report on Sites in Manhattan and Buffalo," by M. Budhu, V. Vijayakumar, R.F. Giese and L. Baumgras, 8/31/87, (PB88-163704/AS).

NCEER-87-0010 "Vertical and Torsional Vibration of Foundations in Inhomogeneous Media," by A.S. Veletsos and K.W. Dotson, 6/1/87, (PB88-134291/AS).

NCEER-87-0011 "Seismic Probabilistic Risk Assessment and Seismic Margins Studies for Nuclear Power Plants," by Howard H.M. Hwang, 6/15/87, (PB88-134267/AS).

NCEER-87-0012 "Parametric Studies of Frequency Response of Secondary Systems Under Ground-Acceleration Excitations," by Y. Yong and Y.K. Lin, 6/10/87, (PB88-134309/AS).

NCEER-87-0013 "Frequency Response of Secondary Systems Under Seismic Excitation," by J.A. HoLung, J. Cai and Y.K. Lin, 7/31/87, (PB88-134317/AS).

NCEER-87-0014 "Modelling Earthquake Ground Motions in Seismically Active Regions Using Parametric Time Series Methods," by G.W. Ellis and A.S. Cakmak, 8/25/87, (PB88-134283/AS).

NCEER-87-0015 "Detection and Assessment of Seismic Structural Damage," by E. DiPasquale and A.S. Cakmak, 8/25/87, (PB88-163712/AS).

NCEER-87-0016 "Pipeline Experiment at Parkfield, California," by J. Isenberg and E. Richardson, 9/15/87, (PB88-163720/AS).

NCEER-87-0017 "Digital Simulation of Seismic Ground Motion," by M. Shinozuka, G. Deodatis and T. Harada, 8/31/87, (PB88-155197/AS).

NCEER-87-0018 "Practical Considerations for Structural Control: System Uncertainty, System Time Delay and Truncation of Small Control Forces," by J. Yang and A. Akbarpour, 8/10/87, (PB88-163738/AS).

NCEER-87-0019 "Modal Analysis of Nonclassically Damped Structural Systems Using Canonical Transformation," by J.N. Yang, S. Sarkani and F.X. Long, 9/27/87, (PB88-187851/AS).

NCEER-87-0020 "A Nonstationary Solution in Random Vibration Theory," by J.R. Red-Horse and P.D. Spanos, 11/3/87, (PB88-163746/AS).

NCEER-87-0021 "Horizontal Impedances for Radially Inhomogeneous Viscoelastic Soil Layers," by A.S. Veletsos and K.W. Dotson, 10/15/87, (PB88-150859/AS).

NCEER-87-0022 "Seismic Damage Assessment of Reinforced Concrete Members," by Y.S. Chung, C. Meyer and M. Shinozuka, 10/9/87, (PB88-150867/AS).

NCEER-87-0023 "Active Structural Control in Civil Engineering," by T.T. Soong, 11/11/87, (PB88-187778/AS).

NCEER-87-0024 "Vertical and Torsional Impedances for Radially Inhomogeneous Viscoelastic Soil Layers," by K.W. Dotson and A.S. Veletsos, 12/87, (PB88-187786/AS).

NCEER-87-0025 "Proceedings from the Symposium on Seismic Hazards, Ground Motions, Soil-Liquefaction and Engineering Practice in Eastern North America, October 20-22, 1987, edited by K.H. Jacob, 12/87, (PB88-188115/AS).

NCEER-87-0026 "Report on the Whittier-Narrows, California, Earthquake of October 1, 1987," by J. Pantelic and A. Reinhorn, 11/87, (PB88-187752/AS).

NCEER-87-0027 "Design of a Modular Program for Transient Nonlinear Analysis of Large 3-D Building Structures," by S. Srivastav and J.F. Abel, 12/30/87, (PB88-187950/AS).

NCEER-87-0028 "Second-Year Program in Research, Education and Technology Transfer," 3/8/88, (PB88-219480/AS).

NCEER-88-0001 "Workshop on Seismic Computer Analysis and Design of Buildings With Interactive Graphics," by J.F. Abel and C.H. Conley, 1/18/88, (PB88-187760/AS).

NCEER-88-0002 "Optimal Control of Nonlinear Flexible Structures," by J.N. Yang, F.X. Long and D. Wong, 1/22/88, (PB88-213772/AS).

NCEER-88-0003 "Substructuring Techniques in the Time Domain for Primary-Secondary Structural Systems," by G. D. Manolis and G. Juhn, 2/10/88, (PB88-213780/AS).

NCEER-88-0004 "Iterative Seismic Analysis of Primary-Secondary Systems," by A. Singhal, L.D. Lutes and P. Spanos, 2/23/88, (PB88-213798/AS).

NCEER-88-0005 "Stochastic Finite Element Expansion for Random Media," by P. D. Spanos and R. Ghanem, 3/14/88, (PB88-213806/AS).

NCEER-88-0006 "Combining Structural Optimization and Structural Control," by F. Y. Cheng and C. P. Pantelides, 1/10/88, (PB88-213814/AS).

NCEER-88-0007 "Seismic Performance Assessment of Code-Designed Structures," by H.H-M. Hwang, J-W. Jaw and H-J. Shau, 3/20/88, (PB88-219423/AS).

NCEER-88-0008 "Reliability Analysis of Code-Designed Structures Under Natural Hazards," by H.H-M. Hwang, H. Ushiba and M. Shinozuka, 2/29/88.

NCEER-88-0009 "Seismic Fragility Analysis of Shear Wall Structures," by J-W Jaw and H.H-M. Hwang, 4/30/88.

NCEER-88-0010 "Base Isolation of a Multi-Story Building Under a Harmonic Ground Motion - A Comparison of Performances of Various Systems," by F-G Fan, G. Ahmadi and I.G. Tadjbakhsh, 5/17/88.

NCEER-88-0011 "Seismic Floor Response Spectra for a Combined System by Green's Functions," by F.M. Lavelle, A. Bergman and P.D. Spanos, 5/1/88.

NCEER-88-0012 "A New Solution Technique for Randomly Excited Hysteretic Structures," by G.Q. Cai and Y.K. Lin, 5/16/88.

NCEER-88-0013 "A Study of Radiation Damping and Soil-Structure Interaction Effects in the Centrifuge," by K. Weissman, supervised by J.H. Prevost, 5/24/88, to be published.

NCEER-88-0014 "Parameter Identification and Implementation of a Kinematic Plasticity Model for Frictional Soils," by J.H. Prevost and D.V. Griffiths, to be published.

NCEER-88-0015 "Two and Three Dimensional Dynamic Finite Element Analyses of the Long Valley Dam," by D.V. Griffiths and J.H. Prevost, to be published.

NCEER-88-0016 "Damage Assessment of Reinforced Concrete Structures in Eastern United States," by A.M. Reinhorn, M.J. Seidel, S.K. Kunnath and Y.J. Park, 6/15/88.

NCEER-88-0017 "Dynamic Compliance of Vertically Loaded Strip Foundations in Multilayered Viscoelastic Soils," by S. Ahmad and A.S.M. Israil, 6/17/88.

NCEER-88-0018 "An Experimental Study of Seismic Structural Response With Added Viscoelastic Dampers," by R.C. Lin, Z. Liang, T.T. Soong and R.H. Zhang, 6/30/88.

NCEER-88-0019 "Experimental Investigation of Primary - Secondary System Interaction," by G.D. Manolis, G. Juhn and A.M. Reinhorn, 5/27/88.

NCEER-88-0020 "A Response Spectrum Approach For Analysis of Nonclassically Damped Structures," by J.N. Yang, S. Sarkani and F.X. Long, 4/22/88.

NCEER-88-0021 "Seismic Interaction of Structures and Soils: Stochastic Approach," by A.S. Veletsos and A.M. Prasad, 7/21/88.

NCEER-88-0022 "Identification of the Serviceability Limit State and Detection of Seismic Structural Damage," by E. DiPasquale and A.S. Cakmak, 6/15/88.

NCEER-88-0023 "Multi-Hazard Risk Analysis: Case of a Simple Offshore Structure," by B.K. Bhartia and E.H. Vanmarcke, 7/21/88, to be published.

NCEER-88-0024 "Automated Seismic Design of Reinforced Concrete Buildings," by Y.S. Chung, C. Meyer and M. Shinozuka, 7/5/88.

NCEER-88-0025 "Experimental Study of Active Control of MDOF Structures Under Seismic Excitations," by L.L. Chung, R.C. Lin, T.T. Soong and A.M. Reinhorn, 7/10/88.

NCEER-88-0026 "Earthquake Simulation Tests of a Low-Rise Metal Structure," by J.S. Hwang, K.C. Chang, G.C. Lee and R.L. Ketter, 8/1/88.

NCEER-88-0027 "Systems Study of Urban Response and Reconstruction Due to Catastrophic Earthquakes," by F. Kozin and H.K. Zhou, 9/22/88, to be published.

NCEER-88-0028 "Seismic Fragility Analysis of Plane Frame Structures," by H.H-M. Hwang and Y.K. Low, 7/31/88.